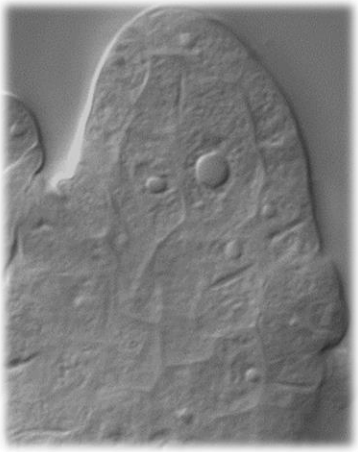

Involvement of *STK* and *REM24* in cellular specification during ovule formation in *Arabidopsis thaliana*

Sara Cristina Mendes Pinto

Biologia Funcional e Biotecnologia de Plantas

Departamento de Biologia

2017

Orientador

Sílvia Coimbra, Professor auxiliar, FCUP

Orientador

Ana Marta Pereira, PhD, FCUP

Coorientador

Matthew Tucker, Professor auxiliar, AFW, University of Adelaide

U.PORTO

FACULDADE DE CIÊNCIAS
UNIVERSIDADE DO PORTO

Todas as correções determinadas pelo júri, e só essas, foram efetuadas.

O Presidente do Júri,

Porto, _____/_____/_____

Acknowledgments

Olá mundo científico! Esta parte não é dedicada a ti, é dedicada aos humanos fantásticos que tornaram possível o trabalho que te dedico. Sabes uma coisa? Eles são mais importantes que tu, apesar de às vezes poder não parecer, por isso aparecem em 1º lugar :)

A primeira pessoa de que te quero falar é do meu Carlos. Foste e és uma pessoa incrível, nunca pensei que pudesse encontrar alguém assim… Mais do que me aturares, o que já é uma tarefa ao estilo missão impossível, quero agradecer-te por acreditares em mim, no meu trabalho, por me dares motivação para continuar mesmo quando penso que já não posso mais, por me amares mesmo do outro lado do mundo, por me levares a tomar cafezinho a sítios novos, por ires ter comigo ao comboio todas as manhãs e tornares a viagem mais pequena… por tudo o resto… tornaste-me uma pessoa mais feliz. Obrigada!

A minha família também foi muito importante para que eu escrevesse estas folhas todas. Obrigada aos meus pais que me apoiaram neste percurso académico. À minha mãe pelas bolachinhas, húngaros (estou mais gorda e a culpa é tua!) e pelas voltas dos tristes para apanhar solzinho na cabeça :P Ao meu irmão por me fazer rir e por me chatear, porque assim pude descarregar o stress ^.^ Ao meu pai pelo apoio à minha ida a Adelaide. À fofa Mini por me deixar brincar com ela e fazer festinhas na barriga quentinha. Um calmante instantâneo aqueles olhinhos doces :) Ao resto dos meus familiares que me enviaram energia positiva durante a minha estadia em Adelaide.

Agora aos meus amigos: as de sempre, os malucos das plantinhas, as oh pá calem-se e à Rosanna, obrigada por me aliviarem o stress, por aturarem os dramas e os delírios xD As de sempre são a Dani e a Eddie, obrigada por, apesar de os nossos caminhos serem paralelos, arranjarmos sempre um momento para que se intersectem: cappuccinos, viagens e passeios na praia para sempre <3 Os malucos das plantinhas são a Mónica, a Leonor (SAMONO power!!!), Nuno mágico, Zuca Bagel e Sr. Aires. São uma família incrível, espero que continue viva depois disto! Quero voltar a recordar os momentos de desespero geral superados com o apoio mútuo e os momentos de estupidezes várias :D Quero voltar a partilhar refeições deliciosas enquanto toda esta tarefa de time travel acontece ;) Rosa e Sofia, desculpem, mas o nome que eu dei ao nosso grupo é o melhor, por isso teve de ser assim xD No Norte, no Sul, nas plantas, nos peixes, nos ratos… nada parece comum, mas a verdade é que a nossa amizade é o melhor fator em comum que podíamos ter ^-^ obrigada por serem quem são! A ver se este ano nos juntamos outra vez todas, leram?

Rosanna you are going to have a whole paragraph! It could actually be a whole chapter right? Our friendship started from serendipity (ah ah), and as we are used to ear, serendipity seems to be the best way to find wonderful things. In truth, it was! Whatever I write here it's not going to be the proper thank you! Just bear in mind that it should sound so much better :P Thank you for being the best lab mate, house mate, friend mate (xD) ever!!! LAB MATES 4 EVER :D You're the nicest person I know, and that is probably why you get along with me. Thank you for taking care of me on the other half of the world. I never thought I could feel at home so easily <3 Thank you for being my fourth supervisor :D You know I couldn't have done all the things I needed by myself, especially if I couldn't remember ;) Thank you for everything, and something more <3 Tinkerbell misses you, you need to come to Porto :)

Quero dar um especial agradecimento aos cientistas do meu lab, o Spred, que me introduziram à beleza do estudo de florzinhas! Sinto-me muito sortuda por ter trabalhado com todos vocês quando ainda nem podia considerar-me cientista ;) Mais ainda, quero agradecer o facto de terem concorrido/escrito um projeto que me levou a Adelaide onde pude crescer pessoalmente e profissionalmente. Foi uma oportunidade incrível e só o devo a vocês! Obrigada: Ana Marta, Ana Lúcia, Mário e Prof. Sílvia!

Talking about my lab leads me to talk about my second lab. I think I can call it mine, maybe not, ups I did it (Petrella *et al*., 2017). Firstly, I want to thank Matthew and Elise because only amazing people would receive a strange in their home and make that person feel so welcome and so at ease. I also want to tell Miriam and Sam that they were a vital component of my Australian journey! I learnt a lot of Troll songs! Amazing kids, thank you for playing with me! Secondly, I called the lab mine because the Arabidopsis and barley scientists that work there welcomed me so nicely. Thank you, Dayton and Weng for introducing me in the lab, showing me how to use a face shield, googles, gloves and lab coat for everything xD And also Dayton, I should thank you for giving us rides to the supermarket and to the house, but c'mon did you really needed to tell me all those disgusting things? No, really, thank you! Thank you, Matt A. and Laura for teaching me about barley :) thank you, Jana for taking me to the chocolate factory (what a dream). Thank you, Cindy and Mia, for showing me that I belong to the Slytherin house and my patronus is a dog, I know myself better now! Thank you, Maple for helping me putting up with Dayton, and for your lovely company ^-^ And also, thank you Cate, the unicorn, you were another European treasure! To finish, I want to thank Matthew again, this time for accepting me in the lab, the scientific support and because now I know more synonyms of the word problem xD

Finally, I want to thank Marta Mendes for providing the *stk* RNA sequencing and for information regarding REM24, Dr Neil Shirley for essential assistance in the qPCR

experiments and Miss Sandy Khor for valuable help in the lab (from the Plant Cell Wall laboratory). From the Adelaide microscopy centre, Dr Gwenda Mayo for assistance with paraffin sections for the *in situ* hybridization.

This work wouldn't have been possible without funding from the SEXSEED project (H2020-MSCA-RISE-2015).

Resumo

O consórcio europeu SEXSEED foi concebido para aumentar o conhecimento sobre o desenvolvimento da semente. O principal objetivo do consórcio é conhecer a rede regulatória controlada por *SEEDSTICK* (*STK*). *STK* é um fator de transcrição (FT) responsável pela identidade dos óvulos de *Arabidopsis thaliana*. Recentemente foi revelado que *STK* pode estar implicado no estabelecimento da identidade da célula mãe dos megásporos (CMM), apesar de nunca ser expresso nesta célula. Primórdios de óvulos *stk* apresentam células nucelares aumentadas que se assemelham à CMM. O trabalho aqui apresentado pretende demonstrar o envolvimento de *STK* neste processo. Dados de transcritómica obtidos de inflorescências *stk*, da CMM de óvulos *wild type* e do nucelo de óvulos *wild type* foram usados para se obter uma lista de genes putativamente regulados por *STK*, importantes para a comunicação entre o nucelo e a CMM. Entre todos os genes, *REPRODUCTIVE MERISTEM 24 (REM24)* surgiu como um interessante alvo putativo de *STK*. De facto, estudos anteriores demonstraram que outro FT *REM*, *VERDANDI*, é um alvo direto de STK. *REM24* foi estudado usando uma abordagem multifacetada: o desenvolvimento de óvulos *rem24* foi caracterizado; para determinar o padrão de expressão do gene candidato, foi criada uma linha marcadora; as vias moleculares desreguladas em *rem24* foram avaliadas através de qPCR. Visto que a identidade de células nucelares aumentadas nunca foi avaliada em *stk*, os defeitos no desenvolvimento do óvulo, tanto em *stk* como em *rem24*, foram investigados usando coloração com azul de anilina, imunolocalização de epítopos de AGP e epítopos de calose, e pelo cruzamento das plantas mutantes com linhas marcadoras relevantes.
Notavelmente, a avaliação molecular de *stk* parece indicar o envolvimento de *SPOROCYTELESS* no desenvolvimento de células nucelares aumentadas. Adicionalmente, também foi revelado que *ARGONAUTE9* e *RNA DEPENDENT RNA polymerase 6* são potencialmente regulados por *STK,* mostrando que o mesmo controlará mecanismos epigenéticos importantes no processo de comunicação nucelo-CMM.

Palavras-chave: AGP; calose; identidade celular; comunicação; megasporogénese; formação da CMM; *REPRODUCTIVE MERISTEM 24*; *SEEDSTICK*; transcritómica.

Abstract

The European consortium SEXSEED was conceived to increase the knowledge on seed development. Its main goal is to assemble the regulatory network controlled by *SEEDSTICK* (*STK*). *STK* is a transcription factor (TF) responsible for specifying the identity of *Arabidopsis thaliana* ovules. Recently, it was revealed that *STK* may be implicated in megaspore mother cell (MMC) identity, although it is never expressed in that cell. *stk* ovule primordia show enlarged sub-epidermal nucellar cells resembling the MMC. The work here presented intends to demonstrate *STK*'s involvement in this process. Transcriptomic data obtained from *stk* inflorescences, the wild type MMC and the wild type nucellus were used to obtain a list of genes putatively regulated by *STK*, important for the cross talk between the nucellus and MMC. Among all the genes, *REPRODUCTIVE MERISTEM 24 (REM24)* was found as an interesting putative *STK* target. In fact, previous studies demonstrated that another *REM* TF, *VERDANDI*, is a STK direct target. *REM24* was studied using a multistep approach: the ovule development of *rem24* was characterized; to determine the expression pattern of the candidate gene, a marker line was developed; the molecular pathways affected in *rem24* were evaluated by qPCR. Since the identity of such enlarged nucellar cells was never investigated in *stk*, the defects in ovule development in both *stk* and *rem24* were further investigated using aniline blue staining, immunolocalization of AGP and callose epitopes, and by crossing the mutant plants with relevant marker lines.
Remarkably, the molecular assessment of *stk* seems to indicate that *SPOROCYTELESS* can be involved in the formation of enlarged nucellar cells. Additionally, it was also revealed that *ARGONAUTE9* and *RNA DEPENDENT RNA polymerase 6* are potentially regulated by *STK,* showing its potential control over epigenetic mechanisms important in the nucellus-MMC cross-talk.

Keywords: AGP; callose; cellular identity; cross-talk; megasporogenesis; MMC formation; *REPRODUCTIVE MERISTEM 24*; *SEEDSTICK*; transcriptomic.

Index

List of figures and tables

List of abbreviations

ABS – Arabidopsis B Sister
AG – AGAMOUS
AGL13 – AGAMOUS LIKE13
AGP – Arabinogalactan protein
ANT – AINTEGUMENTA
AP – APETALA1
ARF – AUXIN RESPONSIVE FACTOR
AGO - ARGONAUTE
BAN/ANR – BANYLUS / ANTHOCYANIDIN REDUCTASE
BEL1 – BELL 1
ChIP-seq – Chromatin immunoprecipitation sequencing
Col-0 – Columbia 0 variety
DAB – Decolorized aniline blue
DEG – Differentially expressed genes
DIC – Differential Interference Contrast
DNA – Deoxyribonucleic acid
ES – Embryo sac
dsRNA – Double stranded ribonucleic acid
FBP – FLOWER BINDING PROTEIN
FDR – False discovery rate
FLA – Fasciclin-like arabinogalactan protein
FG – Female gametophyte
FG1 – Mono-nuclear female gametophyte
FIL – FILAMENTOUS FLOWER
FM – Functional megaspore
gDNA – genomic deoxyribonucleic Acid
GO – Gene Ontology
GUS – β-glucuronidase
H3K27 – Histone 3 lysine 27
H3K9ac – Histone 3 lysine 9 acetylation
HDACs – Histone deacetylases
HSP20 – HEATSHOCK PROTEIN 20-like
INO – INNER NO OUTER
KNU – KNUCKLES
LB – Luria-Bertani
LFY – LEAFY
MEL1 – MEIOSIS ARRESTED AT LEPTOTENE1
MMC – Megaspore mother cell
mRNA – Messenger ribonucleic acid
miRNA – Micro ribonucleic acid
nls – Nuclear localization signal
NUB – NUBBIN
NUC – Nucellus
NZZ – NOZZLE
PAs – Pro-anthocyanidins
PCR – Polymerase chain reaction
PI – PISTILLATA
qPCR – Quantitative polymerase chain reaction
REM – REPRODUCTIVE MERISTEM
REF6 – RELATIVE OF EARLY FLOWERING 6
RdDM – RNA-directed DNA Methylation pathway
RDR – RNA-DEPENDENT RNA POLYMERASE
RNA – Ribonucleic acid
RNA-seq – Ribonucleic acid sequencing
SEP – SEPALLATA
SEU – SEUSS
SHP – SHATERPROOF
siRNA – Short interfering ribonucleic acid

SPL – SPOROCYTELESS

SPL8 – SQUAMOSA PROMOTER BINDING PROTEIN-LIKE 8

ssRNA – Single stranded ribonucleic acid

STK – SEEDSTICK

SUP – SUPERMAN

ta-siRNA – Trans-acting short interfering ribonucleic acid

TF – Transcription Factor

VAL – VALKYRIE

VDD – VERDANDI

UFO – UNUSUAL FLOWER ORGANS

UTR – Untranslated region

UV – Ultraviolet light

WUS – WUSCHEL

WT – Wild Type

Y3H – Yeast three-hybrid

YFP – Yellow Fluorescent Protein

YUC1 – YUCCA1

1. Introduction

1.1. *Arabidopsis thaliana* reproduction

Angiosperms have a life cycle that alternates between a sporophytic (diploid) generation and a gametophytic (haploid) generation. To complete the life cycle the sporophyte must produce two types of haploid spores by meiosis, which subsequently undergo cell proliferation and differentiation and give rise to the gametophytes. Angiosperms such as *Arabidopsis thaliana* possess flowers composed of sepals, petals, stamens and carpels organized in whorls. The syncarpous carpels enclose two rows of ovules, the diploid structures responsible for embryo sac (ES) development, the female gametophyte (FG). In turn, in the anthers of the stamens, the pollen grains, the male gametophytes, are formed. The purpose of the gametophytic generation is to produce the female and male gametes. The passage for the next generation is accomplished when double fertilization - a characteristic feature of angiosperms explained later - occurs and seeds are formed, which harbour the new sporophytes (Fig.1) (Yadegari and Drews, 2004).

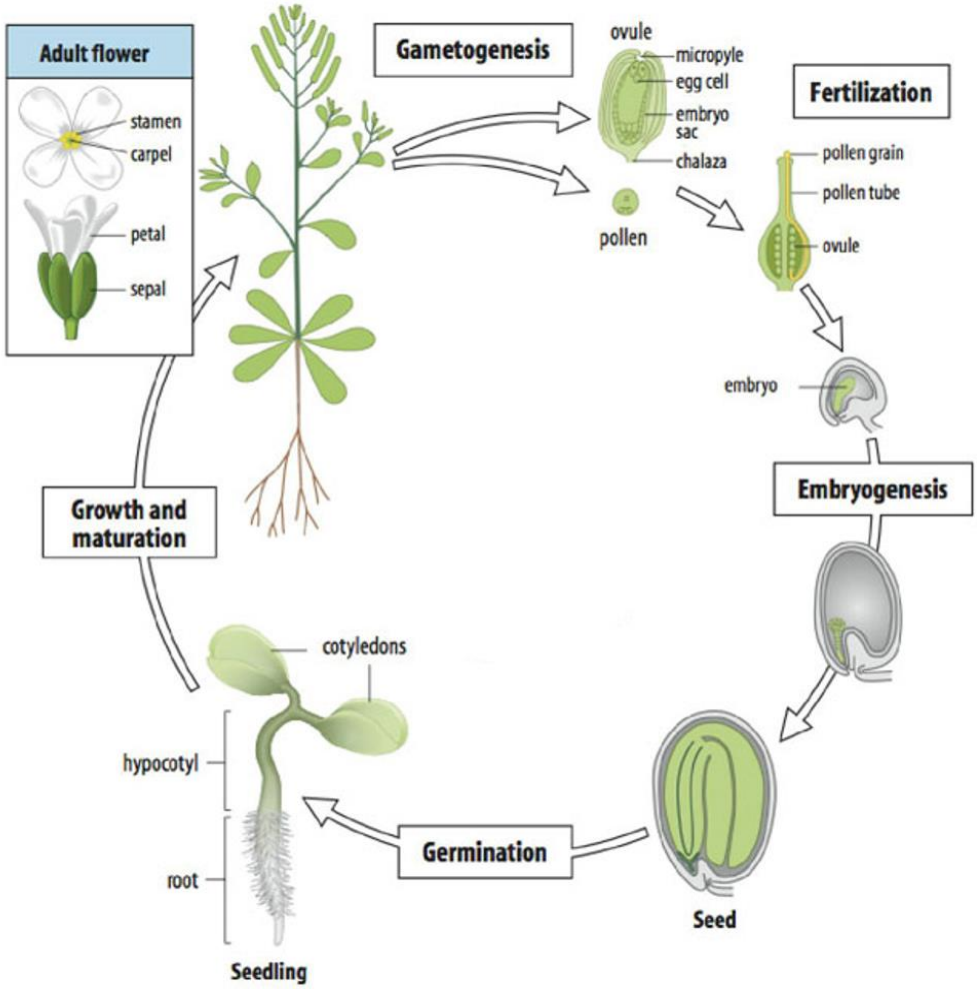

Fig. 1 – Representation of *Arabidopsis thaliana* life cycle. The scheme shows the major stages of development. When the plant is mature it will produce flowers in which male and female gametes are produced by gametogenesis. When

pollen grains land on a stigma, they germinate, and the pollen tube grows towards the micropyle of the ovule. One sperm cell, male gamete, will fuse with the egg cell, female gamete, originating the embryo. The other sperm cell will fuse with the central cell, female gamete, originating the endosperm. The endosperm is a nutritive tissue that supports the growth of the embryo. The life cycle is completed when the seed germinates, giving rise to the new plant. Adapted from: http://www.mun.ca/biology/desmid/brian/BIOL3530/DB_06/DBNPlant.html

1.1.1. The ovule: a mega case of development

In *A. thaliana*, the wild-type (WT) ovule emerges as a finger-like structure only composed of diploid cells: the nucellus, the diploid tissue that will harbour the sporogenous cells, the chalaza, the region between the nucellus and the initiating integuments, and the funiculus, the stalk that connects the ovule to the placenta of the carpel. Early in ovule development, two nucellar layers are distinguishable, an epidermal L1 cell layer and a subepidermal L2 layer which fills the “nucellar dome”. Ovule development can be divided into two main stages: megasporogenesis and megagametogenesis. Within the L2 nucellar layer, during megasporogenesis, the megasporocyte undergoes meiotic division to form four haploid megaspores. The megasporocyte arises as the archesporial cell, a sub-epidermal enlarged cell of the nucellus, which develops into the megaspore mother cell (MMC) without any cell division (Schneitz *et al*., 1995). The MMC enlarges (Schneitz *et al*., 1995), its chromatin setting, including histone modifications and nucleosome remodelling, is altered (Baroux and Autran, 2015), and when mature, the cell wall accumulates large amounts of β-1,3-glucan (callose), distinguishing this cell from the other nucellar cells (Schneitz *et al*., 1995; Lora *et al*., 2016). The MMC is the direct forerunner of the megaspores. Prior to the initiation of meiosis, the two integuments, one inner and one outer, initiate their development. These sporophytic tissues will proliferate around and over the nucellus throughout ovule development, to protect the haploid generation. Megasporogenesis ends with MMC meiosis and the formation of a multiplanar (tetrahedral) or linear spore tetrad (Webb and Gunning 1990; Schneitz *et al*., 1995). Three spores will degenerate and only the chalazal-most megaspore, the functional megaspore (FM), will survive and enter megagametogenesis (morphologically well described, from FG1 to FG7, Christensen *et al*. 1997). The FM after three rounds of mitosis will give rise to the female gametophyte (FG). The ES is composed of two synergid cells, the cells where the pollen tube enters to release its gametes, the egg cell and the central cell, the female gametes, and three antipodals, accessory cells (Fig. 2). When the ovule is successfully fertilized, it will develop into a seed (Schneitz *et al*., 1995). Understanding ovule development has been of considerable interest to the international research community because genes involved in ovule development are potential targets for the optimisation of seed production.

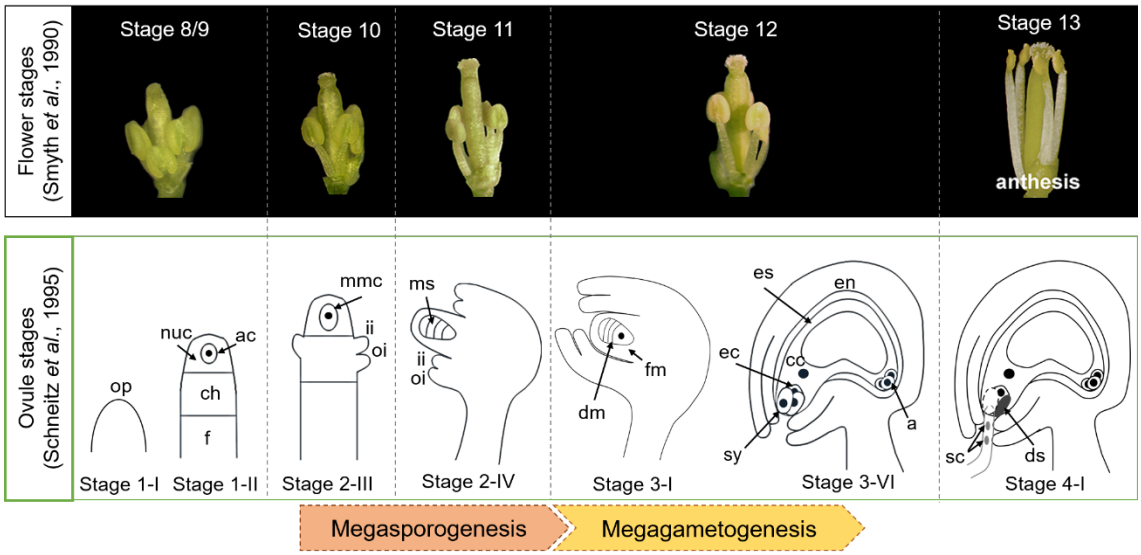

Fig. 2 – *Arabidopsis thaliana* wild type flower developmental stages (according to Smyth *et al*., 1990) and correspondent ovule developmental stages (according to Schneitz *et al*., 1995). Megasporogenesis and megagametogenesis are the two fundamental developmental steps in ovule formation. In flowers stage 8/9 exist finger-like ovules, without integuments, an archesporial cell differentiates in ovules stage 1-II. Megasporogenesis occurs between flowers stage 10 and 11. Flowers stage 10 harbour ovules from stage 2-I to 2-III, with enlarged MMC and integument initiation. Flowers stage 11 contain ovules at stage 2-IV to 2-V, meiosis has finished, and the ovule harbours a tetrad of megaspores. Megagametogenesis occurs in flowers stage 12, with ovules from stage 3-I to 3-VI. In flowers stage 13, ovules may be fertilized and enter stage 4-I. Post-fertilization events occur until flower stage 15 (not represented). These stages were used as reference for this work. For the quantitative PCR analysis, the flowers collected included the sepals and petals, unlike what is portrayed in the flower pictures. a – antipodals; ac – archesporial cell; cc – central cell; ch – chalazal; dm – degenerating megaspores; ds – degenerating synergid; ec – egg cell; en – endothelium; es – embryo sac; f – funiculus; fm – functional megaspore; ii – inner integument; mmc – megaspore mother cell; ms – megaspores; nuc – nucellus; oi – outer integument; op – ovule primordia; sc – sperm cell; sy – synergid. Flower pictures adapted from Cecchetti *et al*. (2008).

1.1.2. Flower development a MADS whorl(d)

MICK MADS transcription factors (TFs) control floral organ specification. These TFs act in a complex fashion to give identity to the sepals, petals, stamens, carpels and ovules. Over 25 years ago, the interactions between the MADS TFs were compiled in the ABC model of flower development for *A. thaliana* and *Antirrinhum majus* (Coen *et al*., 1991). The A-class genes alone determine the identity of the sepals. The B-class together with the A-class genes give identity to the petals. The B-class with the C-class genes control the identity of the stamens. Finally, the C-class genes alone confer identity to the carpels. The A-class genes are *APETALA 1* (*AP1*) and *AP2*. The B-class genes are *AP3* and *PISTILLATA* (*PI*). *AGAMOUS* (*AG*) is the only C-class gene (Fig. 3) (Coen *et al*., 1991). Further genetic-based studies allowed this model to be extended to include the D-class genes, which specify ovule identity, and the E-class genes, which are necessary for the other MADS to regulate transcription. The D-class genes are *SEEDSTICK* (*STK)*,

SHATERPROOF 1 (*SHP1*) and *SHP2*. The E-class genes are *SEPALLATA 1* (*SEP1*), *SEP2*, *SEP3* and *SEP4* (Fig. 3) (Kaufmann *et al.,* 2005). The general mode of transcription regulation by the MADS TFs occurs by the formation of tetramers: one TF dimerizes with another to form a homo or heterodimer, then the two dimers form a heterotetramer. The quartet binds two nearby CArG box, the canonical binding site of the MADS proteins, in the target promoter causing the DNA to loop (reviewed by Yan *et al*., 2016). Through yeast three-hybrid (Y3H) experiments it was demonstrated that STK interacts with AG, SHP1, and SHP2 through SEP3 to form the complexes. Therefore, the ovule identity quartet is composed of STK, AG, SHP1/2 and SEP3 (Fig. 3) (Favaro *et al*., 2003).

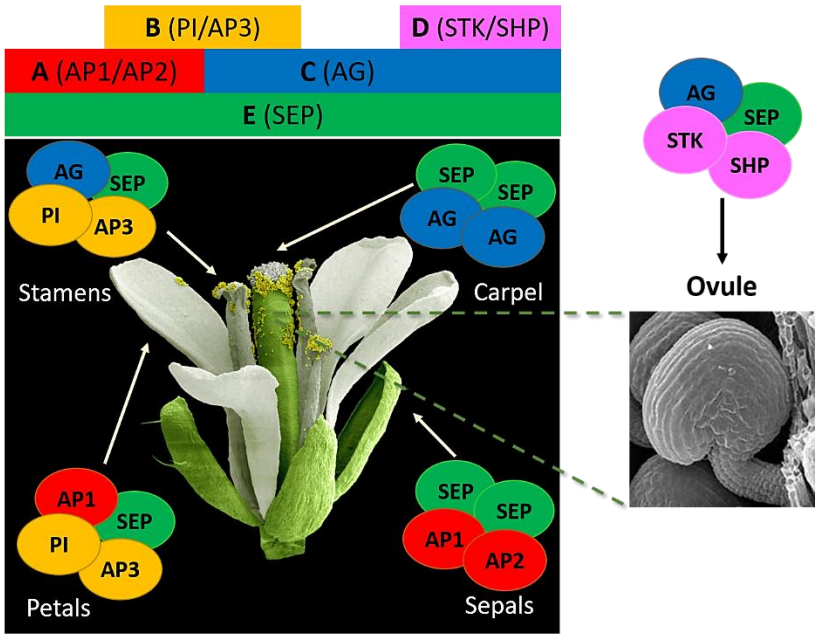

Fig. 3 - Representation of the ABCDE model of flower development. Tetrameric complexes transcriptionally regulate the identity of floral organs. The floral quartets are depicted by each set of four circles. The colours represent the class to which the transcription factor belongs: red for the A-class, yellow for the B-class, blue for the C-class, pink for the D-class and green for the E-class genes. AG – AGAMOUS; AP1 – APETALA1; AP2 – APETALA2; AP3 – APETALA3; SEP – SEPALLATA; SHP – SHATERPROOF; STK – SEEDSTICK.

1.1.3. *STK* as a master regulator of ovule development

STK was proposed to regulate ovule-specific gene expression in *A. thaliana,* since it is orthologous to *FLOWER BINDING PROTEIN 7* (*FBP7*) and *FBP11* from *Petunia hybrida* (Rounsley *et al*., 1995), the first ovule identity genes discovered (Colombo *et al*., 1995). *P. hybrida* plants overexpressing *FBP11* and *A. thaliana* plants overexpressing *STK* are able to convert wild-type sepals into carpelloid organs where ovules develop (Favaro *et al*., 2003; Colombo *et al*., 1995).

During ovule development, *STK* expression is first detected throughout ovule primordia and in placental tissues (Fig. 4.A). When the integuments initiate, *STK* is strongly expressed only in the funiculus and nucellus (Fig. 4.B). At the stage where both integuments cover the nucellus and until later stages of the mature seed, *STK* is still expressed in the funiculus, and becomes expressed in the outer integument and outer layer of the inner integument but is no longer present in the nucellus (Fig. 4.C-E). Importantly, *STK* is not detected in the MMC or its meiotic derivatives (Rounsley *et al*., 1995; Pinyopich *et al*., 2003; Mizzotti *et al*., 2014).

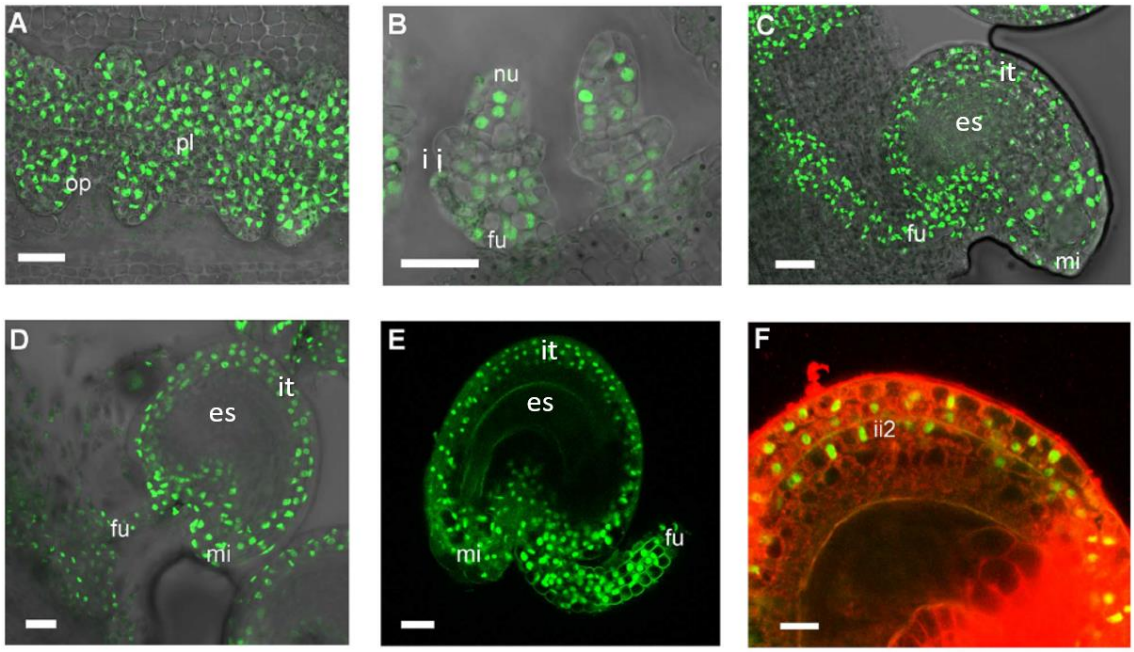

Fig. 4 - Confocal laser-scanning images of *pSTK:STK-GFP* expression patterns during ovule and seed development. **(A)** STK-GFP protein is expressed in the placenta and in the ovule primordia. **(B)** When integuments arise, STK-GFP signal is localized in the nucellus and in the funiculus. **(C, D)** GFP can be detected throughout the integuments, funiculus and the adjacent placental region when the ovule is mature. **(E)** After fertilization, the STK-GFP signal is present in the outer integuments and funiculus of developing seeds. **(F)** Magnification of figure E with an overlay image of propidium iodide staining (specific staining of the cell wall). STK-GFP can be detected in the two layers of the outer integument and also in the outer layer of the inner integument. op - ovule primordia; pl - placenta; nu - nucellus; i - integuments; fu - funiculus; mi - micropyle; ii2 - outer layer of inner integument. Scale bars = 50 μm (A and B), 40 μm (C, D and E) and 20 μm (F). (Adapted from Mizzotti *et al*., 2014).

Many genetic-based studies indicate that *STK* is a master regulator of ovule and seed development. *STK* functions are summarized in Fig. 6. Regarding ovule development, *stk* mutant ovules retain ovule identity, but *stk shp1 shp2* triple mutant ovules are converted to carpel-like structures and seeds do not develop (Pinyopich *et al*., 2003) suggesting that *STK* is responsible for ovule identity redundantly with *SHP1* and *SHP2*. Importantly, *STK* has been implicated in female germline development, since putative

extra MMC-like cells are detected in 46% of *stk* mutant ovules (Fig. 5) (Gatti, 2015). In contrast, in WT pistils only 3-6% of the ovules develop into extra MMC-like cells and these never develop into gametophytes (Schneitz *et al*., 1995; Olmedo-Monfil *et al*., 2010).

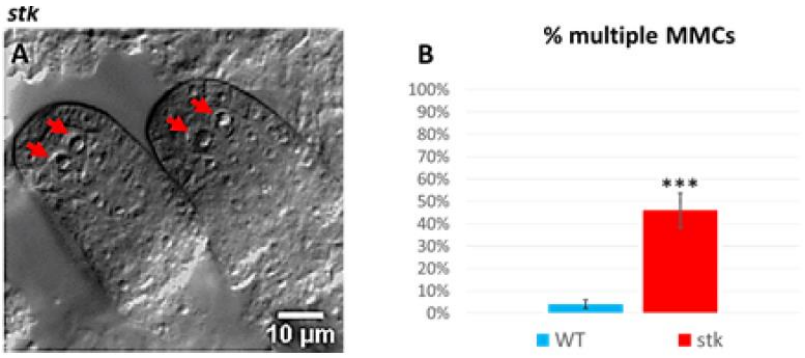

Fig. 5 - *stk* phenotype during early ovule development. **(A)** Finger-like ovules showing the presence of a second putative MMC-like cell (red arrows) in *stk* mutant. **(B)** Frequency of ovules with the depicted phenotype. The asterisks represent the statistical difference observed for *stk* when compared to wild type (adapted from Gatti, 2015).

In addition, studies examining the *bell1* (*bel1) stk shp1 shp2* quadruple mutant phenotype, Y3H and pull down assays concluded that STK controls the development of the outer integument by stabilizing the BEL1-AG-SEP3 complex. This complex then positively regulates *INNER NO OUTER (INO)* (Baker *et al*., 1997), the gene responsible for outer integument outgrowth (Brambilla *et al*., 2007; Brambilla *et al*., 2008; Battaglia *et al*., 2008). *STK* also regulates aspects of the seed formation and post-fertilization processes. *stk* mutant seeds are smaller than WT and the funiculi of these seeds are longer and larger. The abscission zone, a specialized area of the funiculus for seed dehiscence, is also enlarged and therefore the seeds remain attached to the silique (Pinyopich, *et al*., 2003). *STK* regulates endothelium formation with *Arabidopsis B Sister* (*ABS*). The endothelium is the inner most layer of the inner integument. In the *abs* mutant, a deformed endothelium is formed (Nesi *et al*., 2002). However, the double mutant *abs stk* completely lacks the endothelium, and seed set is severely reduced (Mizzotti *et al*., 2012). After fertilization, the ovule accumulates pro-anthocyanidins (PAs) in the endothelium (Debeaujon *et al*., 2003). One of the genes involved in PAs biosynthesis is *BANYLUS/ANTHOCYANIDIN REDUCTASE* (*BAN/ANR*) (Devic *et al*., 1999). *BAN* is transcriptionally activated by *ABS*. *STK* was found to directly repress *ABS* and *BAN* (3-4 days after pollination) in order to restrict PAs production to the endothelium (Mizzotti *et al.,* 2014). *STK* is also responsible for specifying the identity of gametophytic cells. A quartet composed of two STK-SEP3 dimers induce the transcription of *VERDANDI* (*VDD*) and *VALKYRIE* (*VAL*) (Matias-Hernandez *et al*., 2010; Mendes *et al*., 2013; Mendes *et al*., 2016). *VDD* and *VAL* are *REPRODUCTIVE MERISTEM* (*REM*) B3

TFs. *VDD* controls antipodal and synergid cell identity (Matias-Hernandez *et al*., 2010). Both *VDD* and *VAL* are required for pollen tube burst and synergid programmed cell death (Mendes *et al*., 2016).

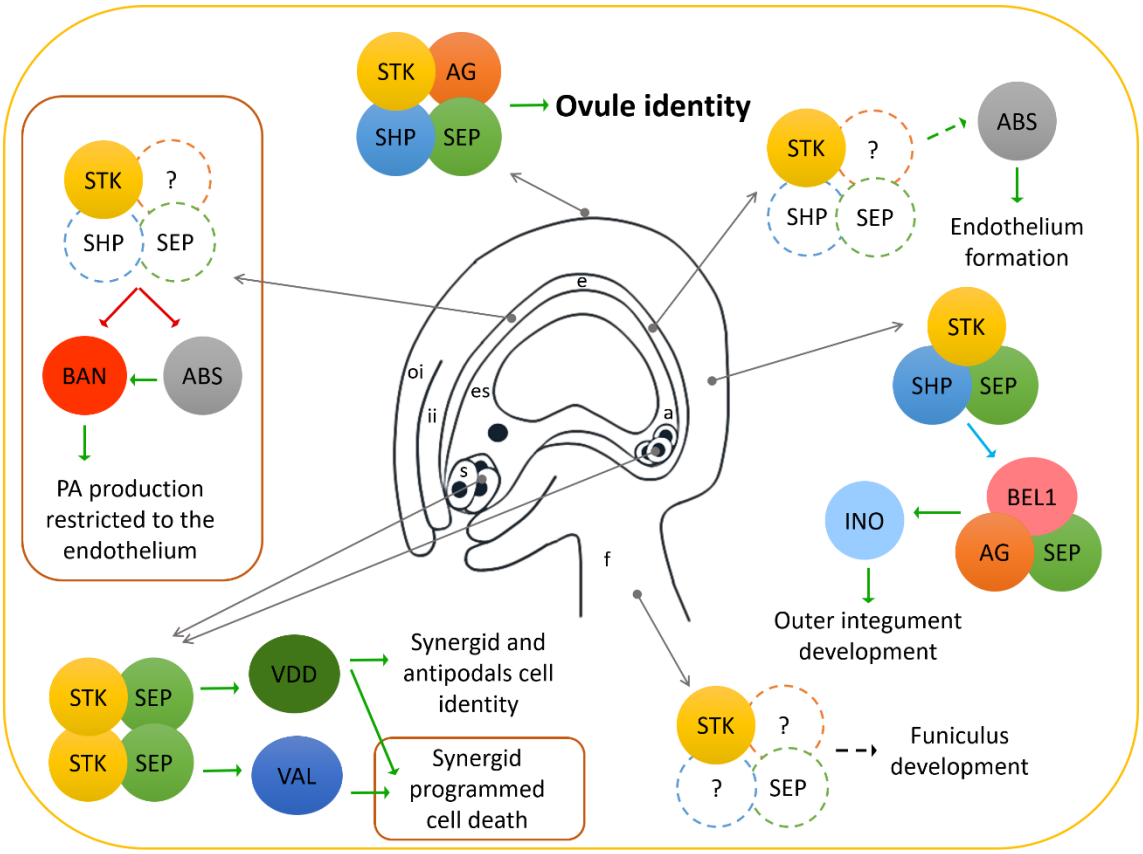

Fig. 6 - Schematic representation of *STK* functions during ovule and seed development. The quartet STK-SHP-AG-SEP promotes ovule identity (Favaro *et al*., 2003). *STK* potentially promotes *ABS* expression leading to endothelium formation. The trimer STK-SHP-SEP putatively stabilizes the complex BEL1-AG-SEP. That complex activates *INO* allowing the outer integument development. *stk* ovules show longer and larger funiculus. *STK* must be required for the correct development of the funiculus. Two dimers STK-SEP promote the transcription of *VDD* and *VAL*. *VDD* confers synergid and antipodals cell identity during embryo sac formation. *VDD* and *VAL* are required for synergid programmed cell death, during fertilization. *STK* binds directly to *BAN* and *ABS* promoters to repress their expression outside the endothelium. ABS promotes *BAN* that is responsible for the production of pro-anthocyanidins (PA) in the endothelium. Each circle represents a transcription factor. The complexes with filled circles were detected by yeast two/three hybrid assays and implicated in the respective processes. Transcriptomic data or *stk* knock-out phenotype analysis indicated that *STK* is involved in certain processes, but their interaction partners weren't identified. The complexes with dashed circles hypothetically regulate the process. In *stk shp1 shp2*, the integuments are converted to carpel like structures. It is likely that *SHP1/2* participate in the quartets acting on the integuments development. *SEP* proteins are required for the formation of the tetramers. *SEP* should be part of all quartets here described. The brown boxes highlight the processes after fertilization. Green arrows – known to promote action; red arrows – known to repress action; blue arrow – stabilize complex formation; dashed arrow – hypothetical relation. a – antipodals; e – endothelium; es – embryo sac; f – funiculus; ii – inner integument; oi – outer integument; s – synergids.

1.1.4. Apomixis: the female power

Plant sexual reproduction results in the production of a seed through double fertilization. Remarkably, some species are able to produce seeds without fertilization, via asexual reproduction. This process is known as apomixis (Schmidt *et al*., 2015). Here the alternation between haploid and diploid generations is evaded. In apomitic species, meiosis doesn't occur, and a process called apomeiosis leads to the formation of unreduced FMs, and then unreduced gametophytes. Apomixis can occur in two ways, the archesporial cell aborts meiosis and directly gives rise to the FM – a phenomenon called diplospory; or a somatic cell adjoining the sexual cells differentiates into a FM – this type of apomixis is named apospory (Fig. 7). Usually male sporogenesis isn't affected, but the production of unreduced pollen occurs sporadically (Bicknell and Koltunow, 2004). Development of the unreduced "FM" leads to the production of an embryo sac containing an egg cell, which will produce an embryo by parthenogenesis, and the central cell, which forms the endosperm autonomously or through fertilization (Whitton *et al*., 2008).

During normal sexual development, it is unclear how the germline fate is established in the MMC and how it is absent in the remaining nucellar cells. However, hypotheses suggest that when communication between somatic ovule cells is defective, both the MMC and adjacent somatic cells can acquire germinal fates. In aposporous apomicts, germline fate should be acquired by a somatic aposporous initial and the sexual MMC, as they both initiate reproductive lineages. The products of apospory interact with the sexual products at a cellular level, either co-existing with them or leading to their degeneration. On the other hand, in diplosporous ovules, only one cell goes through apomeiosis, therefore diplospory directly replaces the sexual process. These differences point to a distinct pathway controlling apospory and diplospory (Schmidt *et al*., 2015; Tucker and Koltunow, 2009). Transcriptomic comparative analysis between the apomitic initials of *Hieracium praealtum* (Okada *et al*., 2013), an aposporous apomitic, and *Boechera gunnisoniana* (Schmidt *et al*., 2015), a diplosporous apomict, unravelled some of those differences. In the aposporous species, some meiosis-related genes weren't active, while in the diplosporous species the core meiotic genes were expressed. These data support the notion that diplospory results from the deviation of the meiotic pathway, whereas in apospory the FM identity is established as a direct change in fate (Schmidt *et al*., 2015).

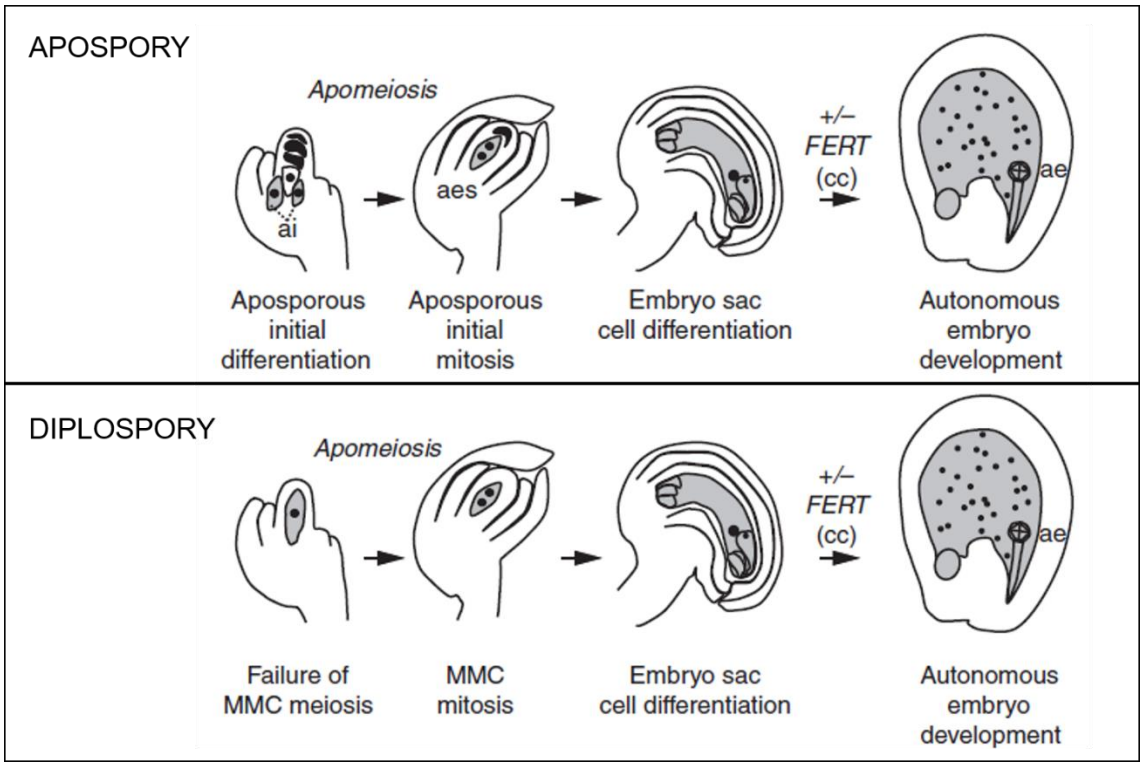

Fig. 7 – Portray of the key steps in apospory and diplospory ovule development and seed formation. ae - autonomous embryo; aes - aposporous embryo sac; ai - aposporous initial; cc – central cell; FERT - fertilisation; Apomictic structures in the ovule/seed diagram are shaded in grey. Adapted from Tucker and Kultonow, 2009.

1.1.5. Incorrect development of the MMC - when neighbours grow together

Before any cell is committed to enter germline fate, the cells within the L2 nucellus layer are very similar in size. Among the uniform nucellar cells, one will perceive certain signals, acquire MMC identity and follow a genetic program much different from the sibling cells. When those signals are integrated, the archesporial cell is under the most distal nucellar epidermal cells and it can be recognized by a difference in cellular volume, relative to the other L2 nucellar cells (Schneitz *et al*., 1995; Lora *et al*., 2016). When the signals are perceived by the neighbouring nucellar cells, they may acquire MMC identity. In 1965, Rédei detected the presence of twin megasporocytes in the *Gf* (female gametophyte factor) mutant. When analysing the WT ovule development, Schneitz *et al*. (1995) noticed that 3% of ovules appeared to have two MMC which were recognized by their similar size. Importantly, the final volume of the WT MMC is always bigger than of the enlarged nucellar cells which don't develop further (Lora *et al*., 2016).

The balance between communication and isolation among the nucellus and the MMC needs to be established to allow MMC development without letting the remaining nucellar cells enter the same germline pathway. The MMC epigenetic state is most distinct of that of the surrounding tissues (She *et al*., 2013) and this may account for the germline versus

somatic fate. Olmedo-Monfil *et al.* (2010) uncovered a sRNA pathway acting in the nucellus, responsible for the correct maintenance of somatic identity. sRNA, such as short interfering RNA (siRNA) or micro RNA (miRNA) are guided by ARGONAUTE (AGO) proteins to cleave target messenger RNA (mRNA) to induce post-transcriptional gene silencing (Borges and Martienssen, 2015). AGO9 is a component of a RNA-directed DNA Methylation pathway (RdDM) (Havecker *et al*., 2010) that leads to silencing of transposable elements in the egg and synergid cells (Olmedo-Monfil *et al*., 2010; Durán-Figueroa *et al*., 2010). The mutants *ago9-2* and *ago9-3* presented 47,7% and 37.16% (respectively) of ovule primordia with an increased number of enlarged nucellar cells, MMC-like, in the L2 layer. While *AGO9* transcript was detected in the epidermal L1 layer of the nucellus, the protein accumulates in the nucleus of the MMC (Olmedo-Monfil *et al*., 2010; Rodríguez-Leal *et al*., 2015; Su *et al*., 2017). In *ago9-3*, the extra cells acquired FM identity and developed into FG without going through meiosis. Another component of the RdDM pathway that is involved in this process is *RNA-DEPENDENT RNA POLYMERASE 6* (*RDR6*). *RDR6* functions in the biogenesis of trans-acting siRNAs (ta-siRNAs) and other siRNAs (Himber *et al*., 2003; Peragine *et al*., 2004; Yoshikawa *et al*., 2005). The *rdr6-11* phenotype showed 43.3% of ovules with extra MMC-like cells that also acquired gametophytic identity without meiosis. *ago9* and *rdr6* ectopic MMC mutant phenotypes resemble apospory, since the enlarged nucellar cells acquire FM identity bypassing meiosis. The authors hypothesized that the pathway involving *AGO9* and *RDR6* leads to gene silencing restricting gametophytic identity in the nucellar cells (Olmedo-Monfil *et al*., 2010) (Fig. 8). In the maize mutant, *ago104*, 70% of the female gametes are unreduced because meiosis is converted to mitosis. *AGO104* is homolog of the *A. thaliana AGO9,* but in this case the AGO protein seems to prevent diplospory in the MMC (Singh *et al*., 2011).

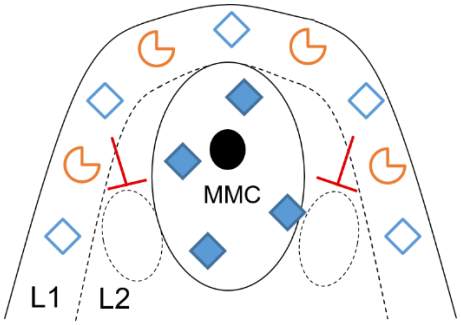

Fig. 8 - Model of *AGO9* and *RDR6* pathways occurring during megasporogenesis. Blue squares indicate *AGO9* expression pattern in the nucellar L1 layer. Filled blue squares represent AGO9 protein accumulation in the MMC. The orange shapes indicate the presence of *RDR6* mRNA in the L1 layer. It is proposed that siRNAs targeted by AGO9 or RDR6 may be silenced in the L2 layer of the nucellus, blocking the development of extra MMC-like cells (dashed ovals) in that layer. MMC – megaspore mother cell; L1 – L1 layer of the nucellus; L2 – L2 layer of the nucellus.

1.1.6. Epigenetics and ovule development – a long distance relationship

Viable seed production is only achieved when all the cells and tissues of the ovule are correctly specified. Otherwise, developmental flaws can translate into ovule defects, and in severe cases, seed abortion. The cross-talk between both generations is well established. For example, ES development and integument formation are linked. The *ino* mutants have a normal inner integument but lack an outer integument, and megagametogenesis is impaired (Villanueva *et al.*, 1999). In *stk shp1 shp2* ovules, integuments are converted to carpelloid structures and FG development is arrested because megagametogenesis doesn't occur normally (Brambilla *et al*., 2007; Battaglia *et al*., 2008). The absence of the endothelium in the *abs stk* double mutant ovules was related with the severe reduced seed set (Mizzotti *et al*., 2012). In *bel1* ovules, integuments are replaced by an inner integument-like structure, which acquires carpel identity (Robinson-Beers *et al*., 1992; Brambilla *et al*., 2007), and ovule development is arrested after megasporogenesis (at FG1). Intriguingly, none of the genes mentioned above are expressed in the haploid cell lineage (Reiser *et al*., 1995; Villanueva *et al*., 1999; Mizzotti *et al*., 2014; Ehlers *et al*., 2016).

Being components of the epigenetic machinery, *ago9*, *ago104* and *rdr6* mutant phenotypes gave clues that epigenetic phenomena are essential for ovule development. Additionally, in *ago9* and *rdr6* mutants, the enlarged nucellar cells have histone modifications similar to those of the MMC (She *et al*., 2013). In rice, mutations in *MEIOSIS ARRESTED AT LEPTOTENE1* (*MEL1*), closely related to *AGO5* from *A. thaliana*, leads to male and female meiotic arrest and sterility (Nonomura *et al*., 2007). The machinery of the ta-siRNAs biogenesis and a specific ta-siRNA were identified as additional players influencing MMC development. When *TEX1* (Jauvion *et al*., 2010; Kumakura *et al*., 2009), part of the THO complex, involved in ta-siRNAs transport from the nucleus to the subcellular location where they're processed into siRNAs (Yelina *et al*., 2010), is mutated, several nucellar cells acquire MMC identity. This mutation also resembles apospory since the ectopic megasporocytes may develop into embryo sacs without going through meiosis. Moreover, *TAS3* transcripts are processed into ta-siRNAs that repress *AUXIN RESPONSIVE FACTOR3* (*ARF3*) and both genes are involved in the same process. In the *tas3* mutant, *ARF3* was more expressed and this was correlated with the supernumerary MMC formation (Su *et al*., 2017).

MICK MADS have been implicated in epigenetic regulation in plant reproduction. *RELATIVE OF EARLY FLOWERING 6* (*REF6*) (Smaczniak *et al*., 2012) encodes a histone 3 lysine 27 (H3K27) demethylase (Lu *et al*., 2011). It was demonstrated that

APETALA1 could interact with REF6 leading to *SEP3* transcriptional activation. Remarkably, *STK* also controls epigenetic mechanisms. Mizzotti *et al*., (2014) discovered an indirect mode of *BAN*/*ANR* transcription regulation by *STK*. In *stk* mutants, *BAN* was upregulated and ectopically expressed in tissues where *STK* was normally expressed. H3K9 acetylation (H3K9ac) marks the transcriptionally active chromatin. The authors identified a correlation between high levels of H3K9ac with an increased active state of the *BAN* promoter in the *stk* mutants. It was proposed that in WT ovules, *STK* repressed histone deacetylases (HDACs) at the *BAN* locus to restrict *BAN* expression (Mizzotti *et al.,* 2014). The evidences connecting MICK MADS TFs and epigenetic alterations lead to an update of the floral quartet model: the floral quartet replaces a nucleosome in inactive chromatin binding to two nearby CArG boxes; besides recruiting the transcription machinery, the protein quartet can then recruit histone-modifying factors which may alter the methylation or acetylation state of nearby nucleosomes (Fig. 9) (Theißen *et al*., 2016).

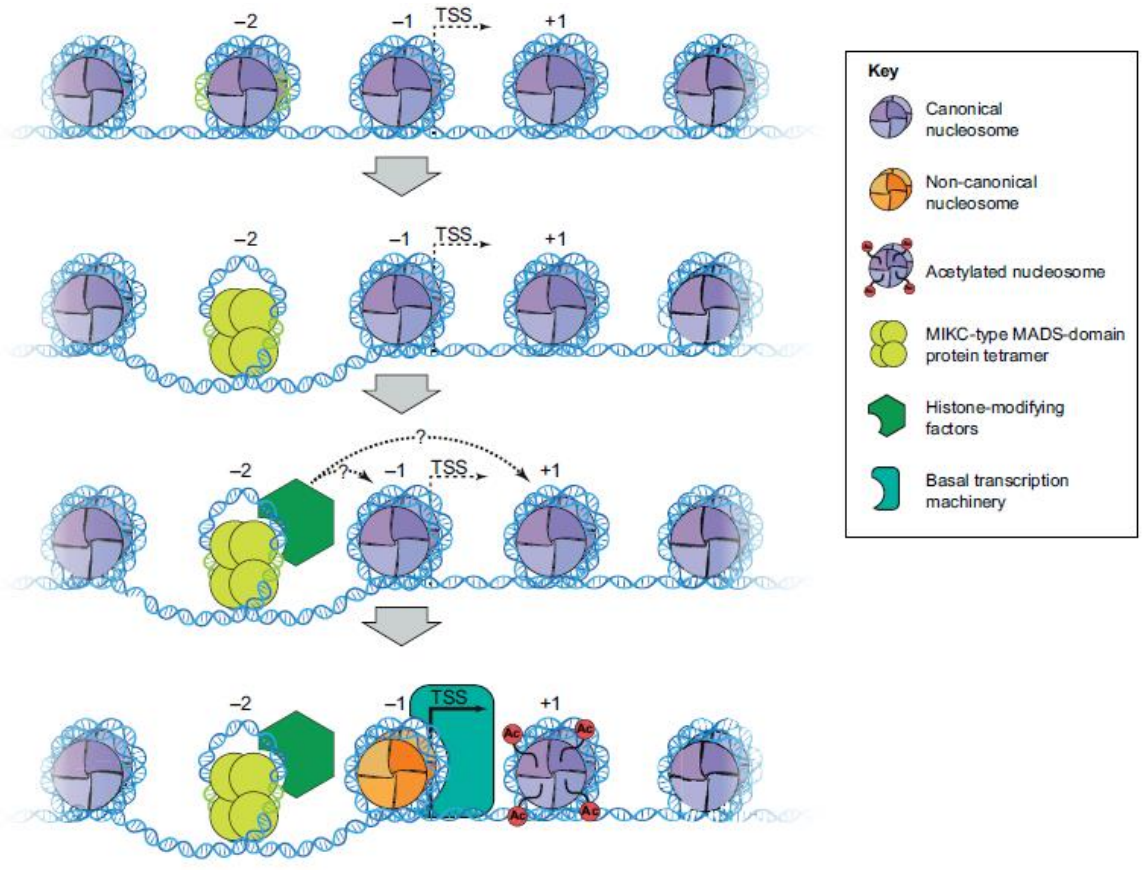

Fig. 9 – Model of the MADS transcription regulation and their influence over epigenetic mechanisms. The quartet replaces the inactive nucleosome, near the transcription start site (TSS) of the target gene, altering the chromatin conformation. The transcription factor complex can then recruit histone-modifying factors such as acetylases and methylases, leading eventually to recruitment of the basal transcriptional machinery. The acetylation of a histone is shown to represent gene activation. Adapted from Theißen *et al*., 2016.

1.1.7. *REM* transcription factors rocking flower development

REPRODUCTIVE MERISTEM (*REM*) TFs contain up to seven B3 DNA-binding domains. 45 *REM* genes constitute the family that probably originated from duplication events (Swaminathan *et al*., 2008; Romanel *et al*., 2009). Genome wide screens and expression analysis strongly implicate the *REM* family in early flower and ovule development (Wellmer *et al*., 2006; Kaufmann *et al*. 2010; Wynn *et al*., 2011; Mantegazza *et al*., 2014). *REM34*/*REM1* was detected in the vegetative and floral meristems, and in specific cell types of the carpel. The elevated level of duplication of the family most likely resulted in the lack of phenotype of *rem34* mutant (Franco-Zorrilla *et al*., 2002). *SEUSS* (*SEU*) and *AINTEGUMENTA* (*ANT*) are transcriptional regulators implicated in ovule initiation from the carpel margins. In WT gynoecia, the ovules emerge from the carpel margin meristem, however in the double *seu ant* mutant the formation of ovules is impaired. With a transcriptomic approach, Wynn *et al.* (2011) identified several *REM* TFs has being de-regulated in the *seu ant* carpels. In fact, *in situ* hybridization experiments showed that *REM15*, *REM16*, *VERDANDI*/*VDD*/*REM20*, *REM34*/*REM1*, and *REM22* are expressed in the carpel margin meristem, in the ovule primordia and tapetal cells of anthers (flowers at the stage 8 to 10, according to Smyth *et al*., 1990) (Wynn *et al*., 2011). Mantegazza *et al*. (2014), performed a meta-analysis of transcriptomic and Chromatin Immunoprecipitation sequencing (ChIP-seq) data and identified two groups of *REM* putatively involved in flower development: *REM23*, *REM24* and *REM25*, and *REM34*, *REM35* and *REM36*. Although *in situ* hybridization assays revealed that the genes from the first group are expressed in flowers at the stage 8 and 9 mostly in stamen primordia, and the second group of genes was expressed in the floral meristem, stamens and carpel primordia; no phenotype was observed for single or double mutants. Remarkably, the ChIP-seq analysis revealed direct targeting of *REM* genes by floral identity TFs, such as *LEAFY* (*LFY*), *APETALA3* (*AP3*) and *PI* (Mantegazza *et al*., 2014). To date, only *VERDANDI* (*VDD*) and *VALKYRIE* (*VAL*) are the *REM* genes with attributed functions. *VDD* controls antipodal and synergid cell identity (Matias-Hernandez *et al*., 2010). In both *vdd*/+ and *VAL* RNA interference line, in ~30% of ovules the pollen tubes don't burst when entering an ovule and synergid cells don't degenerate. *In vivo* interaction studies revealed that VDD and VAL act together. Both *VDD* and *VAL* are required for pollen tube burst and consequently synergid programmed cell death (Mendes *et al*., 2016).

1.2. Objectives

It is known that by 2050, the human population will reach 9.7 billion people (FAO, 2016). This means that current agricultural yields need to double. The food requirements will increase, and we can't increase the arable land. The majority of the calories consumed by humans, the major components of animal feed and the production of high-value-added products are obtained from seeds. Accordingly, it is most important to improve seed production by obtaining plants with higher yields. The work presented here is integrated in the European consortium SEXSEED (H2020-MSCA-RISE-2015), established to improve the knowledge on seed production. One of the factors influencing seed production is the number of ovules correctly formed in each flower. More specifically, SEXSEED aims to analyse the network controlled by *SEEDSTICK* (*STK*), the master regulator of ovule and seed development.

New data indicate that *stk* mutant presents enlarged nucellar cells next to the MMC however, prior to this study, their identity wasn't defined. Since *STK* may regulate epigenetic events, and these are key in MMC formation, the study of this particular aspect of *stk* mutant is of importance. Can *stk* lead to an apospory or diplospory-like defect? What are the players intervening as *STK* targets that can prevent the acquisition of germline fate in the nucellus cells? These are some of the questions raised in this work. To answer the later question, a transcriptomic approach was adopted: the newly obtained *stk* RNA sequencing (RNA-seq) (Mendes *et al*., unpublished) was crossed with the MMC microarray data (Schmidt *et al*., 2011) and with the nucellus transcriptome (Tucker *et al*., 2012). *REM24* was identified as a putative *STK* target that can be involved in MMC cellular specification or formation. Despite a lot of efforts in unravelling *REM* TFs expression patterns, functions haven't been attributed to many of them. Thus, establishing *REM24* function would constitute novel insights into the *REM* family.

2. Materials and Methods

2.1. Plant material and growth conditions

All genotypes of *A. thaliana* (L.) Heynh. plants used in this work were in Columbia (Col-0) background. WT seeds were obtained from the Nottingham Arabidopsis Stock Center (NASC), United Kingdom. *rem24* (SALK_054142) (Mantegazza *et al*., 2014) and *stk* (Pinyopich *et al*., 2003) mutant lines were kindly shared by Marta Adelina Mendes. The marker lines for the megaspore mother cell (*pKNU:3nlsYFP*) (Payne *et al*., 2004), the functional megaspore (*pFM1:GUS*) (Acosta-Garcia and Vielle-Calzada, 2004), and the *dyad*/+ *pKNU:3nlsYFP* were kindly shared by Matthew Tucker. Seeds were sown on soil and incubated at 4ºC, in the dark, for 2 days. Then, all plants were grown in a growth chamber under long-day conditions: 16 hours light at 23ºC and 8 hours dark at 18ºC. The light intensity was set at 180 μmole m^{-2} s^{-1}.

2.1.1. Controlled crosses

Closed *A. thaliana* flowers were emasculated at stages 11 – 12, according to Smyth *et al*. (1990), and immediately hand pollinated with dehiscent anthers. The donor plants were genotyped and/or presence of fluorescent signal checked before crossing.

2.1.2. Preparation of plant material for microscopy

To check the fluorescence of the marker lines and marker line crosses, under a stereo microscope Stemi 2000-C (Zeiss) and using hypodermic needles, pistils were removed from the flowers, mounted on 10% (v/v) glycerol, and gently squashed using the cover slip to release the ovules from the carpels. Then, observation of the ovules occurred using an upright Axio Imager M2 microscope (Zeiss) equipped with a differential interference contrast (DIC) prism for bright field images, and UV light for fluorescence detection (for YFP detection, the filter used was 500/535 nm). Images were captured with an Axiocam MRm camera (Zeiss), using Zen 2 pro software (Zeiss).

To determine the size of seeds resultant from the different crosses, the seeds were placed on a petri dish under the stereo microscope Stemi 2000-C (Zeiss) and the images captured using the AxioCam ERc5s (Zeiss).

2.2. Genotyping

Mutant genotypes were confirmed by Polymerase Chain Reaction (PCR). A crude and rapid DNA extraction from a small leaf disk allowed the isolation of genomic DNA (gDNA) suitable for PCR amplification. The gDNA was extracted according to Edwards, Johnstone, and Thompson (1991). The PCR was carried out using Platinum™ Taq DNA Polymerase (Invitrogen). The reaction mixture was slightly modified, as shown in Table 1.

Table 1 - PCR reaction mixture used with Platinum™ Taq DNA polymerase (Invitrogen).

Reagent	**Final concentration**
10x PCR Buffer	1x
50 mM Magnesium chloride	1.25 mM
2 mM dNTP mix	50 μM
10 μM Forward primer	0.25 μM
10 μM Reverse primer	0.25 μM
Platinum™ Taq DNA polymerase	2.6 U
Template DNA	<500 ng
Nuclease free water	**Up to 20 μL**

Specific oligonucleotides and expected band sizes are listed on Supplemental table 1. The samples were placed on a T100™ Thermal Cycler (BIO-RAD) and general PCR conditions are presented on Table 2.

Table 2 - General PCR conditions used for Platinum™ Taq DNA polymerase (Invitrogen).

Step		**Temperature**	**Time**
Initial denaturation		94ºC	2 min
35 cycles	Denaturation	94ºC	30 sec
	Annealing	55 – 62ºC	30 sec
	Extension	72ºC	1min/kb
Final extension		72ºC	5 min

Specific annealing temperatures are discriminated on Supplemental table 1. PCR products were separated in a 1% - 2% (w/v) agarose gel in 1X TAE (40 mM Tris-acetate and 1 mM EDTA, pH 8.3); SYBR® Safe DNA Gel Stain (Invitrogen) was added prior to polymerisation. 1X loading dye was added to each sample before loading. Using the 1 Kb Plus DNA Ladder (Invitrogen) as a molecular weight marker and 1X TAE as running buffer, the electrophoretic separation was conducted at 110 V and non-limiting amperage for 20 minutes. The DNA was visualized in a UV transilluminator (302-365 nm).

2.3. Gene expression analysis by RT-qPCR

2.3.1. RNA extraction

Target genes' expression level was evaluated across the different flower developmental stages. The stages were nominated considering Smyth *et al*., 1990 and Schneitz *et al*., 1995 floral and ovule development staging, respectively. The stages considered were: stage 1 - 7 (which included the inflorescence meristem and flowers without ovule primordia), stage 8 - 9 (flowers where ovule primordia have initiated, stage 1-I and 1-II), stage 10 (flowers which contained ovules at stage 2-I to 2-III, with enlarged megaspore mother cell), stage 11 (flowers with ovules undergoing megasporogenesis, at stage 2-IV and 2-V), stage 12 early (flowers enclosing ovules at stage 3-I to 3-III, at early stages of megagametogenesis), stage 12 late (flowers with ovules at stage 3-IV to 3-VI, at late stages of megagametogenesis) and stage 13 - 15 (including flowers at anthesis with mature ovules and fertilized ovules, stage 4-I to 4-VI). The flowers were dissected from the inflorescence under the stereo microscope Stemi 2000-C (Zeiss), using hypodermic needles, and placed immediately on liquid nitrogen. At least 5 flowers were collected for each stage, and two biological replicates were collected for each genotype. Total RNA was extracted with the RNeasy Mini Kit (Qiagen) following the instructions manual. After extraction, RNA quality was assessed on a 1% (w/v) agarose gel in 1xTAE, as described before. The electrophoretic separation was conducted at 80 V and non-limiting amperage for 40 minutes. The RNA was treated with TURBO™ DNase (Invitrogen) to remove the remaining gDNA, according to the manufacturer's instructions. The RNA was mixed with the Turbo DNase and its buffer (concentrations displayed in Table 3) and incubated at 37ºC for 30 minutes. Then the resuspended DNase inactivation reagent was added following an incubation at room temperature for 5 minutes. The reaction was centrifuged for 10 000g for 5 minutes, and the supernatant recovered.

Table 3 - Reaction mixture used for removing the gDNA from RNA samples using the TURBO DNA-free™ Kit (Invitrogen).

Reagent	**Final concentration**
10x Turbo DNase Buffer	1X
Turbo DNase	0.04 U/μL
Template RNA	44 μL
DNase inactivation reagent	0.1 volume

2.3.2. cDNA synthesis

RNA was retro-transcribed using Superscript III and and Oligo(dT)$_{12–18}$ Primer (Invitrogen), according to the instructions manual. Reaction mixtures are described in Table 4.

Table 4 - Reaction mixture used for RNA retro-transcription using Supercript III. DTT – 1,4-Dithiothreitol; MM – Master Mix; RT – Reverse Transcriptase.

Reagent		**Final concentration**
MM1	50 μM Oligo(dT)$_{20}$ Primer	2.5 μM
	5 mM dNTP mix	0.5 mM
	Template RNA	3 μL (<5μg)
	H_2O	Up to 11.75 μL
MM2	5X Strand buffer	1X
	0.1 M DTT	0.01 M
	SuperScript™ III RT	100 U/μL
Final volume		**20 μL**

Master Mix 1 (MM1) was incubated at 65ºC for 5 minutes and snap cooled on ice. The MM2 was added and the mixture incubated at 50ºC for 70 minutes. The enzyme was inactivated by heating the mixture at 70ºC for 15 minutes.

The cDNA was tested with *ACT8* (*AT1G49240*) primers by PCR with Platinum™ Taq DNA Polymerase (Invitrogen), as described previously. The electrophoretic separation of the PCR products was performed as described earlier.

2.3.3. qPCR optimization and conditions

Primers for analysing the expression level of *REM24* (*AT2G16210*), *REM23* (*AT2G35310*), *REM1* (*AT4G31610*), *STK* (*AT4G09960*), *AGO9* (*AT5G21150*), *FLA20* (*AT5G40940*), *HSP20* (*AT5G47600*), *SPL* (*AT4G27330*) and *RDR6* (*AT3G49500*) were designed *de novo* (Supplemental table 1) and tested to verify their specificity. The primers for *WUS* (*AT2G17950*), *KNU* (*AT5G14010*) (Payne *et al*., 2004) and *AGO5* (*AT2G27880*) (Tucker *et al*., 2012) were previously designed. Optimization and qPCR experiments occurred as described in Burton *et al*. (2008).

The transcript levels of genes encoding cyclophilin (AtCyclophilin), actin (AtActin), tubulin (AtTublin), and glyceraldehyde 3-phosphate dehydrogenase (AtGAPdH) were used as controls (Supplemental table) (Li *et al*., 2014). Normalization was carried out using these control genes as described by Burton *et al*. (2004) and the Mrna final concentrations of the genes of interest are expressed as arbitrary units that represent the numbers of

copies per microliter of cDNA, normalized against the geometric means of the four control genes that vary the least with respect to each other (Vandesompele *et al*., 2002). The standard error was calculated from the mean of the absolute expression level between the biological replicates for each stage. Since the absolute expression level was calculated as mRNA copies per microliter, to have more homogenous samples, some stages were pulled together: stage 1-7 with 8-9, 10 with 11, and 12 early with 12 late. Therefore, the standard error was recalculated considering the mean obtained for the stages pulled together. For the statistical analysis a two-tailed, paired Student's t-test was performed, $\alpha = 0.05$.

All qPCR experiments and data normalization were kindly performed by Dr Neil Shirley (School of Food Agriculture and Wine, University of Adelaide). The qPCR product HPLC purification was kindly conducted by Mr. Chao Ma (School of Food Agriculture and Wine, University of Adelaide).

2.4. Marker lines production

2.4.1. Cloning the fragments of interest

To produce *pREM24:3nlsYFP* and *pREM24:intron1:3nlsYFP*, the putative *REM24* promoter region considered was from -1161 to -1 (excluding the ATG); the putative *REM24* promoter with the first intron was the region from -1161 to +1037. The fragments were amplified by PCR using the Platinum™ Taq DNA Polymerase High Fidelity (Invitrogen). The oligonucleotides used to produce the fragments were OSP_55 and OSP_57 for *pREM24:3nlsYFP,* and OSP_56 and OSP_61 for *pREM24:intron1:3nlsYFP*, listed on Supplemental table 1. Following the instructions manual, the general PCR conditions are listed on Table 5.

Table 5 - PCR conditions used for Platinum™ Taq DNA Polymerase High Fidelity.

Step		**Temperature**	**Time**
Initial denaturation		94ºC	2 min
35 cycles	Denaturation	94ºC	30 sec
	Annealing	55 – 62ºC	30 sec
	Extension	68ºC	1min/kb
Final extension		68ºC	5 min

Specific annealing temperatures are discriminated on Supplemental table 1. The PCR products were separated on a 1% (w/v) agarose gel, as mentioned previously, and visualized on the blue-light Safe Imager; the desired fragments were excised from the

agarose gel and purified using the illustra GFX PCR DNA and Gel Band Purification Kit (GE healthcare), according to the manufacturer's instructions. The fragments were ligated into the cloning vector pCR™8/GW/TOPO® (Invitrogen) according to the manual.

2.4.2. *Escherischia coli* competent cells transformation

The ligation product was transformed into One Shot® TOP10 Chemically Competent *E. coli* (Invitrogen). 3 μL of the ligation product were added to the competent cells thawed on ice. The mixture was incubated on ice for 30 min. Heat shock was carried out by heating the cells at 42ºC for 45 seconds followed by incubation on ice for 2 minutes. For the cells to recover, 250 μL of pre-warmed Luria-Bertani (LB) medium was added to the cells. The transformed cells were incubated at 37ºC, for one hour. The culture was spined down for 45 seconds, 150 μL of the supernatant removed, the cells were resuspended on the remaining volume and plated on LB media supplemented with 1.2% (w/v) agar and 0.01 mg/mL spectinomycin. The cells were incubated over-night (ON) at 37ºC. Individual colonies were selected for screening by PCR with Platinum™ Taq DNA Polymerase (Invitrogen), as described earlier. A small amount of colony was resuspended in 50 μL of mQH_2O; 5 μL of that dilution were used as DNA template in the reaction mixture. The primer pair used for both *pREM24* and *pREM24:intron1* ligated into pCR8 was M13_F and OSP_057 (Supplemental table 1), at 55ºC, the expected amplification product size was 1297bp.

The colonies positive for the presence of the plasmid of interest were inoculated in LB medium supplemented with 0.01 mg/mL spectinomycin, and incubated ON at 37ºC, with shaking at 180 rpm. Plasmid DNA was isolated from the ON cultures using the PureLink™ Quick Plasmid Miniprep Kit (Invitrogen), following the instructions manual. To further confirm the presence and the orientation of the desired fragment, a restriction digestion assay was performed. All the restriction enzymes used were from New England BioLabs and are described on Supplemental table 2. The expected fragment sizes obtained after digestion are discriminated on Supplemental table 2. The digestion fragments were separated by agarose gel electrophoresis as mentioned in genotyping section.

The colonies that presented the expected digestion fragments were further selected for Sanger sequencing at the Australian Genome Research Facility (AGRF). Prior to sequencing, the plasmid DNA was quantified using the Qubit® dsDNA BR Assay (Invitrogen), according to the instructions manual. The primer used for sequencing was M13_F (Supplemental table 1) for *pREM24* (pCR8) and for *pREM24:intron1* (pCR8).

To obtain the construct of interest, the plasmid DNA with the fragment of interest in the correct orientation was used in a LR reaction with MT589 as a destination vector (Supplemental Fig. 1), using the Gateway™ LR Clonase™ II Enzyme Mix (Invitrogen), according to the instructions manual. 4 μL of the gateway product was used to transform One Shot® TOP10 Chemically Competent *E. coli* (Invitrogen), as described above. The transformed cells were plated on LB medium supplemented with 1.2% (w/v) agar and 0.01 mg/mL kanamycin. The individual *E. coli* colonies grown on selective medium were screened by PCR with Platinum™ Taq DNA polymerase (Invitrogen). The primer pair used for screening was OSP_056 and TL40_R (Supplemental table 1) for *pREM24:3nlsYFP* (MT589) and *pREM24:intron1:3nls:YFP* (MT589), the annealing temperature was 55ºC, and the expected amplification product size was 1429 bp and 2467 bp, respectively. The plasmid DNA of positive colonies was isolated for restriction digestion assay (Supplemental table 2) and Sanger sequencing, all procedures occurred as detailed before. The primer used for sequencing *pREM24:3nlsYFP* (MT589) and *pREM24:intron1:3nlsYFP* (MT589) was OSP_069 (Supplemental table 1).

2.4.3. Agrobacterium transformation

The isolated plasmid DNA was used to transform AGL1 Agrobacterium competent cells by heat shock. The competent cells were thawed on ice. 10 μL of the desired construct was added to the cells and the mixture was incubated on ice for 5 minutes. The cells were heat shocked by placing them on liquid nitrogen for 5 minutes and then incubation at 37ºC for 5 minutes. 1 mL of warmed LB media was added, and the transformed cells were incubated at 28ºC for three hours. The culture was centrifuged at 4000 rcf for one minute and 500 μL of the supernatant removed. The cells were resuspended in the remaining volume and plated on LB media supplemented with 1.2% (w/v) agar, 0.01 mg/mL rifampicin and 0.01 mg/mL kanamycin. The plates were incubated for two ON at 28ºC. Individual colonies were selected for screening by PCR, using the Platinum™ Taq DNA Polymerase (Invitrogen), as detailed earlier. As DNA template, a small amount of each colony was picked with a pipette tip, stroke on LB media supplemented with 1.2% (w/v) agar, 0.01 mg/mL rifampicin and 0.01 mg/mL kanamycin, and the same tip was used to swab the PCR tube. Then, the PCR tubes were microwaved for two minutes (at maximum power) to burst the bacterial cells. The PCR reaction mixture was added and the procedure occurred as mentioned earlier. The primer pair used for screening *pREM24:3nlsYFP* (MT589) and *pREM24:intron1:3nlsYFP* (MT589) colonies were

OSP_056 and TL40_R (Supplemental table 1), the annealing temperature was 55ºC, and the expected amplification product size was 1429 bp and 2476 bp, respectively.

2.4.4. Agrobacterium-mediated plant transformation by floral dip

The procedure followed Clough and Bent (1988) method. The colonies harbouring the correct construct were inoculated in 15 mL of LB media supplemented with 0.01 mg/mL rifampicin and 0.01 mg/mL kanamycin, and incubated ON at 28ºC, with shaking at 180 rpm. To increase the culture volume, that inoculum was added to 250 mL of LB medium supplemented with 0.01 mg/mL rifampicin and 0.01 mg/mL kanamycin. After incubation ON at 28ºC, with shaking at 180 rpm, the culture was centrifuged for 20 minutes, at 4000 rpm, at room temperature. The cell pellet was resuspended in 5% (w/v) sucrose solution, constituting the Agrobacterium solution. Primary stems of WT plants were trimmed off at 6–7 days prior to transformation to encourage secondary stems to emerge. The siliques and opened flowers were removed to increase transformation efficiency. The plants were dipped in the Agrobacterium solution supplemented with 0.03% (v/v) Silwett L-77, and incubated ON in horizontal position, in the growth chamber. To increase transformation efficiency, five days later, the plants were brushed with Agrobacterium solution supplemented with 0.03% (v/v) Silwett L-77 (the solution was obtained as before).

2.5. Immunolocalization of AGP and callose epitopes

2.5.1. Fixation of *A. thaliana* flowers

Individual *A. thaliana* flowers were fixed in 0.25% (w/v) glutaraldehyde, 4% (w/v) paraformaldehyde, 4% (w/v) sucrose in 1X Phosphate Buffered Saline (PBS) [0.8% (w/v) NaCl, 0.02% (w/v) KCl, 0.144% (w/v) Na_2PO_4, 0.024% (w/v) KH_2PO_4, pH 7.4] ON at 4ºC. The flowers were then placed in 1X PBS ON at 4ºC. After dehydration in an ethanol series [from 70% (v/v) ethanol to 100% (v/v) dehydrated ethanol], the samples were incubated in 50% (v/v) LR White resin (in dehydrated ethanol), ON at 4ºC. The material was washed three times with LR White resin before encapsulation in gelatine capsules. The LR white polymerisation of the embedded samples occurred at 60ºC for three ON.

2.5.2. Immunolabelling with fluorophores

1 μM sections were obtained with Leica EM UC6. The sections were placed on glass slides and left unstained for immunolocalization with monoclonal antibodies raised

against AGP and callose epitopes. The monoclonal antibody used to detect AGP epitopes was JIM13 (Knox *et al*., 1991). The monoclonal antibody raised against β-1,3-glucan was used for the detection of callose epitopes. As secondary antibodies AlexaFluor® 555 anti-rat IgG (Invitrogen A-21434) and AlexaFluor® 488 anti-mouse IgG (Invitrogen A-11001) detected AGP and callose primary antibodies, respectively.

The sections were circled with a PAP pen (Pro-Sci-Tech ID300). The slides were rehydrated with 1X PBS for seven minutes, incubated with 0.025 M glycine (in 1X PBS) for 20 minutes, and washed with Incubation Buffer (IB) [1% (w/v) BSA in 1X PBS], two times for 10 minutes. The slides were incubated with the primary antibody (1:100 dilution in IB) in a humid chamber, for one hour. For this step, the negative control slides were incubated with the IB only. After washing the slides three times with IB, the slides were incubated with the secondary antibody (1:200 dilution in IB), in a humid, dark chamber, for two hours. Following one wash with IB and two washes with water (10 minutes each), the sections were stained with 0.1% (w/v) calcofluor white (in water) for 90 seconds and washed three times with water. The slides were mounted with 90% (v/v) glycerol and observed under an upright Axio Imager M2 microscope (Zeiss) [the filters were 365/445 nm for calcofluor, 545/605 nm for AlexaFluor® 555, and 470/525 nm for AlexaFluor® 488]. Images were captured with AxioCam MRm camera (Zeiss) and processed with Zen 2 pro (Zeiss) software.

2.6. *In situ* hybridization of *REM24* mRNA

2.6.1. Probe preparation

2.6.1.1. Cloning the fragment of interest

To discover the genes with nucleotide sequence highly and somewhat similar to *REM24*, *REM24* nucleotide sequence was blasted against *A. thaliana* genome (https://blast.ncbi.nlm.nih.gov/Blast.cgi?PROGRAM=blastn&PAGE_TYPE=BlastSearch&LINK_LOC=blasthome). *REM23* (AT2G35310) and *REM22* (AT3G17010) were the most similar genes, and their nucleotide sequences were aligned with *REM24*'s. Based on this alignment, the region chosen for the probe was the least conserved in the 3'UTR, present in both *REM24* alternative transcripts. All cloning steps occurred as described in section "2.4.1. Cloning fragments of interest". The desired fragment was amplified with the primer pair OSP_059 and OSP_060, using the Platinum™ *Taq* DNA Polymerase High Fidelity (Invitrogen), (oligonucleotide sequences, amplification product size, and annealing temperature are listed on Supplemental table 1). The PCR product was separated by an agarose gel electrophoresis, the fragment with the expected size was

excised from the gel and purified using the illustra GFX PCR DNA and Gel Band Purification Kit (GE healthcare). The purified PCR product was ligated into pCR™II (Invitrogen), and transformed into One Shot TOP10® chemically competent *E. coli* cells (Invitrogen). The transformed cells were plated on LB medium supplemented with 1.2% (w/v) agar, 0.01 mg/mL ampicillin and 0.01 mg/mL kanamycin. The plasmid DNA was isolated using the PureLink™ Quick Plasmid Miniprep Kit (Invitrogen), restriction digestion assay and sequencing were performed to confirm the presence of the insert of interest. The restriction enzymes used and the expected fragment sizes are present on Supplemental table 2. The primer used for sequencing was M13_F (Supplemental table 1).

2.6.1.2. Preparing the DNA template

The plasmid containing the insert on the right orientation was linearized with BamHI-HF (New England Biolabs) for T7 RNA polymerase transcription, and XbaI (New England Biolabs) for SP6 RNA polymerase transcription. Reaction mixture is described on Table 6, the reactions were incubated ON at 37ºC.

Table 6 - Reaction mixture used to linearize the plasmid containing the insert of interest, to serve as DNA template for transcription.

Reagent	**Final concentration**
10X CutSmart® Buffer	1X
Enzyme	2 U
Template DNA	3 μg
Water	Dependent on DNA concentration

To use 3 μg of DNA for each restriction digestion, the purified plasmid DNA was quantified using the Qubit® dsDNA BR Assay (Invitrogen). To check the presence of the linearized plasmid, 2μL of the reaction were separated by electrophoresis on a 1% (w/v) agarose gel, as described before. Because XbaI presented star activity, the fragment of the correct size was excised from the gel and purified using the illustra GFX PCR DNA and Gel Band Purification Kit (GE healthcare). To terminate the restriction digestion of the linearization, a sodium acetate/ethanol precipitation was carried out: 1/20 volume of 0.5 M Ethylenediaminetetraacetic acid (EDTA) (pH8), 1/10 volume of 5 M sodium acetate, and 2 volumes of 100% (v/v) ethanol were added to the reaction mixture, and incubated ON at -20ºC. To remove the restriction enzymes, the mixture was centrifuged at maximum speed for 15 minutes, the supernatant removed completely, and the DNA was resuspended in 15 μL of RNAse-free water.

2.6.1.3. Transcription of the probe

The MAXIscript™ SP6/T7 Transcription Kit (Invitrogen) was used for transcribing the probe. The reaction mixture is detailed on Table 7, following the manufacturer's instructions.

Table 7 - Transcription reaction mixture used for probe production with the MAXIscript™ SP6/T7 Transcription Kit (Invitrogen).

Reagent	Final concentration
10X Transcription Buffer	1X
10 mM ATP	0.5 mM
10 mM CTP	0.5 mM
10 mM GTP	0.5 mM
10 mM UTP	0.3 mM
10 mM Digoxigenin-11-UTP	0.2 mM
T7 or SP6 Enzyme mix	1.5 or 2 U/μL
Template DNA	< 1 μg
Water	Up to 20 μL

To produce the antisense probe, T7 enzyme was used. The sense probe was transcribed with SP6 polymerase. The probe was labelled using Digoxigenin-11-UTP (Roche). The reaction mixture was incubated ON at room temperature. 1 μL of the transcription product was separated by electrophoresis on a 1% (w/v) agarose gel in 1X TAE, stained with 2X GelStar™ Nucleic Acid Gel Stain (Lonza) to detect the single-stranded RNA. Using 1X TAE as running buffer, the electrophoretic run occurred for 15 minutes at 150V, with non-limiting amperage. The gel was visualized as mentioned in the "Genotyping" section. The transcription reaction was treated with TURBO™ DNase (Invitrogen), for 15 minutes at 37ºC, to remove the template plasmid. To inactivate the DNase and to prevent heat-induced RNA-degradation, 0.5M EDTA was added to the mixture. 1μL of this solution was separated by electrophoresis, as detailed above, to check the DNA removal. The RNA probe was precipitated following the suggestions on the transcription kit protocol. To the reaction were added: 30 μL of RNAse-free water, 5 μL of 5 M sodium acetate and 150 μL of cold 100% (v/v) ethanol; the solution was vortexed and incubated ON at -20ºC. The RNA was pelleted at 4ºC, at maximum speed for 15 minutes. The supernatant was discarded, 150 μL of cold 70% (v/v) ethanol was added, and the RNA centrifuged at maximum speed, for 15 minutes, at 4ºC. The pellet was dried on ice and resuspended in 25 μL of water. 1 μL of the probe was verified by electrophoresis, as mentioned before.

Then it was added 25 μL of 100% (v/v) formamide, and the probe was stored at -20ºC until use.

2.6.1.4. Dot blot

In order to check the correct labelling of the probe and the best concentration of probe to use in the *in situ* hybridization, a Dot Blot was conducted. To detect the Digoxigenin-11-UTP present in the probe, the DIG nucleic acid detection kit (Roche) with the Anti-Digoxigenin-AP (Anti-DIG-AP) conjugate antibody and NBT (nitroblue tetrazolium)/BCIP (5-bromo-4-chloro-3-indolyl-phosphate) stock solution (Roche) were used. The DIG Wash and Block Buffer Set (Roche) was used for the chromogenic detection, and as suggested by the manufacturer, the protocol was as follows: the nitrocellulose membrane (0.2 μm, BIO-RAD) was spotted with 3 probe dilutions 1:50, 1:200 and 1:4000 [in 6X SSC (0.9M NaCl, 0.09M $Na_3C_6H_5O_7$) and 7.4% (w/v) paraformaldehyde] and air dried; the membrane was incubated with 1X Washing Buffer for two minutes, with shaking; incubated with 1X Blocking Solution for 30 minutes, with shaking; incubated with Antibody solution (1:5000 dilution of Anti-DIG-AP in 1X Blocking solution) for 30 minutes, with shaking; washed two times for 15 minutes with 1X Washing Buffer; equilibrated in 1X Detection Buffer for 3 minutes; and incubated with Colour Substrate solution (containing NBT/BCIP) ON in the dark, without shaking.

2.6.2. Fixation and embedding of *A. thaliana* inflorescences

WT Arabidopsis inflorescences were fixed in cold FAA [50% (v/v) ethanol, 5% (v/v) glacial acetic acid, 4% (v/v) paraformaldehyde, 0.025% (v/v) Tween 20], placed under vacuum two times for 5 minutes, and incubated ON at 4ºC. After a serial dehydration in ethanol [from 50% to 100% (v/v) dehydrated ethanol], the material was cleared by a series of washes in 33%, 50%, and 66% (v/v) HistoChoice® clearing agent (Sigma-Aldrich) (in ethanol), for 45 minutes each, before incubating ON in 100% (v/v) HistoChoice®. The clearing agent was replaced with fresh Histochoice® to which some paraffin chips were added, incubation occurred at 42ºC. After approximately two hours, more paraffin chips were added. When the paraffin chips were melted the mixture was replaced by 50% (v/v) paraffin in HistoChoice® and incubated ON at 50ºC. The samples were then placed in 75% (v/v) paraffin in HistoChoice® and incubated at 60ºC for six hours. The mixture was removed and 100% (v/v) paraffin was added for incubation ON at 60ºC. Following three washes of 100% (v/v) paraffin (two for six hours, and one ON at 60ºC), the samples were poured on a petri dish on top of a hot plate, and the inflorescences were placed in the correct position. When the paraffin was completely

solidified, the embedded material was stored at 4ºC. 8 μM sections were obtained with a Leica RM2265 microtome, placed on StarFrost® microscope slides, Poly-L-Lysine coated (Pro Sci-Tech), dried at 45ºC on a hot plate and stored at 4ºC until use.

2.6.3. RNA *in situ* hybridization

The paraffin sections were dewaxed by dipping the slides in HistoChoice®, clearing agent (Sigma-Aldrich), two times for 10 minutes. To hydrate the tissue, the slides were dipped in a series of ethanol solutions, in 5 M NaCl: 100%, 90%, 70% (v/v) (10 minutes each wash). From this step, the slides were loaded into the robot InsituPro VSi (intavis Bioanalytical Instruments) which performed all the steps until the colour reaction. The protocol started by continuing the dehydration steps; the slides were washed in 50% and 30% (v/v) ethanol, in 5 M NaCl, and twice in 1X TE (10 mM Tris-HCl, 1 mM EDTA). Following one wash in 1X Proteinase K buffer (100 mM Tri-HCl, 50mM EDTA, pH 8.0), the slides were incubated in 1 μg/mL Proteinase K (in 1X Proteinase K buffer) (both steps at 37ºC). The slides were washed with 10 mg/mL Glycine in 1X PBS. For the post-fixation step the slides were washed in 1X PBS and incubated in 4% (w/v) paraformaldehyde. Before the hybridization, the slides were washed with 50% hybridization mix [25% (v/v) formamide, 0.5X hybridization salts (5 mM Tris-HCl, 0.15 M NaCl, 2.5 mM EDTA, 5 mM Na_2HPO_4, pH 7.5), 0.25 μg/μL tRNA, 0.5X Denhardt's Solution, 25% (v/v) Dextran Sulphate]. Subsequent, the slides were incubated at 55ºC, ON, with the probe solution which was diluted in 100% hybridization mix [50% (v/v) formamide, 1X hybridization salts (10mM Tris-HCl, 0.3M NaCl, 5mM EDTA, 10mM Na_2HPO_4, pH 7.5), 0.5 μg/μL tRNA, 1X Denhardt's Solution, 50% (v/v) Dextran Sulphate]. The slides were subjected to stringent washes with 2X SSC (0.3 M NaCl, 0.03 M $Na_3C_6H_5O_7$) and 0.2X SSC (0.03 M NaCl, 0.003 M $Na_3C_6H_5O_7$), the last one at 55ºC. Then, the RNAse treatment consisted in one wash with 1X RNAse buffer (10 mM Tris-HCl, 1 mM EDTA, 0.5 M NaCl, pH 7.5), incubation with 5 μg/mL RNAse A (in 1X RNAse buffer) at 37ºC, wash with 1X RNAse buffer and a stringent wash with 0.2X SSC at 55ºC.

The immunological detection was performed using the DIG nucleic acid detection kit (Roche) and the DIG Wash and Block Buffer Set (Roche), which started with a blocking step: wash in 1X Washing Buffer and then in 1X Blocking Solution (diluted in 1X Maleic Acid). For the antibody reaction, the slides were incubated with 1:5000 Anti-DIG-AP diluted in 1X Blocking solution and washed in 1X Washing Buffer. The colour reaction started by washing the slides with 1X PBS, and then with 1X Detection Buffer. The slides were removed from the robot and the Colour Substrate (10 μL/mL NBT/BCIP stock

solution in 1X Detection Buffer) was added to each slide. The slides were covered with a glass cover slip for incubation ON, in a humid chamber, in the dark, at room temperature.

The signal on the samples was checked after one, two and three ON of incubation with the Colour Substrate. After the second ON, more Colour substrate was added to prevent the slides to dry. The samples were observed under an upright Axio Imager M2 microscope (Zeiss) equipped with a differential interference contrast (DIC) prism. Images were captured with an Axiocam ERc5s camera (Zeiss) using Zen 2 pro software (Zeiss).

2.7. Clearing *A. thaliana* ovules

For phenotypic characterization, ovules at different developmental stages were cleared and analysed as described previously (Brambilla *et al*., 2007). The inflorescences were fixed in 10% glacial acetic acid in ethanol ON at 4ºC; washed in 90% and 70% (v/v) ethanol for 10 minutes; and placed in a solution containing 160 g of chloral hydrate, 100 mL of water, and 50 mL of glycerol. The flowers were dissected under a stereo microscope Stemi 2000-C (Zeiss) and observed using an upright Axio Imager M2 microscope equipped with DIC optics. Images were captured with an Axiocam MRm camera (Zeiss) using the Zen 2 pro software.

2.8. Aniline blue staining of *A. thaliana* ovules

Flowers were stained with decolorized aniline blue (DAB) following the protocol described by Pereira *et al*. (2016). Arabidopsis flowers at different developmental stages were collected and fixed in 10% (v/v) glacial acetic acid in ethanol, ON at 4ºC. The material was placed in 8 M NaOH, ON at 4ºC, washed three times with water and stained ON in 0.1% (w/v) DAB (in 0.1 M K_3PO_4) at 4°C. The material was observed using an upright Axio Imager M2 microscope (Zeiss), under UV light with the CFP filter (436/480 nm) and images were captured using an AxioCam MRm camera (Zeiss) and processed with Zen 2 pro (Zeiss) software.

2.9. GUS histochemical assay

The GUS assay was performed as described by Liljegren *et al*. (2000). Arabidopsis inflorescences were fixed in 90% (v/v) acetone for 2h, at -20ºC. The inflorescences were washed two times with phosphate buffer (0.1 M NaH_2PO_4, 0.1 M Na_2HPO_4), incubated

in X-gluc solution [50 mM Na_2HPO_4, 50 mM NaH_2PO_4, 0.2% (v/v) Triton X-100, 2 mM potassium hexacyanoferrate(II) trihydrate, 2 mM potassium hexacyanoferrate(III), 1 mg/mL X-gluc (5-bromo-4-chloro-3-indolyl β-D-glucuronic cyclohexylammonium salt)] for three ON, at 37ºC, washed in 90% (v/v) ethanol for 10 minutes and placed in 70% (v/v) ethanol until visualization. The flowers were placed in clearing solution [20% (v/v) lactic acid, 20% (v/v) glycerol in 1× PBS], dissected under a stereo microscope Stemi 2000-C (Zeiss) using hypodermic needles, and observed under an upright Axio Imager M2 microscope (Zeiss) equipped with DIC. Images were captured with an Axiocam ERc5s camera (Zeiss) using Zen 2 pro software (Zeiss).

3. Results

3.1. Bioinformatic analysis

3.1.1. Analysis of the GO terms in the *stk* RNA-seq

Insights into the deregulated pathways in the *stk* inflorescence were uncovered resorting to the Singular Enrichment Analysis (SEA) tool of the AgriGO portal (http://systemsbiology.cau.edu.cn/agriGOv2/classification_analysis.php?category=Plant&&family=Brassicaceae). For this analysis, the genes, detected by RNA-seq, upregulated or downregulated in the *stk* inflorescence (*p*-value < 0.05) were uploaded and the Arabidopsis gene model TAIR10 reference chosen for the analysis. Table 8 shows the top 25 Gene Ontology (GO) terms associated with biological processes enriched among the *stk* downregulated genes. The GO terms are associated with reproduction, microtubule-based movement, mitotic and meiotic cell cycle, and cell division. Interestingly, pollen development is present on this list.

Table 8 - Biological processes gene ontology (GO) terms associated with the genes downregulated in the *stk* transcriptome. The significantly enriched terms (*p*-value < 0.05 and FDR < 0.05) were related to the reproductive process, cell division, mitotic and meiotic cell cycle and pollen development. In this table are presented only the top 25, in ascendant order considering the False Discovery Rate (FDR), all the terms can be accessed in the Supplemental table. 3.

GO term	Description	p-value	FDR
GO:0044699	single-organism process	2.3e-20	6.7e-17
GO:0007018	microtubule-based movement	2.0e-12	2.8e-09
GO:0007049	cell cycle	2.3e-11	1.6e-08
GO:0006928	movement of cell or subcellular component	2.0e-11	1.6e-08
GO:0051301	cell division	1.0e-08	5.8e-06
GO:0007017	microtubule-based process	1.2e-08	5.8e-06
GO:0022402	cell cycle process	1.9e-08	7.0e-06
GO:0000278	mitotic cell cycle	2.0e-08	7.0e-06
GO:0071103	DNA conformation change	2.5e-08	7.7e-06
GO:1903047	mitotic cell cycle process	3.0e-08	8.6e-06
GO:0048229	gametophyte development	6.3e-08	1.5e-05
GO:0007275	multicellular organism development	6.1e-08	1.5e-05
GO:0022414	reproductive process	1.2e-07	2.5e-05
GO:0000003	reproduction	1.3e-07	2.5e-05
GO:0032501	multicellular organismal process	1.3e-07	2.5e-05
GO:0044707	single-multicellular organism process	1.6e-07	2.9e-05
GO:0044702	single organism reproductive process	1.8e-07	3.0e-05
GO:0044767	single-organism developmental process	5.6e-07	8.8e-05
GO:0048827	phyllome development	6.3e-07	9.1e-05
GO:0051321	meiotic cell cycle	6.4e-07	9.1e-05
GO:0048856	anatomical structure development	6.9e-07	9.3e-05
GO:0009555	pollen development	8.2e-07	1.1e-04

GO:0044710	single-organism metabolic process	9.5e-07	1.2e-04
GO:0032502	developmental process	2.2e-06	2.6e-04
GO:0000910	cytokinesis	5.1e-06	5.7e-04

Regarding to the cellular component GO terms: microtubule, cytoskeleton, associated structures like phragmoplast and spindle, plasma membrane, and cell wall were the significative enriched terms (Table 9).

Table 9 - Cellular component gene ontology (GO) terms associated with the genes downregulated in the *stk* transcriptome. The significantly enriched GO (p-value < 0.05 and FRD < 0.05) terms were associated with microtubules, cytoskeleton, plasma membrane, cell wall and chromosomes. False Discovery Rate (FDR).

GO term	Description	p-value	FDR
GO:0099512	supramolecular fiber	4.7e-11	9.4e-09
GO:0099513	polymeric cytoskeletal fiber	4.7e-11	9.4e-09
GO:0005874	microtubule	6.7e-11	9.4e-09
GO:0015630	microtubule cytoskeleton	6.7e-09	7.0e-07
GO:0005871	kinesin complex	1.9e-08	1.6e-06
GO:0071944	cell periphery	2.3e-08	1.6e-06
GO:0044430	cytoskeletal part	3.2e-08	1.9e-06
GO:0005856	cytoskeleton	1.2e-07	6.2e-06
GO:0005887	integral component of plasma membrane	8.0e-07	3.8e-05
GO:0031226	intrinsic component of plasma membrane	1.2e-06	5.1e-05
GO:0043232	intracellular non-membrane-bounded organelle	1.8e-06	5.7e-05
GO:0043228	non-membrane-bounded organelle	1.8e-06	5.7e-05
GO:0005576	extracellular region	1.8e-06	5.7e-05
GO:0009524	phragmoplast	2.4e-06	7.2e-05
GO:0005875	microtubule associated complex	5.2e-06	1.5e-04
GO:0005886	plasma membrane	2.0e-05	5.3e-04
GO:0005694	chromosome	5.5e-05	1.4e-03
GO:0030312	external encapsulating structure	8.2e-05	1.7e-03
GO:0005618	cell wall	8.2e-05	1.7e-03
GO:0044459	plasma membrane part	7.9e-05	1.7e-03
GO:0000793	condensed chromosome	1.7e-04	3.4e-03
GO:0009505	plant-type cell wall	4.9e-04	9.4e-03
GO:0031224	intrinsic component of membrane	8.0e-04	0.015
GO:0005819	spindle	1.3e-03	0.023
GO:0044427	chromosomal part	1.4e-03	0.024
GO:0044425	membrane part	2.5e-03	0.041

When the upregulated genes are considered, the top 25 significantly enriched biological process GO terms were associated with cell wall biogenesis; and to a less extent to response to oxidative stress and photosynthesis (Table 10).

Table 10 – Biological process gene ontology (GO) terms associated with the genes upregulated in the *stk* transcriptome. The significantly (*p*-value < 0.05 and FDR < 0.05) enriched GO terms were associated with cell wall biogenesis and oxi-reduction reactions. In this table are presented only the top 25, in descendant order considering the False Discovery Rate (FDR), all the terms can be accessed in the Supplemental table. 4.

GO term	Description	p-value	FDR
GO:0009834	plant-type secondary cell wall biogenesis	8.8e-15	3.9e-11
GO:0044085	cellular component biogenesis	8.3e-14	1.8e-10
GO:0071669	plant-type cell wall organization or biogenesis	6.5e-12	9.5e-09
GO:0042546	cell wall biogenesis	1.6e-10	1.8e-07
GO:0045491	xylan metabolic process	2.4e-10	2.1e-07
GO:0045492	xylan biosynthetic process	7.3e-10	5.3e-07
GO:0009832	plant-type cell wall biogenesis	1.0e-09	6.4e-07
GO:0071554	cell wall organization or biogenesis	3.5e-09	1.9e-06
GO:0071840	cellular component organization or biogenesis	8.3e-09	4.1e-06
GO:0070592	cell wall polysaccharide biosynthetic process	1.7e-08	7.4e-06
GO:0022900	electron transport chain	2.1e-08	8.2e-06
GO:0044038	cell wall macromolecule biosynthetic process	2.7e-08	9.0e-06
GO:0070589	cellular component macromolecule biosynthetic process	2.7e-08	9.0e-06
GO:0022613	ribonucleoprotein complex biogenesis	6.5e-08	2.0e-05
GO:0055114	oxidation-reduction process	1.4e-07	4.0e-05
GO:0010410	hemicellulose metabolic process	5.6e-07	1.5e-04
GO:0042254	ribosome biogenesis	7.7e-07	2.0e-04
GO:0010383	cell wall polysaccharide metabolic process	2.4e-06	5.9e-04
GO:0006979	response to oxidative stress	3.7e-06	8.6e-04
GO:0015979	photosynthesis	7.4e-06	1.6e-03
GO:0034637	cellular carbohydrate biosynthetic process	1.1e-05	2.3e-03
GO:0033692	cellular polysaccharide biosynthetic process	1.4e-05	2.8e-03
GO:0006869	lipid transport	1.8e-05	3.4e-03
GO:0009698	phenylpropanoid metabolic process	2.2e-05	4.0e-03
GO:0044264	cellular polysaccharide metabolic process	2.8e-05	4.8e-03

The top 25 significant cellular component GO terms retrieved from *stk* upregulated genes are present on Table 11. The terms were related to ribosome, mitochondrial respiration, and photosynthesis.

Table 11 – Cellular component gene ontology (GO) terms associated with the genes upregulated in the *stk* transcriptome. The significantly (*p*-value < 0.05 and FDR < 0.05) enriched GO terms were related to ribosome, mitochondrial respiration, and photosynthesis. In this table are presented only the top 25, in descendant order considering the False Discovery Rate (FDR), all the terms can be accessed in the Supplemental table. 5.

GO term	Description	p-value	FDR
GO:0005840	ribosome	3.5e-23	3.3e-20
GO:0022626	cytosolic ribosome	8.0e-21	3.8e-18
GO:0032991	macromolecular complex	1.4e-20	4.4e-18
GO:0044391	ribosomal subunit	2.8e-20	6.7e-18
GO:0044445	cytosolic part	7.9e-20	1.5e-17
GO:0044444	cytoplasmic part	1.1e-19	1.8e-17
GO:0005746	mitochondrial respiratory chain	2.1e-19	2.9e-17
GO:1990204	oxidoreductase complex	2.4e-19	2.9e-17
GO:0098796	membrane protein complex	9.5e-19	1.0e-16
GO:1990904	ribonucleoprotein complex	1.2e-18	1.0e-16
GO:0030529	intracellular ribonucleoprotein complex	1.2e-18	1.0e-16
GO:0044436	thylakoid part	1.8e-18	1.4e-16
GO:0044422	organelle part	2.3e-18	1.6e-16
GO:0070469	respiratory chain	2.2e-18	1.6e-16
GO:0034357	photosynthetic membrane	2.7e-18	1.6e-16
GO:0009535	chloroplast thylakoid membrane	2.7e-18	1.6e-16
GO:0044446	intracellular organelle part	2.8e-18	1.6e-16
GO:0055035	plastid thylakoid membrane	3.0e-18	1.6e-16
GO:0009534	chloroplast thylakoid	5.2e-18	2.6e-16
GO:0031976	plastid thylakoid	5.8e-18	2.8e-16
GO:0009579	thylakoid	8.0e-18	3.4e-16
GO:0042651	thylakoid membrane	8.2e-18	3.4e-16
GO:0098803	respiratory chain complex	7.8e-18	3.4e-16
GO:0098798	mitochondrial protein complex	5.5e-17	2.2e-15
GO:0022625	cytosolic large ribosomal subunit	4.4e-16	1.7e-14

3.1.2. Crossing the transcriptomic data

In order to find *STK* putative targets, the transcriptomic data of the *stk* inflorescence (Mendes *et al*., unpublished), the nucellus (Tucker *et al*., 2012), and the MMC (Schmidt *et al*., 2011) were overlapped.

From the 17741 genes detected in *stk* the RNA-seq, 1822 were Differentially Expressed Genes (DEG) (10.3%), not considering the False Discovery Rate (FDR). Crossing the DEG from the three transcriptomes revealed that: 437 genes were common to the three transcriptomes, 1070 genes were present exclusively in the MMC and the *stk* inflorescence, 66 genes were found in the *stk* and nucellus data, and 4577 genes were expressed both in the nucellus and MMC data (Fig. 10).

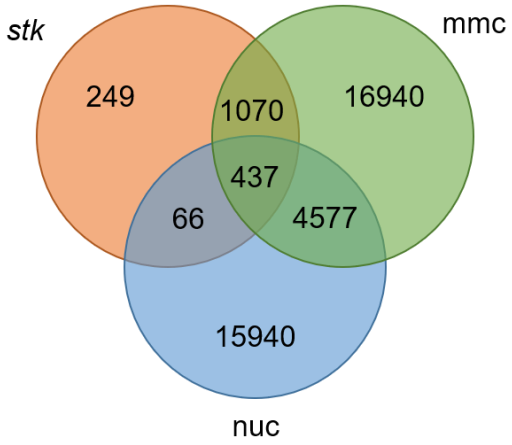

Fig. 10 - Venn diagram representing the overlap of the Differentially Expressed Genes (DEG of the MMC microarray (mmc), the nucellus microarray (nuc) with the *stk* RNA sequencing (*stk*).

15 genes were commonly present in the downregulated genes in *stk*, upregulated in the nucellus and downregulated in the MMC (Fig. 11). In contrast, when crossing the downregulated genes in *stk*, upregulated in the nucellus and upregulated in the MMC 23 genes were found (Fig. 11).

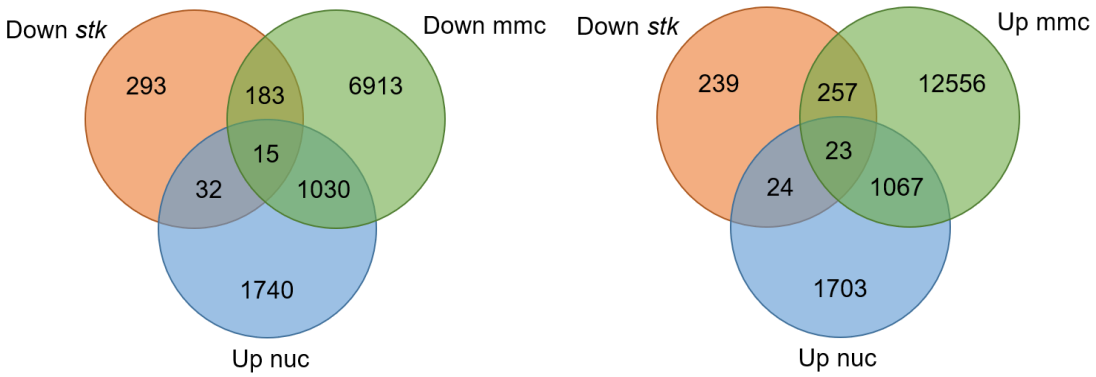

Fig. 11 - Venn diagrams showing the cross of the downregulated genes in *stk* RNA sequencing (Down *stk*), upregulated in the nucellus microarray (Up nuc) with the downregulated genes in the MMC microarray (Down mmc, on the left) or upregulated in the MMC microarray (Up mmc, on the right).

For the lists acquired by overlapping the transcriptomes, based on TAIR (http://www.arabidopsis.org/), each gene was briefly described (as is in what it encodes) and known functions annotated. A qualitative assessment of the putative expression pattern of the genes was perfomed using e-FP Brower (http://bar.utoronto.ca/efp/cgi-bin/efpWeb.cgi), to find genes expressed preferentially in the reproductive tissues. Based on the information collected, the interesting genes were further studied resorting to the literature. Also, known *STK* targets was another element to reflect on for the choice of the final candidate to be investigated.

Among the genes downregulated in the *stk* inflorescence, upregulated in the nucellus, and downregulated in the MMC (Table 12) the gene with the highest absolute fold change (0.8x) in the *stk* inflorescence was *AGO9*. The fold change in the nucellus was 0.9, and in the MMC was 0.1. Importantly the FDR for *AGO9* was below 0.05, likewise, *AGO9* was considered an interesting candidate to study. *CELL WALL INVERTASE 4* (*AT2G36190*) was the only other gene with FDR < 0.05 in the *stk* inflorescence in this list.

Table 12 - List of genes downregulated in the *stk* RNA sequencing (*stk*), upregulated in the nucellus microarray (NUC-OV) and downregulated in the MMC microarray (MMC-NUC). Gene locus, Log_2 of fold change (FC), a brief description of the gene's function and expression profile according to eFP Browser are detailed for each gene. It is also presented the false discovery rate (FDR) for *stk* RNA-seq. The list is organized in an ascendant order according to the fold changes in the *stk* RNA-seq. From this group of genes, *AGO9* is the gene with the highest absolute fold change in *stk* RNA-seq and also has a FDR lower than 0.05.

	stk-WT		NUC-OV	MMC-NUC			
Gene	Log_2FC	FDR	Log_2FC	Log_2FC	Gene Description	Expression - eFP Browser	Reference
AT5G21150	-0,8	0,01	0,9	-0,1	***AGO9*, *ARGONAUTE 9***. Argonaute family protein.	Specific of reproductive structures. Higher in carpels of flowers stage 12 and 15.	Olmedo-Monfil *et al*., 2010
AT1G17460	-0,8	0,08	1,0	-0,6	*TRFL3*, *TRF-like 3.* MYB family transcription factor	Specific of reproductive structures. Higher in shoot apex inflorescence and flower stage 9 to 11.	
AT2G36190	-0,7	0,01	0,1	-0,4	*CWINV4*, *CELL WALL INVERTASE 4.* Catalyzes the hydrolysis of sucrose into fructose and glucose	Specific expression in the stamens of flowers stage 12, and whole flower stage 15.	Ruhlmann *et al*., 2009
AT1G13710	-0,7	0,10	1,3	-1,9	*CYP78A5*, *KLUH*. Cytochrome P450, family 78, subfamily A, polypeptide 5	Specific expression in the shoot apex transition and shoot apex inflorescence.	Anastasiou *et al*., 2007
AT2G18260	-0,6	0,45	1,4	-0,6	*SYP112*, *SYNTAXIN OF PLANTS 112.* Syntaxin part of *SYP11* gene family	Specific of reproductive structures. Higher in seeds stage 4 and 5 and flowers stage 9.	
AT1G75640	-0,6	0,06	0,2	-0,8	*MUS*, *MUSTACHES*. Leucine-rich receptor-like protein kinase family protein	Specific of reproductive structures. Higher in shoot apex inflorescence and seed stage 6. Expressed in flower stage 9.	Keerthisinghe *et al*., 2015
AT5G61460	-0,5	0,13	0,7	-0,8	*SMC6B*, *STRUCTURAL MAINTENANCE OF CHROMOSOMES 6B*. Component of the SMC5/6 complex	Higher expression in the shoot apex transition and shoot apex inflorescence and flowers stage 9 to 11.	Watanabe *et al*., 2009
AT1G59540	-0,5	0,20	0,4	-0,4	*ZCF125*. Contains a kinesin motor domain	Mainly expressed in reproductive structures. Higher in the shoot apex and flowers stage 9.	
AT4G14330	-0,5	0,15	0,4	-0,4	*AtPAKRP2 Arabidopsis thaliana Phragmoplast-Associated Kinesin-Related Protein* 2. P-loop containing nucleoside triphosphate hydrolases superfamily protein	Specific of reproductive structures. Higher in the shoot apex and flowers stage 9.	Lee *et al*., 2001
AT1G79490	-0,5	0,32	0,8	-1,2	*EMB2217*, *EMBRYO DEFECTIVE 2217*. Pentatricopeptide repeat (PPR) superfamily protein	Higher expression in the shoot apex inflorescence and seed stages 8 to 9. Equally expressed across flower stages.	
AT1G77410	-0,5	0,47	1,0	-0,9	*BGAL16, BETA-GALACTOSIDASE 16*. Glycoside hydrolase	Specific of flower stage 9 and mature pollen grains.	Macquet *et al*., 2007
AT1G34355	-0,4	0,32	0,7	-1,0	*PS1, PARALLEL SPINDLE 1.* Forkhead-associated (FHA) domain-containing protein	Higher expression in the shoot apex and flower stage 9.	d'Erfurth *et al*., 2008

AT5G50210	-0,4	0,41	1,2	-3,2	*OLD5*, *ONSET OF LEAF DEATH 5*. Quinolinate synthase and cysteine desulfurase activator	Higher expression in the leaves. Medially expressed in flower stage 9 to 11.	Jing *et al*., 2005
AT1G32190	-0,4	0,38	0,8	-1,2	alpha/beta - hydrolases superfamily protein	Specific of reproductive structures. Higher in shoot apex inflorescence, flower stage 9 to 11 and seed stage 6 and 7.	
AT3G06030	-0,4	0,42	0,3	-0,3	*ATANP3, NPK1-RELATED PROTEIN KINASE 3.*	Higher in shoot apex inflorescence, flower stage 9 to 11 and seed stage 6.	Saito *et al*., 2015

When crossing the genes downregulated in the *stk* inflorescence, upregulated in the nucellus and upregulated in the MMC (Table 13), the gene with the highest absolute fold change for the MMC data was *REM24*, 1.3x more expressed in the MMC than in the surrounding nucellus. In the nucellar tissue, at a later stage of development, *REM24* was upregulated 1.9x. In the *stk* inflorescence, *REM24* was downregulated 0.5x. In this list, most genes were expressed at the flower stage 9. The genes with FDR < 0.05 in the *stk* RNA-seq were *AT1G73050*, *AT1G74150*, *PECTIN METHYLESTERASE* (*AT5G49180*) and *EXORDIUM LIKE 1* (*AT1G35140*).

Table 13 - List of genes downregulated in the *stk* RNA sequencing (*stk*), upregulated in the nucellus microarray (NUC-OV) and upregulated in the MMC microarray (MMC-NUC). Gene locus, Log_2 of fold change (FC), a brief description of the gene's function and expression profile according to eFP Browser are detailed for each gene. It is also presented the false discovery rate (FDR) for *stk* RNA-seq. The list is organized in a descendant order according to the fold changes in the MMC microarray. From this group of genes, *REM24* is the gene with the highest absolute fold change in MMC microarray; the FDR in *stk* RNA-seq is higher than 0.05. *FLA20* was the gene chosen to verify the *stk* RNA-seq through qPCR analysis (presented later).

	stk-WT		NUC-OV	MMC-NUC			
Gene	Log_2FC	FDR	Log_2FC	Log_2FC	Gene Description	Expression - eFP Browser	Reference
AT2G16210	-0,5	0,45	1,9	1,3	***REM24*, *REPRODUCTIVE MERISTEM 24*.** Transcriptional factor B3 family protein	Specifically expressed in the shoot apex inflorescence and flower stage 9.	Mantegazza *et al*., 2014
AT1G15190	-0,7	0,36	0,9	1,2	Fasciclin-like arabinogalactan family protein	Specifically expressed in the flower stage 9.	
AT4G10950	-0,8	0,19	2,3	1,0	SGNH hydrolase-type esterase superfamily protein	Specifically expressed in the flower stage 9.	
AT4G33870	-0,8	0,18	2,0	1,0	Peroxidase superfamily protein	Specifically expressed in the flower stage 9.	
AT3G11010	-0,6	0,22	1,0	1,0	*RLP34*, *RECEPTOR LIKE PROTEIN 34*. Leucine-rich repeat receptor	Specific of vegetative structures. Medially expressed in flower stage 15.	
AT1G73050	-1,1	0,01	1,1	0,9	Glucose-methanol-choline (GMC) oxidoreductase family protein	Specifically expressed in the flower stage 9.	Kurdyukov *et al*., 2006
AT5G60090	-0,8	0,36	0,4	0,7	Protein kinase superfamily protein	Specifically expressed in the flower stage 9.	
AT2G33000	-0,8	0,32	0,7	0,7	Ubiquitin-associated (UBA) / TS-N domain-containing protein-like protein	Higher expression in the flower stage 9.	
AT1G74150	-1,1	0,02	0,7	0,7	Galactose oxidase/kelch repeat superfamily protein	Higher expression in the flower stage 9 and shoot apex transition	
AT5G40940	-0,7	0,34	2,2	0,6	*FLA20*, *FASCICLIN-LIKE ARABINOGALACTAN PROTEIN 20*.	Specifically expressed in the flower stage 9.	
AT1G32300	-0,6	0,38	2,1	0,6	D-arabinono-1,4-lactone oxidase family protein	Specifically expressed in carpels of flowers stage 12 and flowers stage 15.	
AT5G49180	-1,2	0,00	1,3	0,6	*PME58*, *PECTIN METHYLESTERASE 58*. Pectin methylesterase	Specifically expressed in seeds stage 3 to 5.	Turbant *et al*., 2016
AT1G67630	-0,4	0,38	0,3	0,6	*EMB2814*, *EMBRYO DEFECTIVE 2814*. DNA polymerase alpha 2	Higher in the shoot apex transition and shoot apex inflorescence.	
AT5G06820	-0,9	0,05	2,2	0,5	*SRF2*, *STRUBBELIG-RECEPTOR FAMILY 2*. Leucine-rich repeat receptor	Specifically expressed in the flower stage 9.	Chevalier *et al*., 2005
AT1G55740	-0,6	0,45	1,4	0,5	*SIP1*, *SEED IMBIBITION 1*. Raffinose synthase	Specific of the different seed stages.	

AT1G35140	-1,0	0,00	1,2	0,5	*EXL1*, *EXORDIUM LIKE 1*. Phosphate-induced protein	Specifically expressed in leaves.	Schröder *et al*., 2011
AT3G62430	-0,7	0,43	0,2	0,4	Protein with RNI-like/FBD-like domains	Higher expression in the flower stage 9.	
AT5G17540	-0,6	0,12	0,2	0,4	HXXXD-type acyl-transferase family protein	Higher expression in the flower stage 9 to 12.	
AT1G68320	-0,7	0,33	0,1	0,3	*MYB62, MYB DOMAIN PROTEIN 62*. R2R3-MYB transcription factor	Specifically expressed in the flower stage 15.	Devaiah *et al*., 2009
AT1G75040	-0,5	0,35	0,1	0,3	*PR5, PATHOGENESIS-RELATED GENE 5.* Thaumatin-like protein	Higher in rosette after transition to flower and flower stage 15.	Liu *et al*., 2013
AT3G44050	-0,4	0,31	0,5	0,2	P-loop containing nucleoside triphosphate hydrolases superfamily protein	Higher in the shoot apex inflorescence and flower stage 9.	
AT5G24470	-0,7	0,17	1,1	0,1	*PRR5*, *PSEUDO-RESPONSE REGULATOR 5*. Transcriptional repressor of *CIRCADIAN CLOCK ASSOCIATED 1* and *LATE ELONGATED HYPOCOTYL 1*.	Specifically expressed in seed stage 7.	Nakamichi *et al*., 2016

3.1.3. Candidate genes

The evidences showed that both *AGO9* and *REM24* seemed to be good candidates to investigate. However, *AGO9* associated functions are vastly known, on the contrary, the *REM* family is poorly studied. Altogether, the results pointed *REM24* as the best candidate gene to be studied in this work. A *rem24* mutant (SALK_054142), with a T-DNA insertion in the 3'UTR was reported as a *knock-down* line, where *REM24* was 2.6-fold downregulated. To investigate *REM24* function, this mutant line was used for all the experiments.

3.1.4. Understanding the network

3.1.4.1. Analysis of genes putatively co-expressed with *REM24*

A tool developed at the Plant Cell Wall (PCW) lab allows to find genes putatively co-expressed with the gene of interest, based on the similarity of the expression profile. The expression profiles are based on RNA-seq data obtained from different WT plant structures, vegetative and reproductive (collected as published in Klepikova *et al*., 2016). *REM24* co-expressed genes were evaluated to provide further insights into *REM24* putative function. The data was analysed considering all the tissues sampled (Table 14) or just the floral tissues (Table 15). *REM24* expression profile used for this analysis are depicted on Supplemental Fig. 4 and 5. The function of the listed genes (Table 14 and 15) was briefly investigated resorting to Tair, Araport or PlantTFDF (http://planttfdb.cbi.pku.edu.cn/). In both cases, the 18 genes with the most similar expression profile were enriched for TFs, especially other *REM* TFs. *REM15* and *REM9* were present in both sets. *SQUAMOSA PROMOTER BINDING PROTEIN-LIKE 8* (*SPL8*) expression profile is similar to *REM24* in both situations.

When vegetative and reproductive structures were included in the analysis, most genes were of unknown functions (Table 14). The gene with the most similar expression pattern was *HEAT SHOCK PROTEIN 20-like (AT5G47600).* Four other *REM* TFs are putatively co-expressed with *REM24*.

Table 14 - List of the 18 genes with the most similar expression pattern to *REM24,* considering vegetative and floral tissues. For each gene the locus, gene description and known functions are presented. The list is organized in an ascendant order according to the deltasum. Deltasum measures the similarity of expression pattern, relative to *REM24* expression pattern. Most similar expression patterns have a deltasum value closer to zero. A heatshock protein AT5G47600 has the most similar expression pattern to *REM24*. In green are indicated the genes that were downregulated in the *stk* RNA sequencing.

Deltasum	Locus	Gene name/Description	Known functions	Reference
31.63	AT5G47600	HSP20-like chaperones superfamily protein	Unknown	
32.78	AT5G57720	*REPRODUCTIVE MERISTEM 15 (REM15)*. AP2/B3-like transcriptional factor family protein	Unknown	Mantegazza *et al*., 2014
35.86	AT5G37860	Heavy metal transport/detoxification superfamily protein	Unknown	
36.99	AT1G10980	Lung seven transmembrane receptor family protein	Unknown	
37.45	AT1G02065	*SQUAMOSA PROMOTER BINDING PROTEIN-LIKE 8 (SPL8).* SBP-box transcription factor	Megasporogenesis and microsporogenesis	Unte *et al*., 2003
38.52	AT4G31690	*REM9.* Transcriptional factor B3 family protein	Response to cold	Mantegazza *et al*., 2014
41.42	AT5G64910	Serine/Threonine-kinase	Unknown	
41.92	AT4G34400	*REM17.* AP2/B3-like transcriptional factor family protein	Unknown	Mantegazza *et al*., 2014
42.93	AT3G12470	Polynucleotidyl transferase, ribonuclease H-like superfamily protein	Unknown	
43.42	AT5G17080	Cysteine proteinases superfamily protein	Unknown	
45.18	AT3G12440	Polynucleotidyl transferase, ribonuclease H-like superfamily protein	Unknown	
45.54	AT5G58610	PHD finger transcription factor, putative	Unknown	
45.59	AT4G16560	HSP20-like chaperone	Unknown	
45.79	AT4G16550	HSP20-like chaperone	Unknown	
47.10	AT1G31310	Hydroxyproline-rich glycoprotein family protein. Transcription factor	Unknown	
47.43	AT1G62500	Bifunctional inhibitor/lipid-transfer protein/seed storage 2S albumin superfamily protein	Unknown	
47.44	AT2G19910	RNA-dependent RNA polymerase family protein	Unknown	
48.81	AT5G09780	*REM23.* Transcriptional factor B3 family protein	Unknown	Mantegazza *et al*., 2014

Considering only the floral tissues, the gene with the most similar expression profile was *NUBBIN* (*NUB*). *REM15*, *REM35* and *REM16* are potentially co-expressed with *REM24* (Table 15).

Table 15 - List of the 18 genes with the most similar expression pattern to *REM24,* considering only floral tissues. For each gene the locus, gene description and known functions are presented. The list is organized in an ascendant order according to the deltasum. Deltasum measures the similarity of expression pattern, relative to *REM24* expression pattern. Most similar expression patterns have a deltasum value closer to zero. *NUB* is the gene with the most similar expression pattern to *REM24*. Other five *REM* are potentially co-expressed with *REM24*. Highlighted in green are genes downregulated in the *stk* RNA sequencing.

Deltasum	Locus	Gene name/Description	Known functions	Reference
3.94	AT1G13400	*NUBBIN (NUB).* C2H2 and C2HC zinc fingers superfamily protein	Stamen and carpel development	Dinneny *et al*., 2005
4.80	AT5G64910	Serine/Threonine-kinase	Unknown	
5.29	AT1G35730	*PUMILIO 9 (PUM9)*	Regulates mRNA stability and translation through sequence-specific binding to the 3' UTR of target mRNA transcripts	Xiang *et al*., 2014
5.69	AT5G17810	*WUSCHEL related homeobox 12 (WOX12)*	Adventitious root development	Liu *et al*., 2014
6.15	AT5G37860	Heavy metal transport/detoxification superfamily protein	Unknown	
6.19	AT5G47600	HSP20-like chaperones superfamily protein	Unknown	
6.55	AT5G57720	*REPRODUCTIVE MERISTEM 15 (REM15).* AP2/B3-like transcriptional factor family protein	Unknown	Mantegazza *et al*., 2014
6.74	AT1G28360	*ERF DOMAIN PROTEIN 12* (*ERF12).* Ethylene response factor transcription factor.	Unknown	
6.96	AT4G31615	*REM35.* Transcriptional factor B3 family protein	Unknown	Mantegazza *et al*., 2014
7.04	AT3G58770	Hypothetical protein	Unknown	
7.08	AT4G08840	*PUMILIO 11* (*PUM11*)	Regulates mRNA stability and translation through sequence-specific binding to the 3' UTR of target mRNA transcripts	Xiang *et al*., 2014
7.12	AT3G53310	*REM16.* AP2/B3-like transcriptional factor family protein	Unknown	Mantegazza *et al*., 2014
7.20	AT1G02065	*SQUAMOSA PROMOTER BINDING PROTEIN-LIKE 8 (SPL8).* SBP-box transcription factor	Megasporogenesis and microsporogenesis	Unte *et al*., 2003
7.20	AT4G32540	*YUCCA1 (YUC1).* Flavin-binding monooxygenase family protein	Auxin biosynthesis	Stepanova *et al*., 2011
7.26	AT4G31690	*REM9.* Transcriptional factor B3 family protein	Response to cold	Mantegazza *et al*., 2014

7.41	AT2G45190	*FILAMENTOUS FLOWER (FIL).* Plant-specific transcription factor YABBY family protein	Meristem structural organization; specification of floral organ identity; fruit development	Lugassi *et al*., 2010
7.44	AT3G60670	*PLATZ* transcription factor family protein	Unknown	
7.49	AT2G17770	*BASIC REGION/LEUCINE ZIPPER MOTIF 27* (*ATBZIP27*).	Regulation of photoperiodism, flowering	Abe *et al*., 2005

3.1.4.2. *STK* positively regulated genes

Similarly, to the previous approach, it was obtained a list of 18 genes potentially co-expressed with *STK*, considering both vegetative and reproductive tissues (Table 16) or just reproductive tissues (Table 17). The profiles used for this analysis are shown on Supplemental Fig. 6 and 7. These targets were then crossed with the genes downregulated in the *stk* inflorescence.

If vegetative and floral tissues were included in the analysis *VALKYRIE* (*VAL*) was the gene with the most similar expression profile to *STK*. *COMPANION OF CELLULOSE SYNTHASE 3* (*CC3*), *ATP-BINDING CASSETTE A9* (*ABCA9*), *TRANSPARENT TESTA 1* (*TT1*), and *PEPTIDE TRANSPORTER 5* (*PTR5*) are related to seed development and shared a similar expression pattern with *STK*. One argonaute, AGO3 seems to have a similar expression pattern to *STK* (Table 16).

Table 16 - List of the 18 genes with the most similar expression pattern to *STK* considering vegetative and floral tissues. For each gene the locus, gene description and known functions are presented. The list is organized in an ascendant order according to the deltasum. Deltasum measures the similarity of expression pattern, relative to *STK* expression pattern. Most similar expression patterns have a deltasum value closer to zero. *VAL* is the gene with the most similar expression pattern. None of these genes was downregulated in the *stk* inflorescence.

Deltasum	Locus	Gene name/Description	Known functions	Reference
14.21	AT5G60140	*VALKYRIE (VAL).* AP2/B3-like transcriptional factor family protein	Pollen tube burst and synergid cell death	Mendes *et al*., 2016
14.81	AT5G11360	Interleukin-1 receptor-associated kinase 4 protein	Unknown	
15.09	AT3G20520	*SHV3-like 3* (*SVL3*). Member of the glycerophosphodiester phosphodiesterase like (GDPD-like) family.	Unknown	Hayashi *et al*., 2008
17.26	AT4G32170	*CYTOCHROME P450, FAMILY 96, SUBFAMILY A, POLYPEPTIDE 2* (*CYP96A2*)	Unknown	
17.76	AT1G24540	*CYTOCHROME P450, FAMILY 86, SUBFAMILY C, POLYPEPTIDE 1* (*CYP86C1*)	Unknown	
20.50	AT4G17480	Alpha/beta-Hydrolases superfamily protein	Unknown	

20.64	AT5G46300	Hypothetical protein	Unknown	
22.17	AT1G05490	*CHROMATIN REMODELING 31* (*CHR31*). DEAD-like helicase	Unknown	
22.73	AT3G05460	Sporozoite surface protein-related	Unknown	
23.28	AT2G41990	*COMPANION OF CELLULOSE SYNTHASE 3* (*CC3*). Late embryogenesis abundant protein	Unknown	
23.98	AT1G31290	*ARGONAUTE 3* (*AGO3*)	Gene silencing by RNA, regulation of transcription	Zhang *et al*., 2016
24.21	AT3G60900	*FASCICLIN-LIKE ARABINOGALACTAN PROTEIN 10* (*FLA10)*	Unknown	
24.40	AT4G21640	Subtilase family protein	Unknown	
2495	AT5G61730	*ATP-BINDING CASSETTE A9* (*ABCA9*)	ER-localized ABC transporter with a role in the supply of fatty acid substrates for TAG biosynthesis at the ER during the seed-filling stage	Kim *et al*., 2013
25.66	AT1G34790	*TRANSPARENT TESTA 1* (*TT1*). C2H2 and C2HC zinc fingers superfamily protein	Involved in photomorphogenesis, flavonoid biosynthesis, flower and seed development.	Appelhagen *et al*., 2011
25.93	AT5G01180	*PEPTIDE TRANSPORTER 5* (*PTR5*)	Dipeptide transporter expressed in pollen and ovules during early seed development	Komarova *et al*., 2008
26.13	AT5G61120	Zinc ion-binding protein	Unknown	

Just considering reproductive tissues, *VAL* is still the gene with the most similar expression profile relative to *STK*. Other reproduction-related TFs appear to be expressed in a similar manner as *STK*: *SUPERMAN* (*SUP*), *SHP2*, and *AGAMOUS LIKE13 (AGL13)*. Also appear genes involved in seed development in this list: *TRANSLOCASE INNER MEMBRANE SUBUNIT 17-1* (*TIM17-1*), *UNICORN-LIKE* (*UCNL*), and *COBRA-LIKE PROTEIN 2 PRECURSOR (COBL2)*. Besides *AGO3*, *AGO9* has a similar expression pattern to *STK* when just considering reproductive tissue. *AGO9* was the only gene also downregulated in *stk* inflorescence (Table 17).

Table 17 - List of the 18 genes with the most similar expression pattern to *STK* considering only floral tissues. For each gene the locus, gene description and known functions are presented. The list is organized in an ascendant order according to the deltasum. Deltasum measures the similarity of expression pattern, relative to *STK* expression pattern. Most similar expression patterns have a deltasum value closer to zero. Like for the previous list, *VAL* is the gene with the most similar expression pattern. *AGO9* is highlighted in green because *AGO9* was also downregulated in the *stk* RNA sequencing.

Deltasum	Locus	Gene name/Description	Known functions	Reference
1,85	AT5G60140	*VALKYRIE (VAL).* AP2/B3-like transcriptional factor family protein	Pollen tube burst and synergid cell death	Mendes *et al*., 2016
2,81	AT1G12890	ERF (Ethylene Response Factor) subfamily B-1 of ERF/AP2 transcription factor family	Unknown	
3,79	AT3G23130	*SUPERMAN* (*SUP*)	Flower-specific gene controlling the boundary of the stamen and carpel whorls. Similar to zinc finger transcription factors.	Sakai *et al.*, 1995
3,98	AT1G30160	Protein of unknown function (DUF295)	Unknown	
4,01	AT5G04660	*CYTOCHROME P450, FAMILY 77, SUBFAMILY A, POLYPEPTIDE 4* (*CYP77A4*)	Fatty acid oxidation	Sauveplane *et al*., 2009
4,04	AT2G42830	*SHATTERPROOF 2* (*SHP2*). K-box region and MADS-box transcription factor family protein	Fruit development (valve margin and dehiscence zone differentiation)	Liljegren *et al*., 2000
4,12	AT1G20350	*TRANSLOCASE INNER MEMBRANE SUBUNIT 17-1* (*TIM17-1*). Mitochondrial inner membrane translocase	Alters seed germination rate	Wang *et al*., 2014
4,13	AT1G05490	*CHROMATIN REMODELING 31* (*CHR31*). DEAD-like helicase	Unknown	
4,25	AT5G56880	Hypothetical protein	Unknown	
4,33	AT3G20830	*UNICORN-LIKE* (*UCNL*). AGC (cAMP-dependent, cGMP-dependent and protein kinase C) kinase family protein	Redundant with *UNICORN.* In *uncl* occurs aberrant embryogenesis	Enugutti *et al*., 2012
4,40	AT3G29810	*COBRA-LIKE PROTEIN 2 PRECURSOR* (*COBL2*)	Affects mucilage solubility and cellulosic ray formation in mucilage secretory cells of seeds	Ben-Tov *et al*., 2015
4,61	AT4G14730	*LIFEGUARD 1* (*LFG1*). Bax inhibitor-1 family protein	Supports plant colonization by biotrophic powdery mildew	Weis *et al*., 2013
4,63	AT5G21150	*ARGONAUTE 9* (*AGO9*)	sRNA silencing is crucial to specify cell fate in the ovule	Olmedo-Monfil et al., 2010
4,67	AT1G65150	TRAF-like family protein	Unknown	
4,68	AT3G61120	*AGAMOUS-LIKE 13* (*AGL13*)	Functions in male and female gametophyte morphogenesis.	Hsu *et al*., 2014
4,76	AT1G31290	*ARGONAUTE 3* (*AGO3*)	Gene silencing by RNA, regulation of transcription	Zhang *et al*., 2016
4,83	AT1G75520	*SHI-RELATED SEQUENCE 5* (*SRS5*)	Promote gynoecium, stamen and leaf development	Kuusk *et al*., 2006

3.1.5. qPCR assay to confirm *stk* RNA-seq indicated targets

As detected by the previous RNA-seq, other putative *STK* targets were tested by qPCR to determine whether their expression was altered in *stk*, and during which floral stage.

AGO9 was found in the list of genes downregulated in the *stk* inflorescence, downregulated in the MMC and upregulated in the nucellus. The *AGO9* transcript profile during WT flower development, present on Fig. 12.a, shows that *AGO9* expression level increased during floral development, reaching its maximum in the flowers at the stage 13-15. While the expression increased in the WT flowers, in the *stk* mutant, the absolute expression level of *AGO9* was stable across the developmental stages, yet, no statistical differences were found against WT (Fig. 12.b).

FASCICLIN-like ARABINOGALACTAN protein 20 (*FLA20)* was detected upregulated in the nucellus and in the MMC transcriptomes and downregulated in *stk*. *FLA20* expression level was the highest in the WT samples stage 1-7, decreased brusquely, and it was practically null from the flower stage 12i (Fig. 12.c). Despite *FLA20* absolute expression level was considerably higher in *stk* sample stage 1-9, relative to WT, no significant differences were found for all the stages (Fig. 12.d).

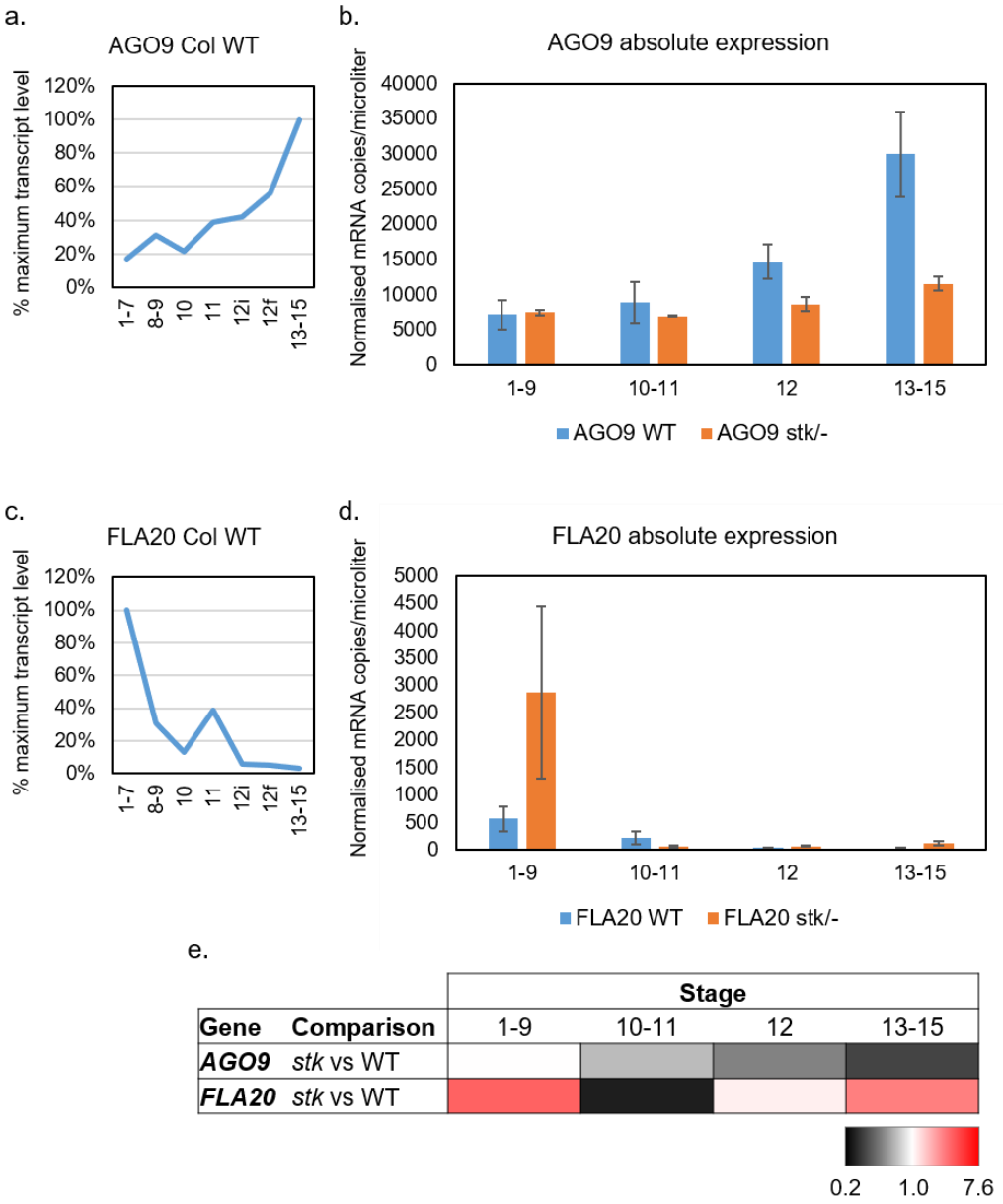

Fig. 12 – *AGO9* and *FLA20* qPCR expression analysis throughout floral development. *AGO9* **(a)** and *FLA20* **(c)** transcript abundance across all the stages collected for WT plants. Transcript abundance was plotted considering the maximum absolute expression level corresponds to 100%. *AGO9* **(b)** and *FLA20* **(d)** absolute gene expression level in pulled stages of floral development. Error bars are the (±) standard error calculated from the biological replicates for each stage (calculated from the mean between the technical replicates). **(e)** Heat map of fold change relative to one. The gene expression between *stk* and WT were compared. Fold change values aren't indicated since no statistical differences were found between absolute gene expression levels. Student's t-test, α = 0.05. Stage 1-9: flower meristem and flowers with ovule primordia (stage 1-I to 1-II). Stage 10-11: flowers with ovules at megasporogenesis (from stage 2-I to 2-V). Stage 12: flowers with ovules at megagametogenesis (from stage 3-I to 3-VI). Stage 13-15: flowers with fertilized ovules (stage 4-I to 4-VI). Red fill indicates upregulated genes. Black fill indicates downregulated genes.

3.2. *REM24* expression pattern during ovule development

3.2.1. Confirming the nature of the mutant line *rem24*

REM24 mRNA level was evaluated by qPCR on WT flowers. The maximum transcript level was in the sample 1-7. In the flowers at the stage 8-9, the percentage of maximum transcript level decreased abruptly to 25%, and it was very low in the other developmental stages, being practically null at the stage 13-15 (only 5% of maximum transcript level) (Figure 13.a). Relative to WT, *REM24* absolute expression level was very similar in *rem24* flowers, consequently, it wasn't significantly different (Figure 13.b, c).

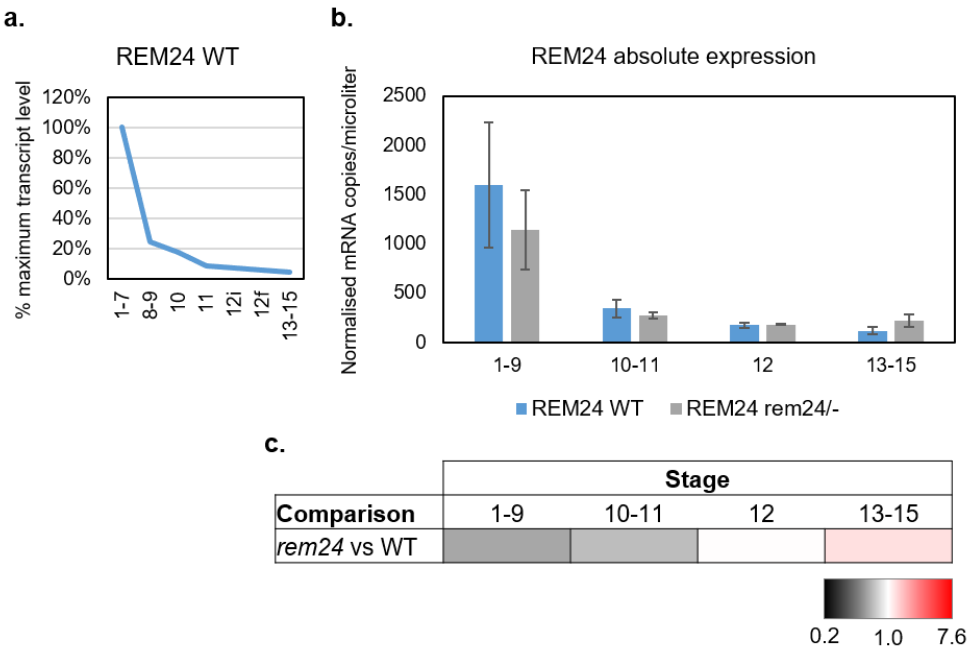

Fig. 13 – *REM24* qPCR expression analysis throughout floral development. **(a)** *REM24* transcript abundance across all the stages collected for WT plants. Transcript abundance was plotted considering the maximum absolute expression level corresponds to 100%. **(b)** *REM24* absolute gene expression level in pulled stages of floral development. Error bars are the (±) standard error calculated from the biological replicates for each stage (calculated from the mean between the technical replicates). **(c)** Heat map of fold change relative to one. The gene expression between *rem24* and WT were compared. Fold change values aren't indicated since no statistical differences were found. Student's t-test, α = 0.05. Stage 1-9: flower meristem and flowers with ovule primordia (stage 1-I to 1-II). Stage 10-11: flowers with ovules at megasporogenesis (from stage 2-I to 2-V). Stage 12: flowers with ovules at megagametogenesis (from stage 3-I to 3-VI). Stage 13-15: flowers with fertilized ovules (stage 4-I to 4-VI). Red fill indicates upregulated genes. Black fill indicates downregulated genes.

3.2.2. *REM24* marker lines

To uncover *REM24* expression pattern during ovule development, two marker lines were developed: *pREM24:3nlsYFP* and *pREM24_intron1:3nlsYFP* (Fig. 14). In these constructs, the *REM24* putative promoter region, the putative start codon and the 5'UTR (Fig. 14.a) or the *REM24* putative promoter, putative start codon, 5'UTR and first intron (Fig. 14.b) were cloned into the destination vector to drive the expression of three Yellow Fluorescent Proteins (YFP). The nuclear localization signal (nls) aimed to concentrate the fluorescent protein in the nuclei.

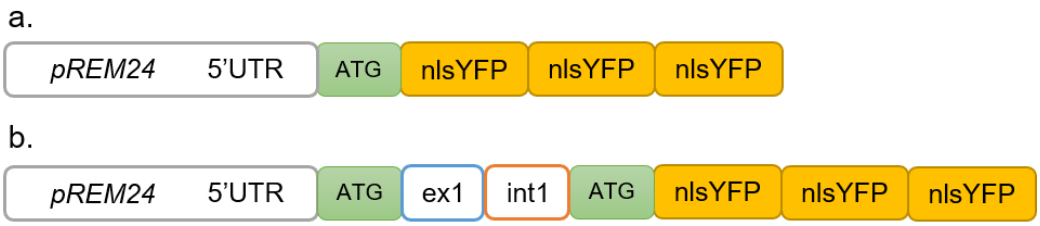

Fig. 14 – Constructs transformed into *Arabidopsis thaliana* to determine *REM24* expression pattern. **(a)** *pREM24*:*3nlsYFP*, the putative promoter sequence (*pREM24*) amplified contain the 5' untranslated region (5'UTR). **(b)** *pREM24_intron1*:*3nlsYFP,* the genomic *REM24* sequence from the putative promoter until the first intron (int1) were cloned. This includes the putative *REM24* start codon (ATG) and its first exon (ex1). The MT589 construct used as a destination vector contained a start codon (ATG) followed by three repeats of the nuclear localization signal (nls) fused to the yellow fluorescent protein (YFP) to concentrate the signal.

The designed constructs were successfully cloned into the destination vector MT589, as demonstrated by the restriction profiles (Fig. 15). For the restriction assay of *pREM24:3nlsYFP* construct, as expected, two fragments of around 1700 and 10500 bp were obtained (Fig. 15.a). The expected fragments for *pREM24_intron1:3nlsYFP* construct were 3000 and 10200 bp, however the profiles showed fragments of around 10200 bp, 3000 bp and between 2000 and 3000 bp (Fig. 15.b). Therefore, all the constructs were sequenced. The sequencing results allowed to identify the correct constructions for both cases.

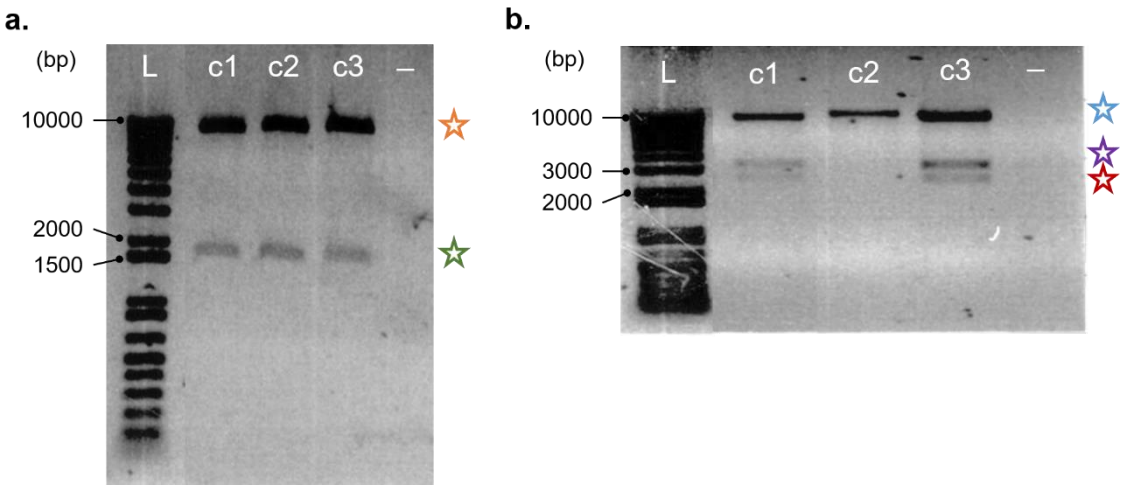

Fig. 15 - Electrophoretic separation of DNA fragments obtained from restriction digestion assay performed on plasmid DNA. **(a)** Digestion of *pREM24:3nlsYFP* with HindIII-HF and NcoI-HF produced two DNA fragments of around 10500 bp (yellow star) and 1700 bp (green star). **(b)** Digestion of *pREM24_intron1:3nlsYFP* with XbaI produced three fragments: 10200 bp (blue star), 3000 bp (purple star) and one between 2000 and 3000 bp (red star). In **(b)**, in the case of c2, the plasmid mustn't contain any insert and only the linearized plasmid (10200 bp) was separated. For each situation are presented restriction assays on DNA obtained from three different colonies (c1-c3). L – Molecular DNA weight ladder; – negative control without DNA.

The plants were transformed and the T1 generation was sown on soil. Unfortunately, until this moment, it wasn't possible to analyse the transformed plants since they are still being selected.

3.2.3. *In situ* hybridization

An RNA *in situ* hybridization was performed to determine the *REM24* mRNA expression pattern in the ovule, and to confirm the data obtained with the marker line. The desired sequence was cloned into pCRII® as shown by the correct restriction digestion profile obtained when the sequence for the probe was cloned in the right orientation into pCRII (Fig. 16.a). The sequencing results further confirmed the correct identity of the constructs. The construct was linearized to serve as DNA template for SP6 and T7 RNA polymerases for sense and antisense probe production, respectively, as demonstrated on Fig. 16.b.

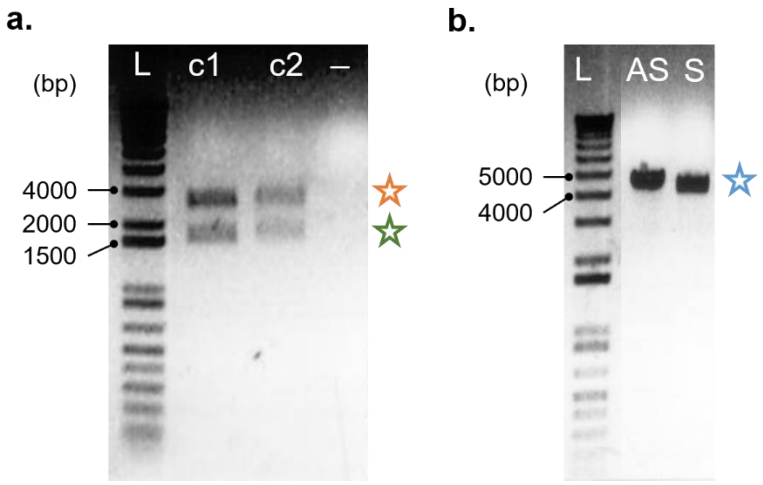

Fig. 16 - Electrophoretic separation of DNA fragments obtained from restriction digestion assay performed on plasmid DNA. **(a)** Digestion of the probe sequence cloned into pCRII with NdeI-HF and NcoI-HF produced two DNA fragments of around 2500 bp (yellow star) and 1700 bp (green star). It is shown the restriction assay on DNA obtained from two different colonies (c1-c2). – negative control without DNA; **(b)** Linearization of the probe sequence cloned into pCRII. For the transcription of the antisense (AS) probe the construct was digested with BamHI. For the transcription of the sense (S) probe, the construct was digested with XbaI. In both cases the produced fragments were around 4100 bp (blue star). L – Molecular DNA weight ladder.

The Dot Blot performed on a nitrocellulose membrane revealed that the probe was successfully transcribed incorporating the labelled UTP (Fig. 17). The assay also helped determining the probe concentration to use in the *in situ* hybridization. Dilution 1 was used for the hybridization of both sense and antisense probes.

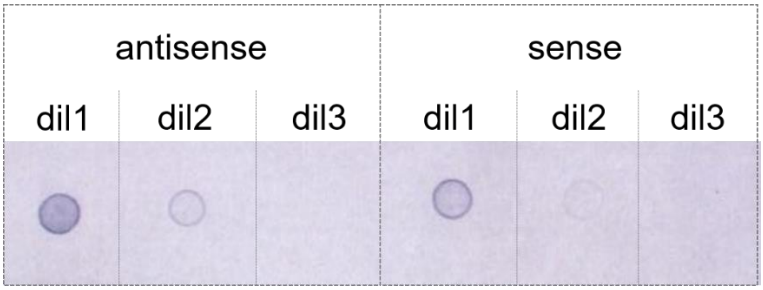

Fig. 17 - Dot Blot – Colour reaction of probe on a nitrocellulose membrane. The antisense and sense probes were diluted for this experiment. Dil1 represents the most concentrated solution, and dil3 represents the least concentrated solution. For both probes the dilution chosen to be used in the *in situ* hybridization was dil1. dil1 – dilution 1; dil2 – dilution 2; dil3 – dilution 3.

The results of the *in situ* hybridization are present on Fig. 18. No signal or background signal were detected on the antisense and sense sections, after one, two or three over-night incubation with the colour substrate.

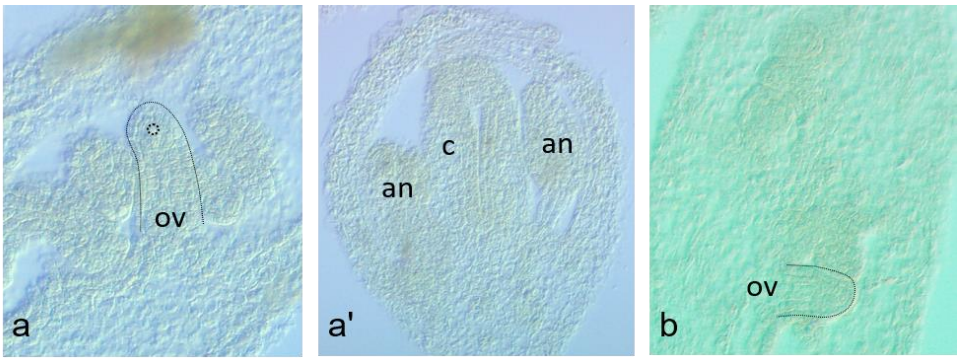

Fig. 18 - *REM24* Expression analysis by *in situ* hybridization in wild type flowers. **(a-a')** representative sections obtained for antisense probe. **(a)** An ovule (ov) and the nucleolus of the megaspore mother cell (small circle) is visible but no staining is detected. **(a')** Flower primordium where anther (an) and carpel (c) primordia are evidenced, and no staining is visible. **(b)** Representative section obtained for the sense probe. An ovule at approximately the same stage as the ovule in picture **(a)** is outlined. No background signal was observed.

3.3. *rem24* phenotype during ovule development

3.3.1. Checking the presence of abnormal nucellar cells – clearing method

Abnormal cellular composition of mutant and WT ovules was verified using a clearing method. For this analysis, *rem24*, *stk* and WT ovules at the stages 2-I to 2-III (according to Schneitz *et al*., 1995) (from now called MMC stage) were cleared, categorized according to their morphology and each category scored (Fig. 19 and 20). The categories were: the "WT", ovules harbouring one MMC with its prominent nucleolus in the central region of the nucellus, the MMC seemed to occupy the entire nucellar sub-epidermal region, and no other cells/nucleoli were visible (Fig. 19.a, a', a''); the "squashed MMC", in these ovules was possible to observe that the position of the MMC nucleolus was deviated from the centre, and there was no other visible nucleoli next to the MMC (Fig. 19.b, b', b''); the "MMC + small nucleolus" category was described has the ovules with the MMC nucleolus deviated from the centre and a lateral smaller nucleolus by its side, the smaller nucleolus could belong to an enlarged or a small sub-epidermal cell (Fig. 19.c, c', c'').

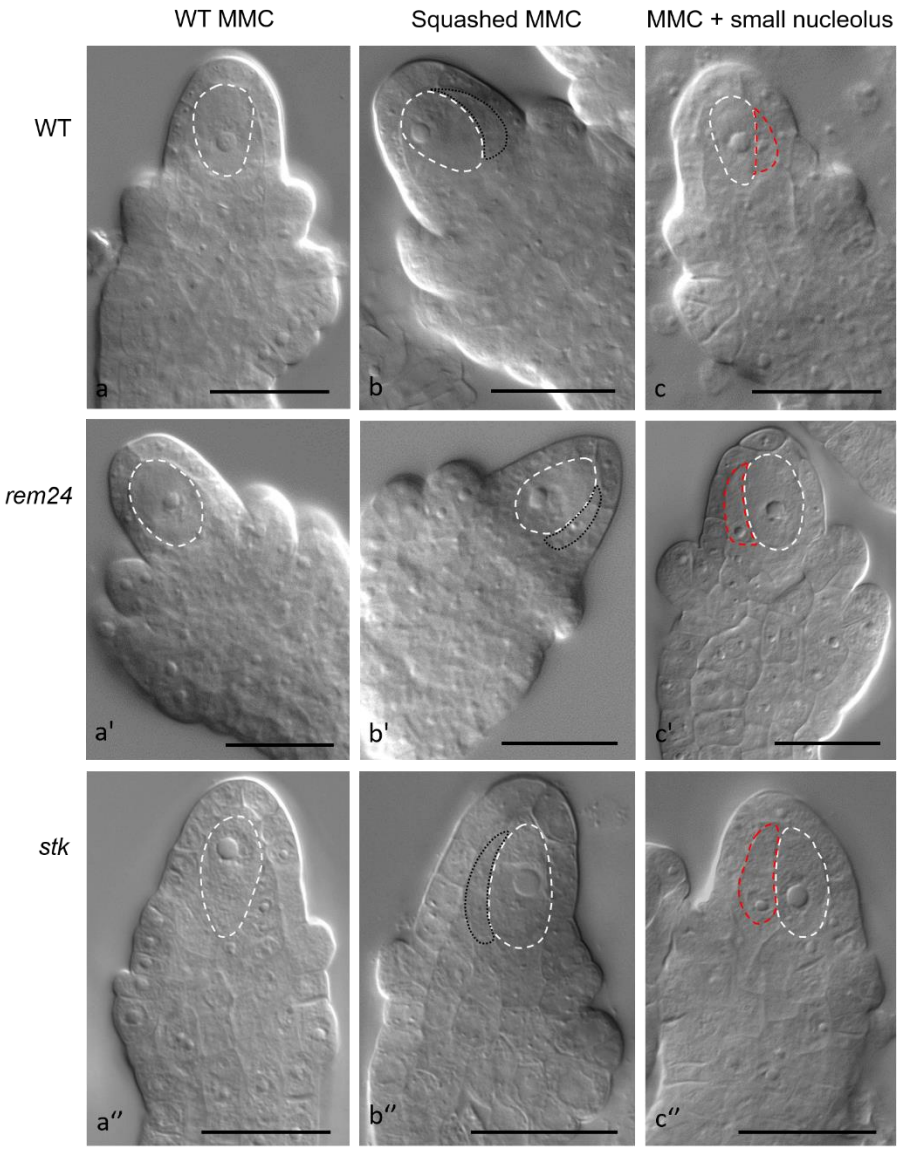

Fig. 19 - Representative ovule constitutions at megaspore mother cell (MMC) stage for wild type (WT), *rem24* and *stk*. MMC stage stands for ovules from stage 2-I to 2-III (according to Schneitz *et al*., 1995). **(a, a', a'')** WT MMC: ovules with one MMC that occupies the nucellar dome. **(b, b', b'')** Squashed MMC: ovules with one MMC to the side of the nucellar dome. **(c, c', c'')** MMC + small nucleolus: ovules with one MMC to the side of the nucellar dome and a prominent nucleolus by its side. **(a – c)** WT ovules. **(a' – c')** *rem24* ovules **(a'' – c'')** *stk* ovules. White dashed line outlines the MMC; black spotted line indicates the "gap" between the MMC and the nucellus epidermis; red dashed lines highlights the presence of a sub-epidermal nucellar cell next to the MMC. Scale bars = 20 μm.

In Fig. 20 are plotted the results obtained by analysing: 232 *rem24* ovules (among two plants), 156 *stk* ovules (among two plants) and 254 WT ovules (among three plants). The results indicate that the frequency of each ovule morphology wasn't significantly different between each mutant and the WT.

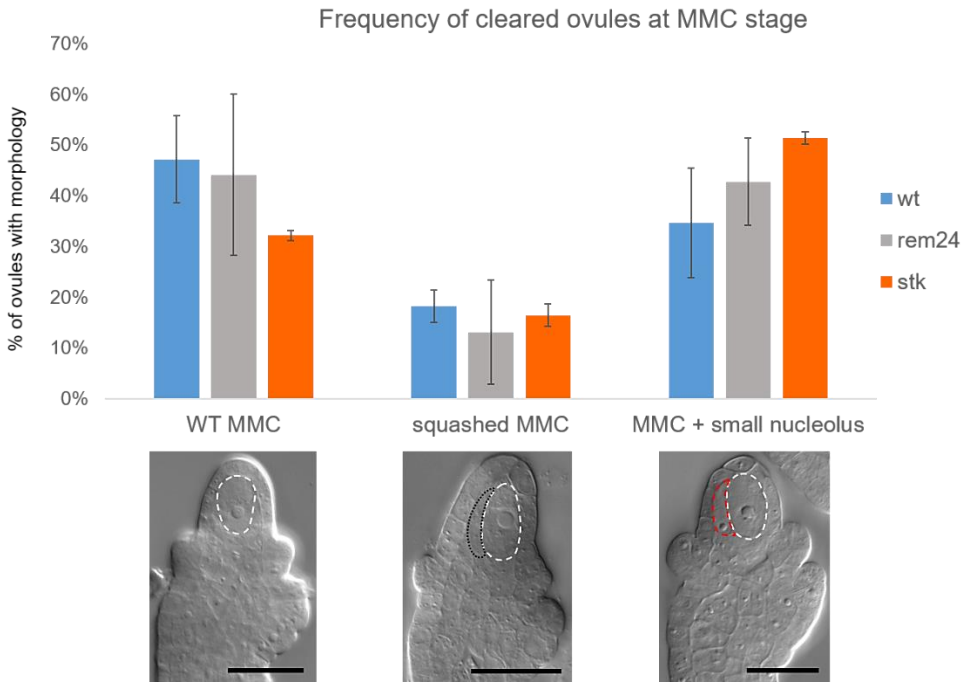

Fig. 20 - Frequency of wild type (WT), *rem24* and *stk* ovules at megaspore mother cell (MMC) stage with different cellular constitutions. MMC stage stands for ovules from stage 2-I to 2-III (according to Schneitz *et al*., 1995). Error bars are the ± standard deviation calculated from the biological replicates. A paired Student's t-test was performed, and no statistical differences were found (α = 0.05). Insets show the representative morphologies observed. WT MMC: ovules with one MMC that occupies the nucellar dome. Squashed MMC: ovules with one MMC with its nucleolus to the side of the nucellar dome. MMC + small nucleolus: ovules with the MMC nucleolus pushed to the side of the nucellar dome and a prominent smaller nucleolus by its side. White dashed line outlines the MMC; black spotted line indicates the "gap" between the MMC and the nucellar epidermis; red dashed lines highlights the presence of a sub-epidermal nucellar cell next to the MMC. Scale bars = 20 μm.

To understand whether the enlarged nucellar cells develop further, mutant and WT ovules at stage 3-VI were also cleared (Fig. 21). Around 80 mature ovules of each genotype were observed, and all showed a normal embryo sac and no extra cell or clear structure were identified next to the embryo sac.

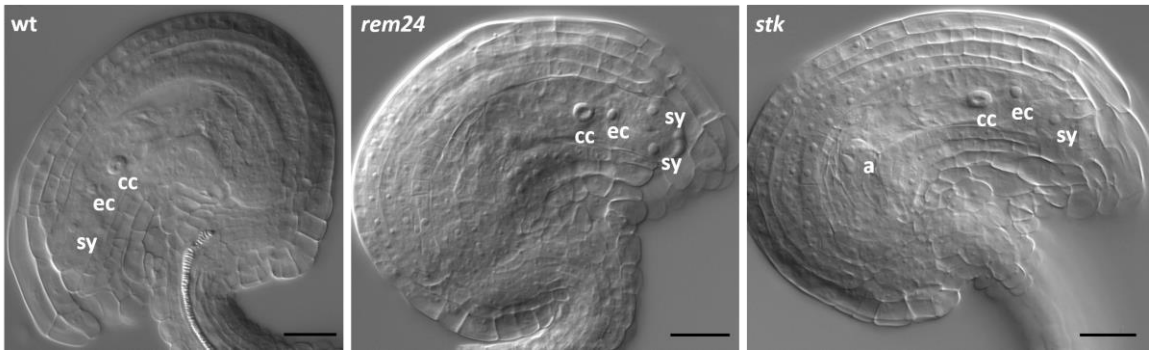

Fig. 21 - Cleared mature ovules of wild type (WT), *rem24* and *stk* plants. The ovules analysed presented a normal cellular constitution of the embryo sac. In general, the ovules contained at least one synergid cell, one egg cell and one central cell. a – antipodals; ec – egg cell; sy – synergid. Scale bars = 20 μm.

3.3.2. Analysis of callose deposition during megasporogenesis – aniline blue staining

It was possible to follow megasporogenesis using DAB staining and track that pattern of callose deposition in WT ovules (Fig. 22), as described by others.

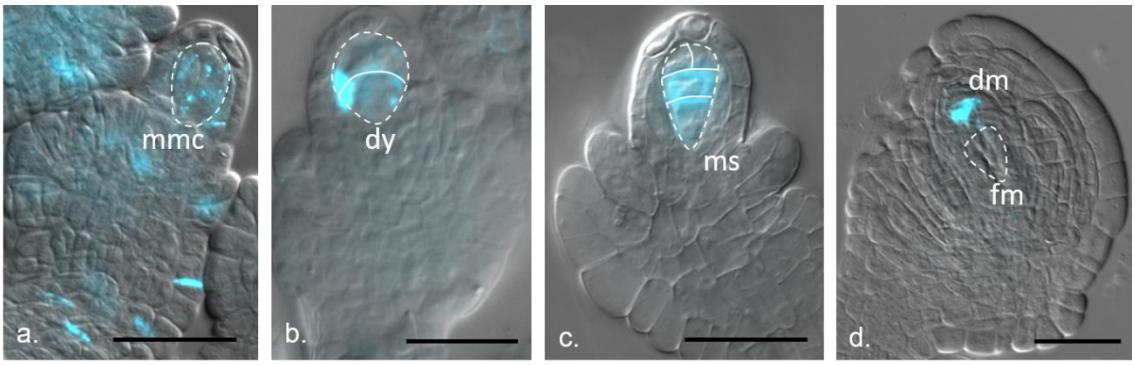

Fig. 22 – Developmental callose deposition pattern during megasporogensis, indicated by decolorized aniline blue staining. **(a)** Callose deposited in a wild type-like punctate pattern around the megaspore mother cell (mmc), stained by the aniline blue. **(b)** When the first meiotic division occurs, aniline blue stains the cellular plate diving the new cells. **(c)** The megaspores of the tetrad are separated by cellular plates stained with aniline blue. **(d)** The micropylar-most megaspore degenerate and accumulate callose which is indicated by the staining with aniline blue. Around the functional megaspore, no staining is observed. Pictures represent a merge of bright-field DIC and UV channel images. The blue signal corresponds to the aniline blue fluorescence under UV light. White dashed lines highlight the megaspore mother cell (mmc in **a.**), dyad (dy in **b.**), megaspore tetrad (ms in **c.**) or functional megaspore (fm in **d.**). dm – degenerated megaspores. Scale bars = 20 μm.

If the enlarged nucellar cells acquire MMC identity or if they undergo meiosis, maybe they accumulate callose in a similar manner as the MMC or megaspores. On the other hand, if the enlarged nucellar cells are perceived by the ovule as being aberrant, maybe that cell would accumulate callose to be separated from the rest. With DAB staining, one can easily track these events and answer those questions. The different patterns of DAB staining at MMC stage were categorized and scored (Fig. 23 and 24). The "WT" category was described as small punctate pattern, surrounding the MMC, on the border between the MMC and the nucellar epidermis (Fig. 23.a, a', a''); the "bigger spots" term corresponded to the ovules showing a bigger accumulation of DAB creating bigger puncta, but on the same relative position as in "WT" (Fig. 23.b, b', b''); "blobby" refered to the staining where the DAB accumulated in blobs, usually not forming a punctate pattern, but still surrounding the MMC (Fig. 23.c, c', c'').

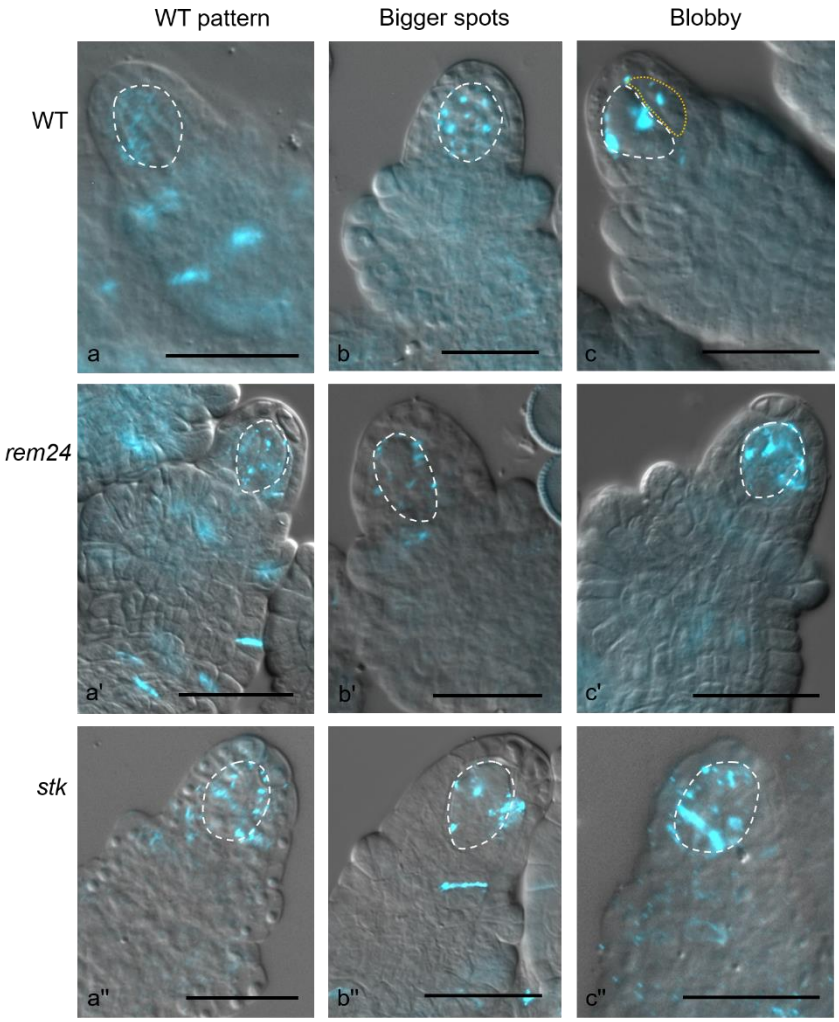

Fig. 23 – Representative decolorized aniline blue staining patterns observed for wild type (WT), *rem24* and *stk* ovules at megaspore mother cell (MMC) stage. MMC stage stands for ovules from stage 2-I to stage 2-III (according to Schneitz *et al*., 1995). **(a, a', a'')** WT pattern: the aniline blue stains in small punctate pattern, surrounding the MMC, on the border between the MMC and the nucellar epidermis. **(b, b', b'')** Bigger spots: ovules showing a bigger accumulation of the stain creating bigger puncta, but on the same relative position as in W category. **(c, c', c'')** Blobby: the aniline blue accumulates in blobs,

usually not forming a punctate pattern, but still surrounding the MMC. **(a – c)** WT, **(a' – c')** *rem24* and **(a'' – c'')** *stk* ovules. White dashed lines outline the MMC. Yellow spotted line highlights the potential presence of nucellar cells next to the MMC. Pictures represent a merge of bright-field DIC and UV channel images. The blue signal corresponds to the aniline blue fluorescence under UV light. Scale bars = 20 μm.

As seen in Fig. 24, there were no significant differences between the mutants and the WT. To stress, a staining indicating the individualization of an enlarged nucellar cell next to the MMC was never observed, in any of the genotypes.

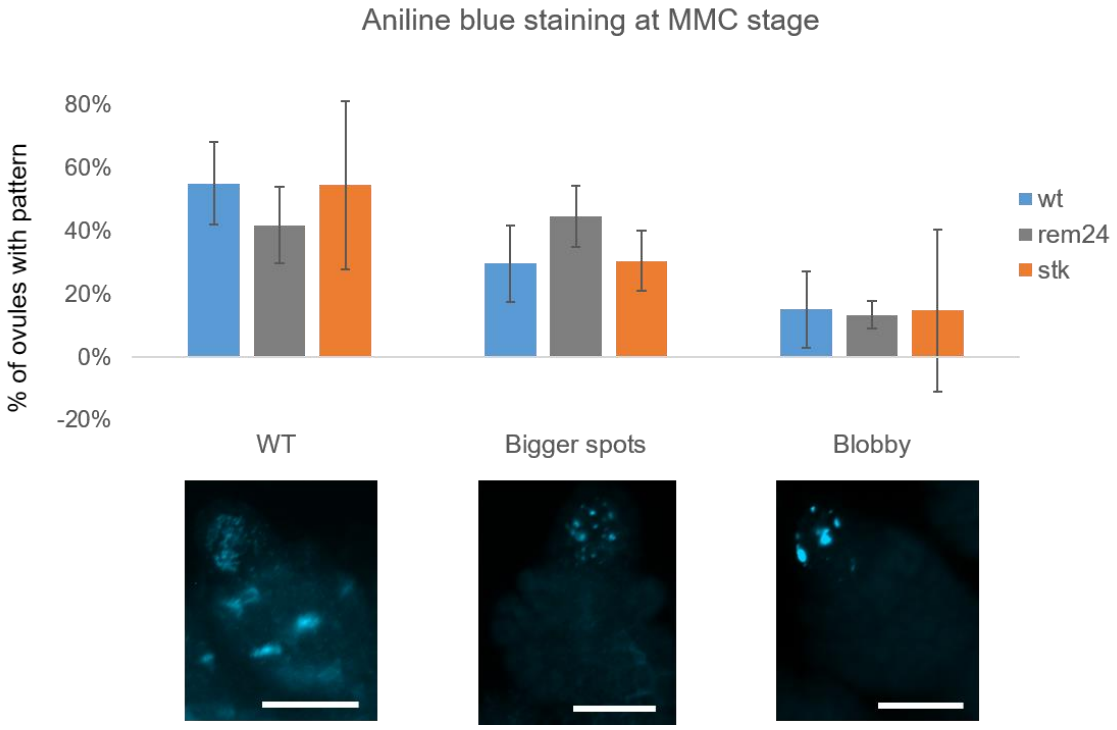

Fig. 24 - Frequency of wild type (WT), *rem24* and *stk* ovules at megaspore mother cell (MMC) stage with different aniline blue staining patterns. MMC stage stands for ovules from stage 2-I to stage 2-III (according to Schneitz *et al*., 1995). Error bars are the ± standard deviation calculated from the biological replicates. A paired Student's t-test was performed and no statistical differences were found ($\alpha = 0.05$). Insets show the representative morphologies observed. WT category: the aniline blue stains in small punctate pattern, surrounding the MMC, on the border between the MMC and the nucellar epidermis. Bigger spots: ovules showing a bigger accumulation of the stain creating bigger puncta, but on the same relative position as in WT category. Blobby: the aniline blue accumulates in blobs, usually not forming a punctate pattern, but still surrounding the MMC. The blue signal corresponds to the aniline blue fluorescence under UV light. Scale bars = 20 μm.

Ovules at stage 2-IV/V (from now named tetrad stage), were also stained. It was possible to verify that the orientation of the meiotic division is not always linear (as described before). In Fig. 25 (a – c) are presented the WT-like tetrads for *rem24*, *stk* and WT. It was also possible to find some tetrads that were pushed to the side, which indicated the presence of an enlarged nucellar cell (squashed tetrad, Fig. 25 a' – c'). But again, that cell never showed

any staining, the meiosis of a second MMC-like cell was never observed, in any of the genotypes

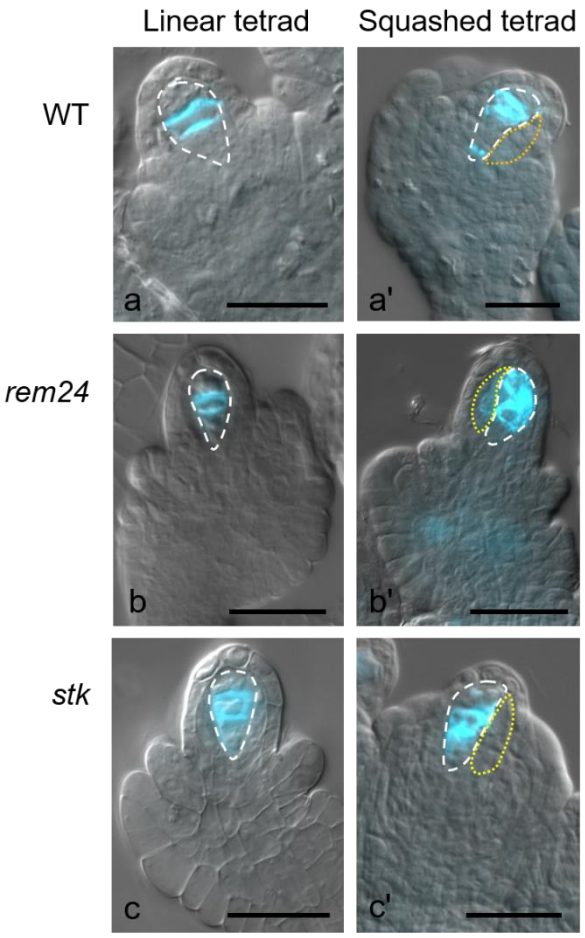

Fig. 25 - Representative decolorized aniline blue staining patterns observed for wild type (WT), *rem24* and *stk* ovules at tetrad stage. Tetrad stage stands for ovules at stage 2-IV/V (according to Schneitz *et al*., 1995). **(a - c)** Linear tetrad: the tetrad occupies the nucellar dome, the aniline blue stains the cell plates dividing the spores parallelly, indicative of a linear tetrad. **(a' - c')** Squashed tetrad: considering the aniline blue staining pattern, the tetrad is still linear, but it in is a lateral position pushed by a potential enlarged nucellar cell. **(a – a')** WT, **(b – b')** *rem24* and **(c – c')** *stk* ovules. White dashed lines outline the megaspore tetrad. Yellow spotted line highlights the presence of potential enlarged nucellar cells next to the MMC. Pictures represent a merge of bright-field DIC and UV channel images. The blue signal corresponds to the aniline blue fluorescence under UV light. Scale bars = 20 μm.

3.3.3. Characterising the identity of the enlarged nucellar cells

3.3.3.1. Crosses with marker lines

rem24 and *stk* mutant plants were crossed with *pKNU:3nlsYFP* (*pKNU-YFP*) or *pFM1:GUS* (*pFM1-GUS*) transgenic plants. The plants were screened for the mutation prior to observation. *pKNU-YFP* was crossed with mutant plants to determine if the enlarged nucellar cells had MMC identity. As a control, plants segregating for the construct, but without a mutant allele were examined. In WT (Fig. 26 a – c), *rem24*/+ (Fig. 26 d – f) and *stk*/+ (Fig. 26 g – i) ovules at MMC stage the YFP signal was detected only in the MMC nuclei. However, it was possible to find one WT ovule, among 371 WT ovules, with ectopic *pKNU-YFP* expression (Fig. 26 a' – c'). In this ovule, the promoter of *KNU* drove YFP expression in an enlarged nucellar cell next to the MMC (Fig. 26.b'). It was even possible to distinguish the prominent nucleolus of the abnormal cell (Fig. 26.c'). 72% of the *pKNU-YFP*/+, 50% of *pKNU-YFP*/+ *rem24*/+ and 64% of *pKNU-YFP*/+ *stk*/+ ovules expressed the construct.

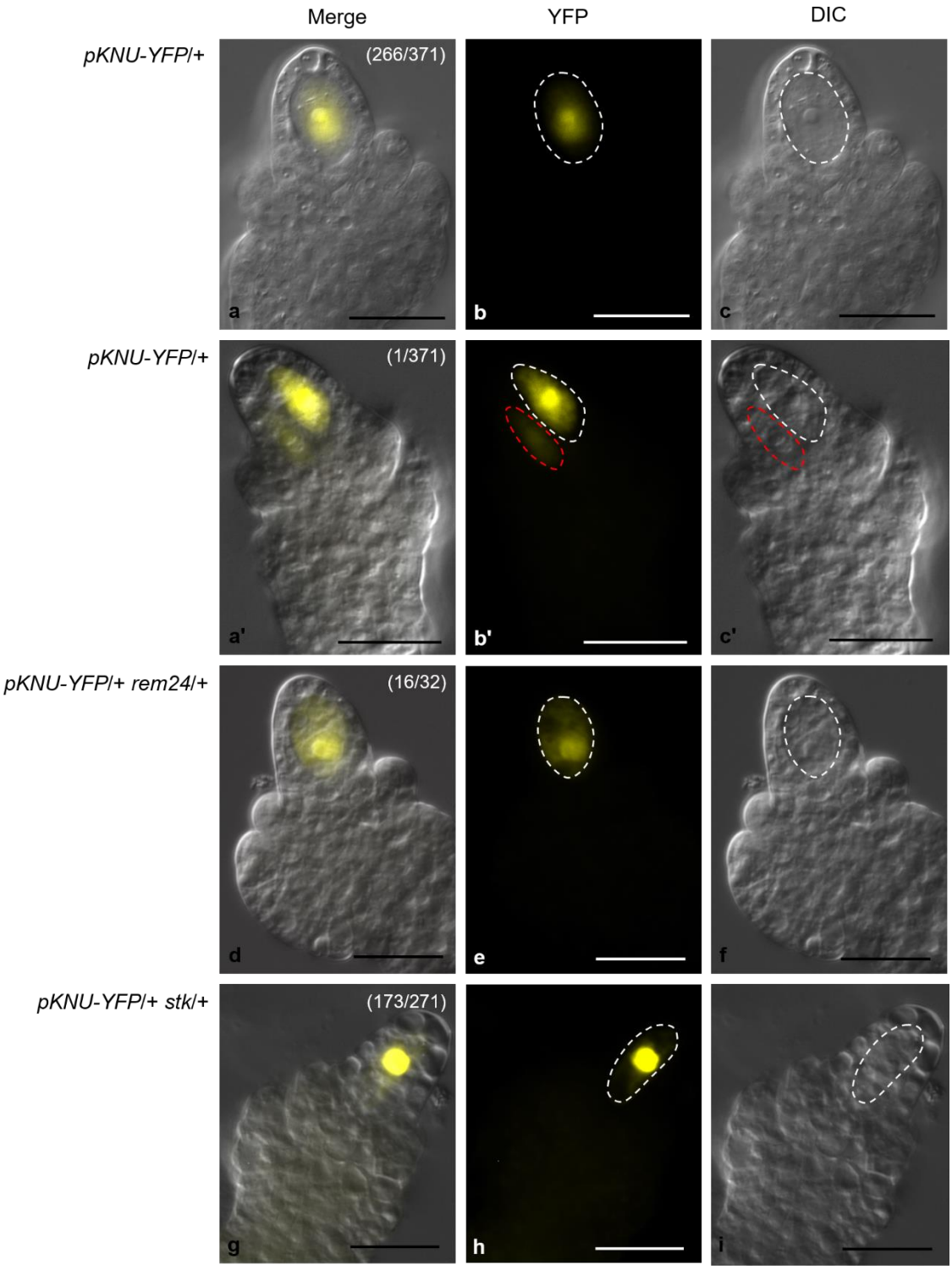

Fig. 26 – *pKNU-YFP* expression in wild type (WT), *rem24*/+ and *stk*/+ ovules at megaspore mother cell (MMC) stage. MMC stage stands for ovules from stage 2-I to 2-III (according to Schneitz *et al*., 1995). The promoter of *KNU* (*pKNU*) drives the expression of the yellow fluorescent protein (YFP) in the MMC nucleus in WT **(a – c),** *rem24*/+ **(d – f)** or *stk*/+ **(g – i)** background. **(a' – c')** YFP signal was detected in an enlarged nucellar cell in a WT ovule. In parenthesis is the calculation of the penetrance of the construct, the ratio of stained ovules showing the same signal against the total number of ovules observed. The remaining ovules didn't show any fluorescent signal. White dashed lines outline the MMC. Red dashed line highlights the presence of an enlarged nucellar cells next to the MMC showing fluorescent signal. Merge: pictures represent a merge of bright-field DIC and UV channel images. YFP: the yellow signal corresponds to the YFP fluorescence under UV light. DIC: bright-field Differential Interference Contrast microscopy. Scale bars = 20 μm.

As to determine if the enlarged nucellar cells had female gametophyte identity, the mutant plants were crossed with plants transformed with *pFM1-GUS*. Ovules at MMC stage and ovules at the stage 3-I (from now called FG1 stage) were also examined. For *rem24*/+ or *stk*/+, ovules at MMC stage didn't show any β-glucuronidase activity (Fig. 27 a-b), even if the MMC was squashed (Fig. 27 d, e); while the staining developed in the FG1 in *rem24*/+ or *stk*/+ ovules at the FG1 stage (Fig. 27 c, f). In some ovules, the staining was broader spreading to the nucellar cells, this occurred for the two genotypes. 37% of the *pFM1-GUS*/+ *rem24*/+ and 42% of *pFM1-GUS*/+ *stk*/+ ovules expressed the construct.

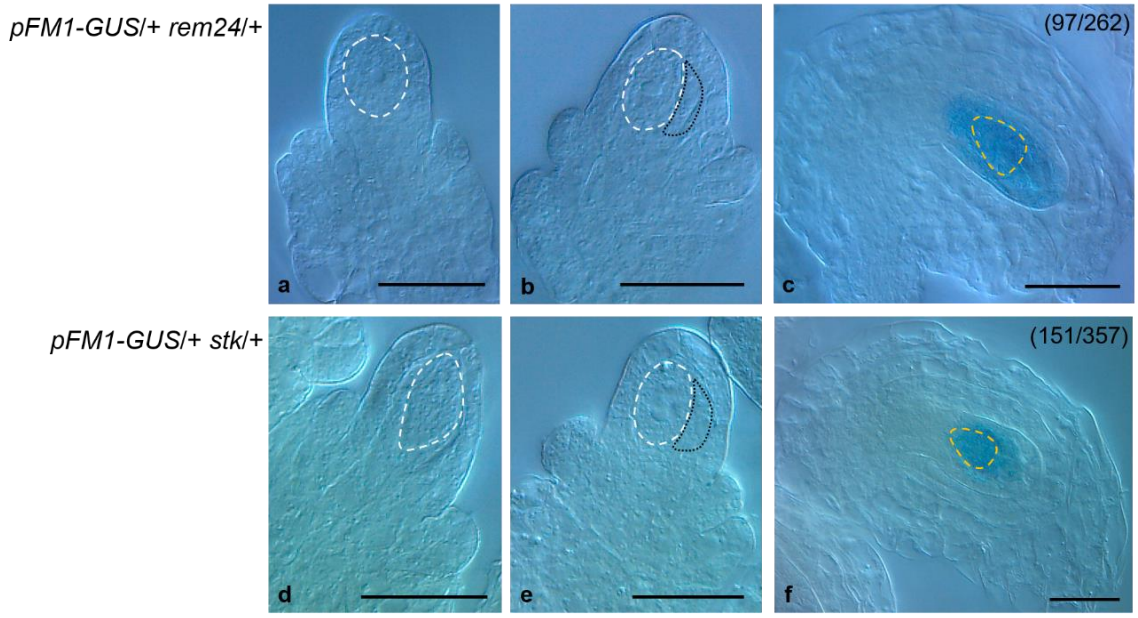

Fig. 27 - Histochemical detection of β-glucuronidase (GUS) activity driven by the *FM1* promoter (*pFM1-GUS*) in *rem24*/+ and *stk*/+ ovules at megaspore mother cell (MMC) and mono-nuclear female gametophyte (FG1) stages. MMC stage stands for ovules from stage 2-I to 2-III; FG1 stage is the stage 3-I (according to Schneitz *et al*., 1995). In ovules where the MMC fills the nucellar dome no staining was observed for *rem24*/+ **(a)** or *stk*/+ **(d)**. When ovules present an MMC in a lateral position in the nucellar dome, no staining was visualized in the "gap" between the MMC and the nucellar epidermis for *rem24*/+ **(b)** or *stk*/+ **(e)**. *pFM1* drives the expression of GUS in the FG1 where staining was visualized in *rem24*/+ **(c)** and *stk*/+ **(f)** ovules. In parenthesis: the penetrance of the construct was calculated, the ratio of staining ovules against the total number of ovules visualized. White dashed line outlines the MMC. Black spotted line highlights the "gap" between the MMC and the nucellar epidermis. Yellow dashed line indicates the FG1. Scale bars = 20 μm.

3.3.3.2. Immunolabelling of AGP and callose epitopes

Monoclonal antibodies that detect AGP sugars (JIM13) and callose (β-1,3-gucan) epitopes were used as indicators of gametophytic lineage or MMC/megaspores identities, respectively.

The MMC cell wall of *rem24* ovules was labelled by callose and AGP monoclonal antibodies (Fig. 28). The *rem24* ovules at MMC stage presented this type of labelling (across different sections of the same ovule and among different ovules). Unfortunately, it wasn't possible to obtain sections of WT ovules at MMC stage in time. Moreover, it wasn't possible to obtain sections with ovules at MMC stage with enlarged nucellar cells for both genotypes.

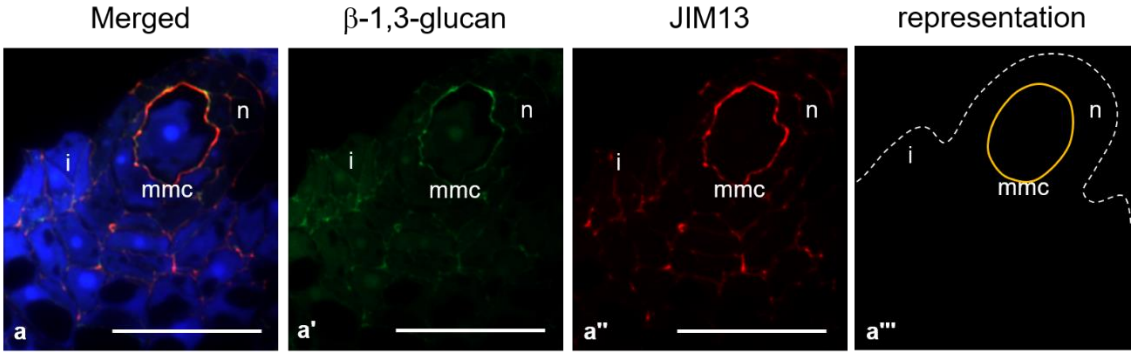

Fig. 28 - Fluorescence microscopy of *rem24* ovule at megaspore mother cell (mmc) stage labelled with monoclonal antibodies specific for callose (β-1,3-glucan) with AlexaFluor® 488 secondary antibody and for AGPs (JIM13) with AlexaFluor® 555 secondary antibody. mmc stage corresponds to ovules at stage 2-I to 2-III (according to Schneitz *et al*., 1995). (a) Merged image of calcofluor fluorescence under UV light with a' and a'' showing that callose and AGP epitopes are labelled in the cell wall of the mmc. (a') β-1,3-glucan antibody recognizes callose epitopes on the cells wall of the mmc. (a'') AGP epitopes are labelled by JIM13 in the cell wall of the MMC. (a''') schematic representation portraying the overlap of the callose and AGP epitopes localization. i – integuments; mmc – megaspore mother cell; n – nucellus. Scale bars = 20 μm.

At the tetrad stage, both *rem24* and WT ovules showed labelling for callose and AGP sugar epitopes on the cell plates dividing the megaspores (Fig. 29). Interestingly, in a WT ovule with a non-linear tetrad, the labelling can be detected around the megaspore in the odd position (Fig. 29 b – b'''). In Fig. 29 are depicted WT (c - c''') and *rem24* (e – e''') ovules at the tetrad stage, where the tetrad was pushed to the side due to the presence of an enlarged nucellar cell. No labelling was detected around those cells, for both genotypes. This situation was observed for other sections of the same ovule. In *rem24*, the AGP labelling seemed more intense than what was observed for WT (compare Fig. 29. a''-c'' with Fig. 29. d''- e'').

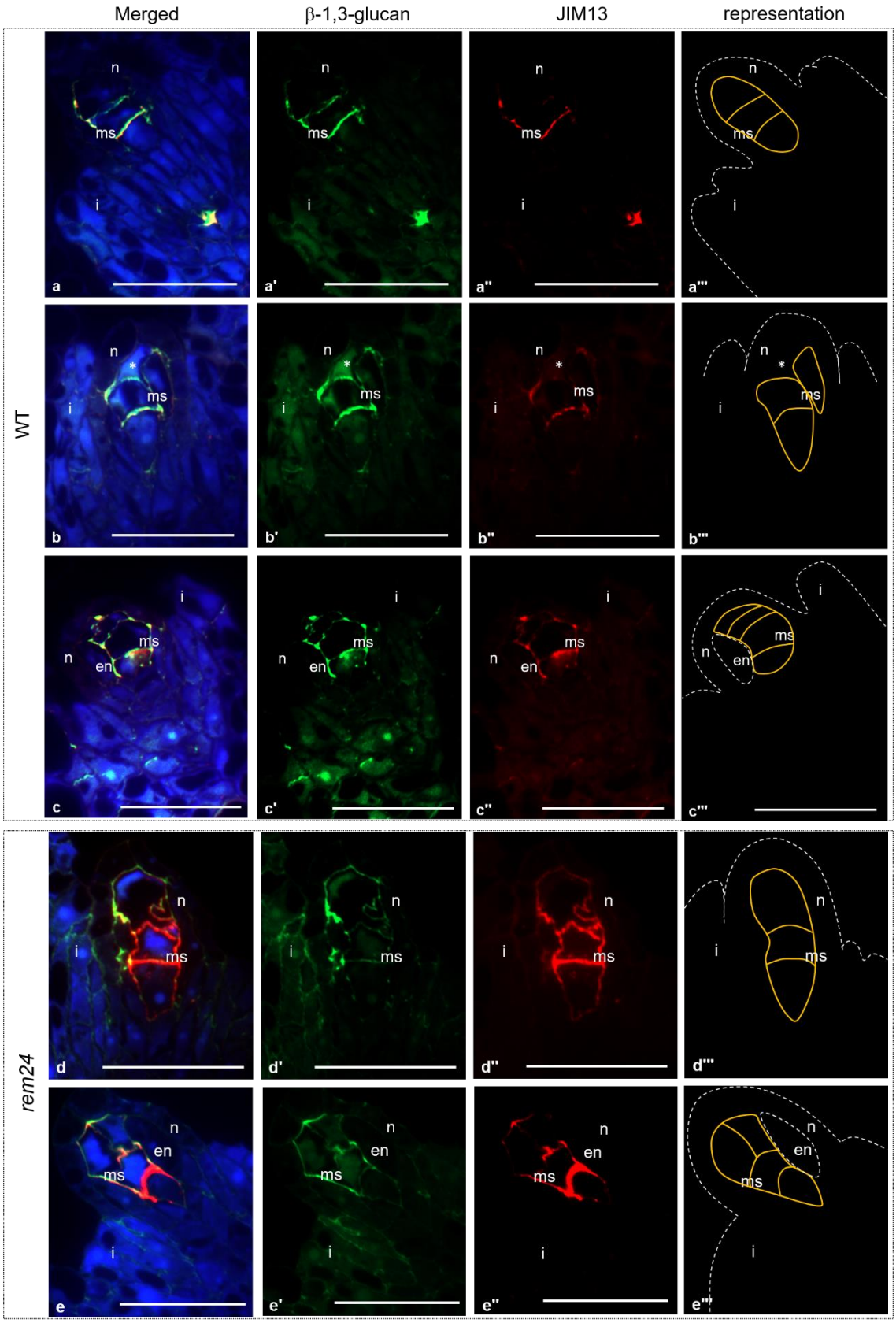

Fig. 29 - Fluorescence microscopy of wild type (WT) and *rem24* ovules at tetrad stage labelled with monoclonal antibodies specific for callose (β-1,3-glucan) with AlexaFluor® 488 secondary antibody and for AGPs (JIM13) with AlexaFluor® 555 secondary antibody. Tetrad stage corresponds to ovules at stage 2-V (according to Schneitz *et al*., 1995). Merged images of the AlexaFluor® 488 (β-1,3-glucan), AlexaFluor® 555 (JIM13) and calcofluor white fluorescence under UV light showing the overlap of localization of the callose and AGP epitopes in WT **(a, b, c)** and *rem24* ovules **(d, e)**. Fluorescent signal obtained

from the labelling of callose epitopes on the megaspores cell walls both in WT **(a', b', c')** and *rem24* **(d', e')** situations. JIM13 binds to AGP epitopes in the cell wall of the WT **(a'', b'', c'')** and *rem24* **(d'', e'')** spore tetrad. Schematic representation portraying the overlap of the callose and AGP epitopes localization in WT **(a''', b''', c''')** and *rem24* **(d''', e''')** ovules. The yellow line demonstrates the overlay of the green and red channels. Enlarged nucellar cells do not show any labelling in WT **(c – c''')** and *rem24* **(e – e''')**. en – enlarged nucellar cell; i – integuments; ms – megaspores; n – nucellus; * - degenerating megaspore. Scale bars = 20 μm.

3.4. Evaluating *REM24* and *STK* relation

3.4.1. Obtaining a double mutant *rem24 stk*

To obtain the double mutant *rem24 stk*, the reciprocal cross *rem24* with *stk* was performed. The seeds of these crosses were compared with the *rem24*, *stk*, and WT seeds (Fig. 30). *stk* seeds were smaller and rounder, as described previously (Pinyopich *et al*., 2003). *rem24* seeds were similar to WT, nonetheless, some seeds were similar to *stk* seeds; this was also verifiable among WT seeds. Qualitatively, the size of the *rem24* x *stk* seeds appeared to be larger than WT seeds, whilst fertile. Observing the *stk* x *rem24* seeds in the silique it was possible to conclude that the seeds aborted. When removing the *stk* x *rem24* seeds from the siliques, the integuments separated from the aborted embryo. Only a very small portion of the seeds looked fertile. The cross was repeated a second time and the same results were obtained.

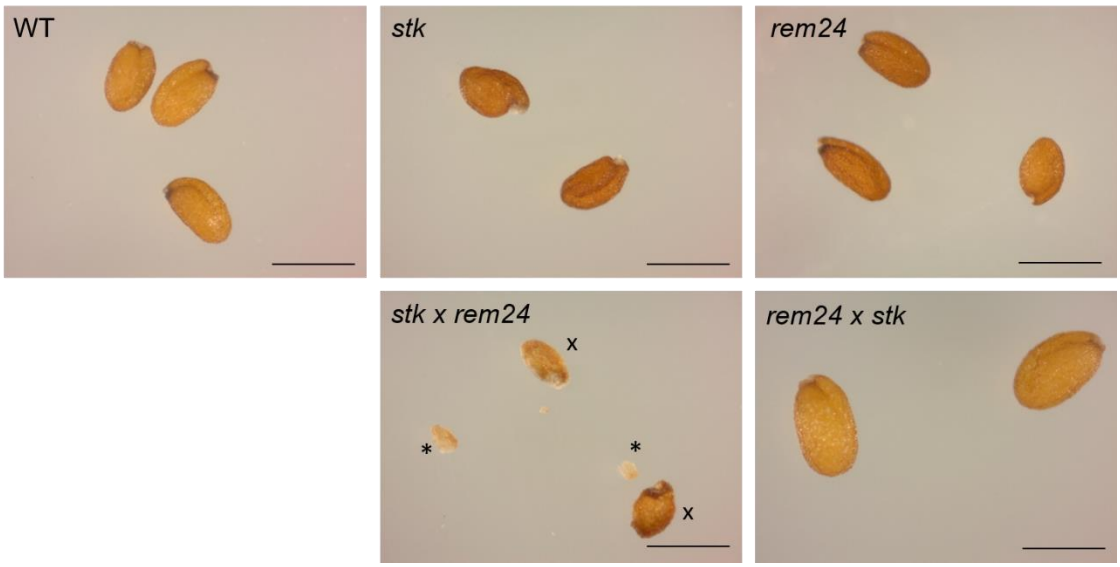

Fig. 30 - Magnification of wild type (WT), *rem24*, *stk*, *stk* x *rem24* and *rem24* x *stk* seeds. *stk* seeds are smaller and rounder than WT seeds. *rem24* seeds are WT-like but also some are *stk*-like (this happens in WT as well). When *rem24* is the pollen donor, the seeds abort (*stk* x *rem24*). Because *stk* seeds remain attached to the septum of the *stk* pistil, removing the seeds from the pistil results in separating the seed integuments (x) from the aborted embryo structure (*). When *stk* is the pollen donor, the resultant seeds are larger than WT ones (*rem24* x *stk*). Scale bars = 1mm.

3.4.2. qPCR analysis of *STK* and *REM24* expression

To confirm the RNA-seq indication of *REM24* downregulation in *stk*, *REM24* transcript abundance was quantified by qPCR in the *stk* mutant flowers (Fig. 31). In *stk*, the absolute expression level of *REM24* was higher during flower development but followed a similar trend as in WT. Likewise, *REM24* was upregulated in the *stk* flowers at the stage 10-11 and 12 (Fig. 31.a). The upregulation corresponds to a 1.8-fold change, when comparing with WT expression level (Fig. 31.b). As previously mentioned, *REM24* transcript abundance in *rem24* wasn't different from the WT level; yet, between *rem24* and *stk* a significant difference, although small, in absolute gene expression was present in the sample stage 1-9 and 10-11, 0.6 and 0.4-fold downregulation, respectively (Fig 31.b).

a.

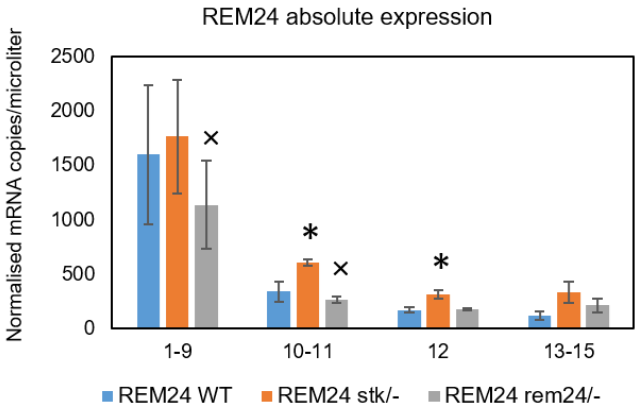

b.

	Stage			
Comparison	1-9	10-11	12	13-15
stk vs WT		1.8	1.8	
rem24 vs WT				
rem24 vs *stk*	0.6	0.4		

0.2 1.0 7.6

Fig. 31 – *REM24* qPCR expression analysis throughout floral development in different genotypes. **(a)** *REM24* absolute gene expression level in pulled stages of floral development for wild type (WT), *stk* and *rem24*. Error bars are the (±) standard error calculated from the biological replicates for each stage (calculated from the mean between the technical replicates). **(b)** Heat map of fold change relative to one. The gene expression between *stk* with WT, *rem24* with WT, and *rem24* with *stk* were compared. Fold change values are indicated for statistical differences between absolute gene expression levels. * indicates statistical differences when comparing *stk* to WT. ^{x} indicates statistical differences from the *rem24* versus stk comparison. Student's t-test, $\alpha = 0.05$. Stage 1-9: flower meristem and flowers with ovule primordia (stage 1-I to 1-II). Stage 10-11: flowers with ovules at megasporogenesis (from stage 2-I to 2-V). Stage 12: flowers with ovules at megagametogenesis (from stage 3-I to 3-VI). Stage 13-15: flowers with fertilized ovules (stage 4-I to 4-VI). Red fill indicates upregulated genes. Black fill indicates downregulated genes.

STK expression level was evaluated to understand *STK* WT expression profile during flower development, its possible deregulation in *rem24* and to confirm the *knock-out* mutation in *stk* (Fig. 32). *STK* transcript profile indicates that its expression increased along the WT flower development. In fact, only 10% of maximum transcript level was detected in the flowers at the stage 1-7, and it reached maximum transcript abundance at stage 13-15. Importantly, it seems that in WT there was a peak in the transcript level in the flowers at the stage 8-9, reaching 47% of maximum transcript level, while in stage 10, *STK* mRNA level is only 23% of maximum transcript level (Fig. 32.a). In the *stk* mutant, the absolute expression level didn't alter much, after the stage 1-9. Accordingly, a downregulation was verified, for stages 12 and 13-15 with a fold change of 0.3 and 0.2, respectively. On the other hand, *STK* expression in *rem24* wasn't significantly different in relation to WT, in any of the developmental stages. Statistical differences were present in the flowers at the stages 10-11 and 12, fold changes of 1.8 and 2.5, when comparing *rem24* to *stk* (Fig. 32.b, c).

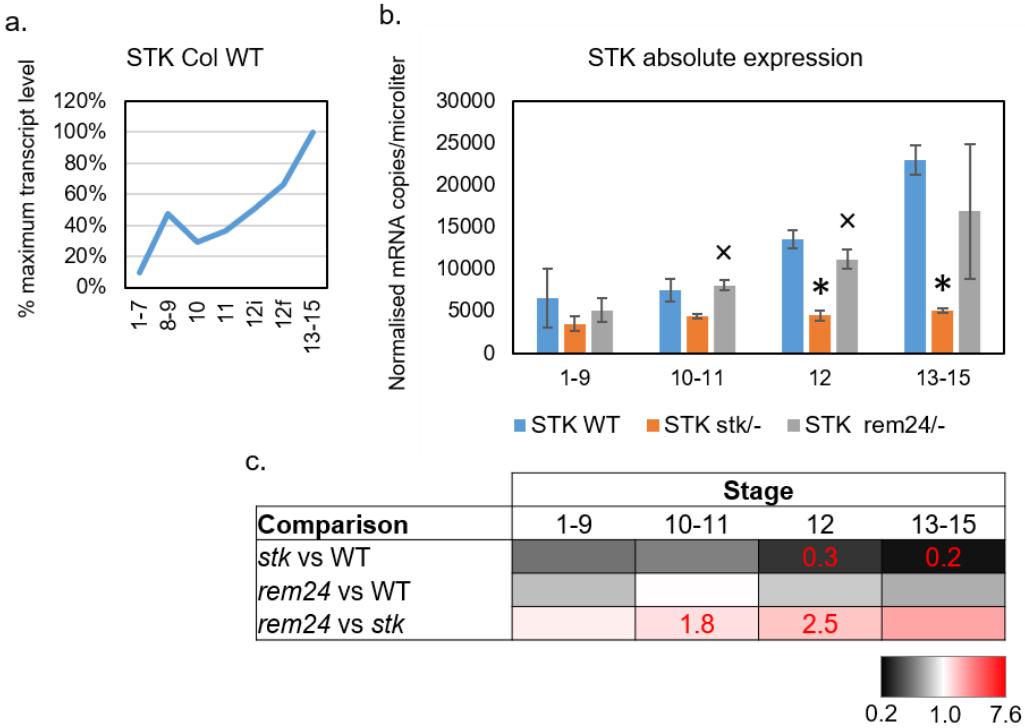

Fig. 32 - *STK* qPCR expression analysis throughout floral development. **(a)** *STK* transcript abundance across all the stages collected for WT plants. Transcript abundance was plotted considering the maximum absolute expression level corresponds to 100%. **(b)** *STK* absolute gene expression level in pulled stages of floral development for WT, *stk* and *rem24*. Error bars are the (±) standard error calculated from the biological replicates for each stage (calculated from the mean between the technical replicates). **(c)** Heat map of fold change relative to one. The gene expression between *stk* with WT, *rem24* with WT, and *rem24* with *stk* were compared. Fold change values are indicated for statistical differences found between absolute gene expression levels. * indicates statistical differences when comparing *stk* to WT. ˣ indicates statistical differences from the *rem24* versus *stk* comparison. Student's t-test, α = 0.05. Red fill indicates upregulated genes. Black fill indicates downregulated genes.

3.5. Designing a molecular pathway involving *REM24* and *STK*: qPCR analysis of relevant genes

The molecular pathways potentially altered in *rem24* and *stk* were examined performing qPCR. cDNA synthesized from the RNA of the various floral stages was used to determine the expression of other *STK* putative targets, genes relevant during ovule development, and genes potentially co-expressed with *REM24*.

3.5.1. *STK* putative targets

The expression level of the *STK* putative targets, revealed on the bioinformatic analysis (Table 12 and 13), were assessed also in *rem24*.

In *rem24* flowers, *AGO9* transcript levels weren't distinct from the WT, in terms of absolute gene expression (Fig. 33.a). Significant changes in gene expression were detected, when comparing *AGO9* absolute expression level between *rem24* and *stk* flowers at the stages 10-11 and 12, with the fold change 1.6 and 1.9x, respectively (Fig. 33.c). *AGO9* absolute gene expression in *rem24* was very similar to WT flowers, across development (Fig. 33.a). Therefore, no statistical differences were accounted between *rem24* and WT.

As seen for *stk*, *FLA20* absolute transcript level was higher in flowers at the stage 1-9 in *rem24,* but follows the same trend as in WT. No statistical alterations were detected when comparing *rem24* to WT or to *stk* (Fig. 33.b).

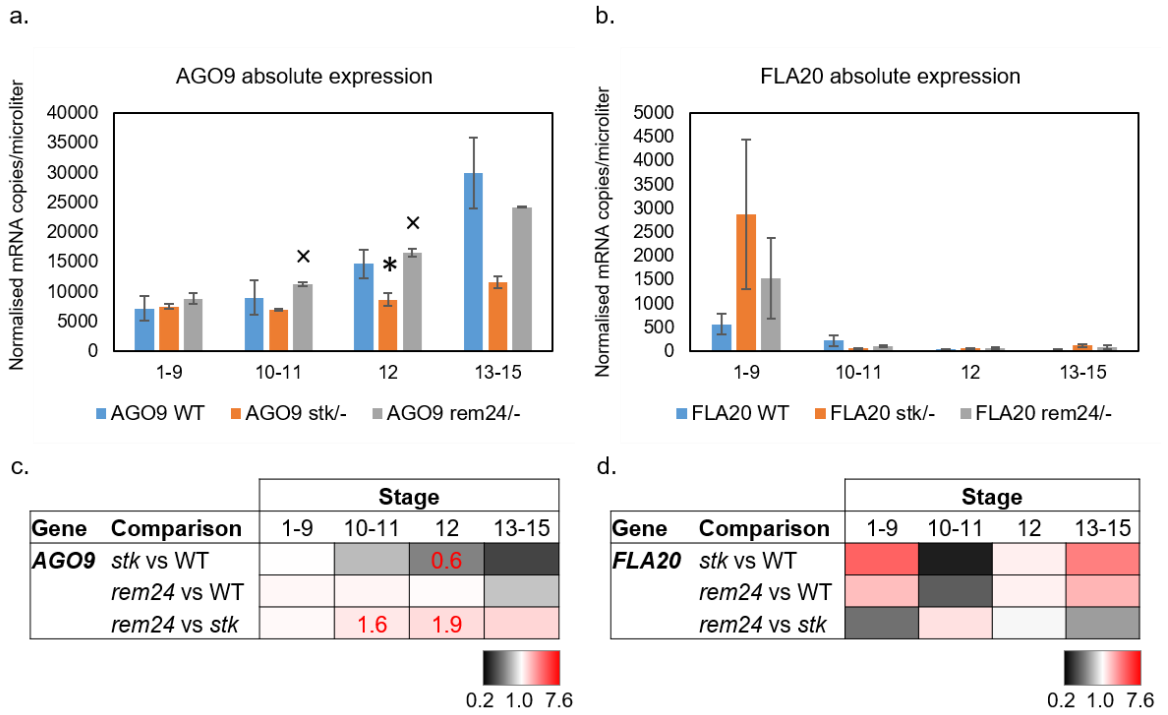

Fig. 33 - *AGO9* and *FLA20* qPCR expression analysis throughout floral development. *AGO9* **(a)** and *FLA20* **(b)** absolute gene expression level in pulled stages of floral development for WT, *stk* and *rem24*. Error bars are the (±) standard error calculated from the biological replicates for each stage (calculated from the mean between the technical replicates). Heat map of fold change relative to one for *AGO9* **(c)** and *FLA20* **(d)**. The gene expression between *stk* with WT, *rem24* with WT, and *rem24* with *stk* were compared. Fold change values are indicated for statistical differences found between absolute gene expression level. * indicates statistical differences when comparing *stk* to WT. ^{x} indicates statistical differences from the *rem24* versus *stk* comparison. Student's t-test, $\alpha = 0.05$. Stage 1-9: flower meristem and flowers with ovule primordia (stage 1-I to 1-II). Stage 10-11: flowers with ovules at megasporogenesis (from stage 2-I to 2-V). Stage 12: flowers with ovules at megagametogenesis (from stage 3-I to 3-VI). Stage 13-15: flowers with fertilized ovules (stage 4-I to 4-VI). Red fill indicates upregulated genes. Black fill indicates downregulated genes.

3.5.2. Genes involved in ovule development

Genes known to be relevant in ovule development were investigated by means of qPCR in *stk* and *rem24* in order to understand what molecular pathways are deregulated in the mutants.

In WT flowers, *WUSCHEL* (*WUS)* transcript abundance increased along the flower development until the stage 12f, where its maximum level was observed; in the flowers at the stage 13-15 *WUS* was absent (Fig. 34.a). This profile was also present in *rem24* and *stk* mutants. Relative to WT, only in *rem24* flowers at the stage 10-11 an upregulation was detected (Fig. 34.b). The gene was 2.4x upregulated at that stage (Fig. 34.c). While *WUS* absolute expression was higher in *stk* flowers stage 10-11 and 12, compared to WT, the difference wasn't statistically significant. No significant differences were found between *stk* and *rem24* (Fig. 34.b).

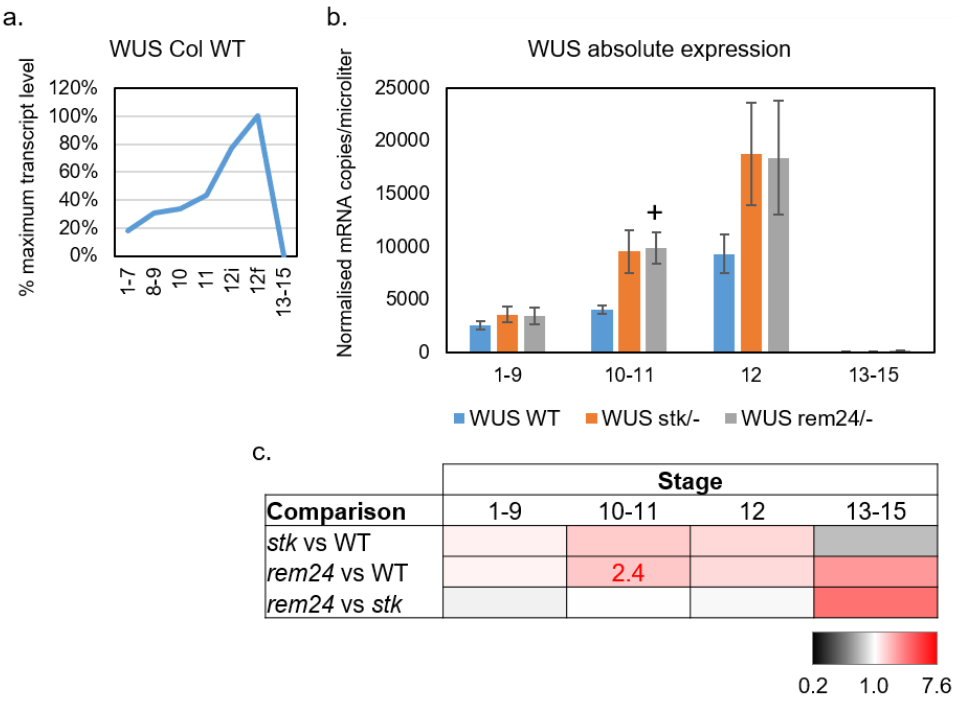

Fig. 34 - *WUS* qPCR expression analysis throughout floral development. **(a)** *WUS* transcript abundance across all the stages collected for WT plants. Transcript abundance was plotted considering the maximum absolute expression level corresponds to 100%. **(b)** *WUS* absolute gene expression level in pulled stages of floral development for WT, *stk* and *rem24*. Error bars are the (±) standard error calculated from the biological replicates for each stage (calculated from the mean between the technical replicates). **(c)** Heat map of fold change relative to one. The gene expression between *stk* with WT, *rem24* with WT, and *rem24* with *stk* were compared. Fold change values are indicated for statistical differences found between absolute gene expression levels. + indicates statistical differences from the *rem24* versus WT comparison. Student's t-test, $\alpha = 0.05$. Red fill indicates upregulated genes. Black fill indicates downregulated genes.

RDR6 transcript profile in WT flowers shows that *RDR6* mRNA level decreased along development. The maximum transcript level was observed at the stage 1-7. Accordingly, only 32% of the maximum transcript level was detected at the stage 13-15 (Fig. 35.a). *RDR6* absolute expression in *rem24* was similar to WT in the first stages of flower development. However, in flowers at the stage 12 it was detected an upregulation of 1.7-fold change. Despite not significative, the absolute expression level was also higher in *rem24* flowers stage 13-15, relative to WT. For *stk*, the expression profile was more dissimilar: *RDR6* was highly expressed in all stages of development. In fact, in flowers at the stage 1-9, 12 and 13-15 *RDR6* was upregulated. The fold change was always above two: 2.5, 4.4 and 7.6, respectively. When comparing *RDR6* expression level between *rem24* and *stk*, a downregulation was detected in *rem24* flowers at the stage 12 (Fig. 35.b, c).

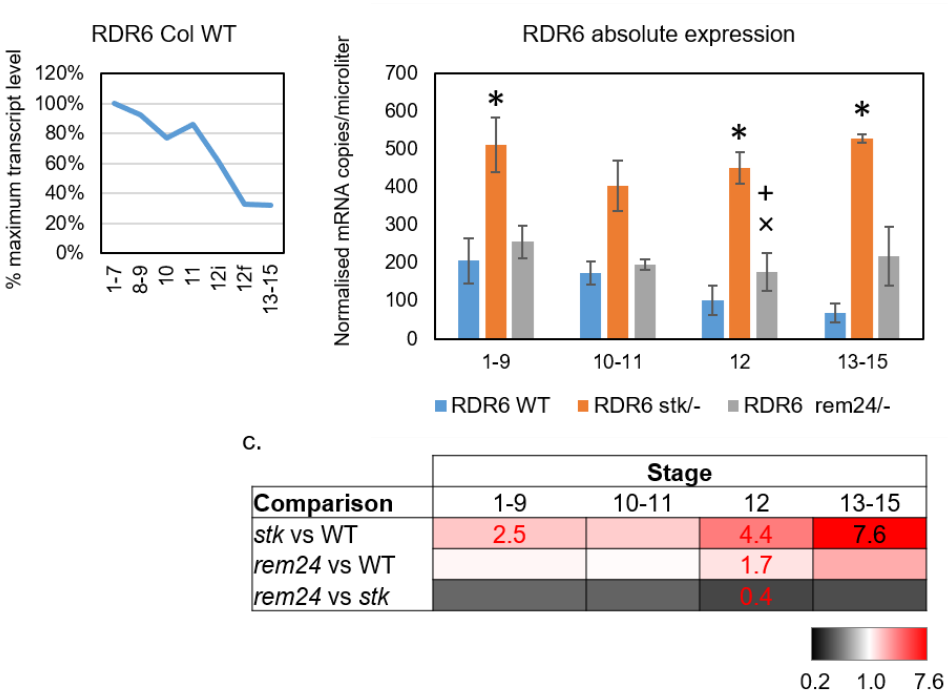

c.

Comparison	Stage 1-9	10-11	12	13-15
stk vs WT	2.5		4.4	7.6
rem24 vs WT			1.7	
rem24 vs *stk*			0.4	

0.2 1.0 7.6

Fig. 35 – *RDR6* qPCR expression analysis throughout floral development. **(a)** *RDR6* transcript abundance across all the stages collected for WT plants. Transcript abundance was plotted considering the maximum absolute expression level corresponds to 100%. **(b)** *RDR6* absolute gene expression level in pulled stages of floral development for WT, *stk* and *rem24*. Error bars are the (±) standard error calculated from the biological replicates for each stage (calculated from the mean between the technical replicates). **(c)** Heat map of fold change relative to one. The gene expression between *stk* with WT, *rem24* with WT, and *rem24* with *stk* were compared. Fold change values are indicated for statistical differences found between absolute gene expression levels. * indicates statistical differences when comparing *stk* to WT. x indicates statistical differences from the *rem24* versus *stk* comparison. + indicates statistical differences between *rem24* and WT. Student's t-test, $\alpha = 0.05$. Red fill indicates upregulated genes. Black fill indicates downregulated genes.

SPOROCYTELESS (SPL) WT expression was initially high, the maximum transcript level was verified at the stage 8-9, and it decreased along development, being almost absent from the stage 12f (Fig. 36.a). Generally, *SPL* absolute transcript profile was similar in *rem24* and *stk*, yet at higher level. In *rem24, SPL* upregulation was observed in the flowers at the stage 10-11, with 1.8-fold change. In *stk*, *SPL* was upregulated 2.1x in the flowers at the stage 1-9, and 2.2x in the flowers at the stage 10-11 (Fig. 36.b-c).

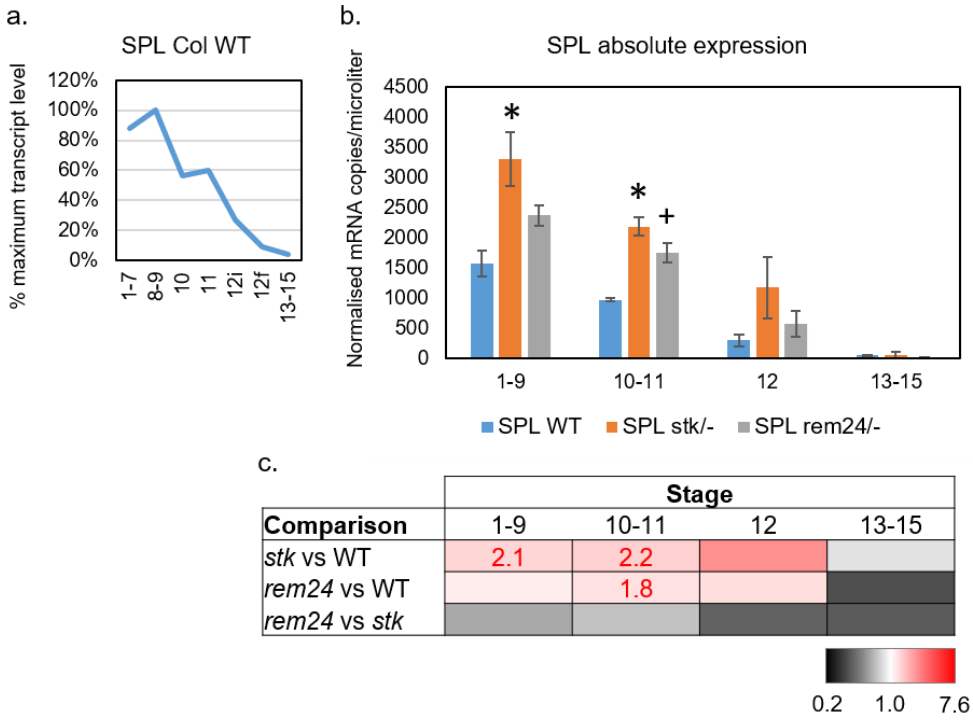

Fig. 36 - *SPL* qPCR expression analysis throughout floral development. **(a)** *SPL* transcript abundance across all the stages collected for WT plants. Transcript abundance was plotted considering the maximum absolute expression level corresponds to 100%. **(b)** *SPL* absolute gene expression level in pulled stages of floral development for WT, *stk* and *rem24*. Error bars are the (±) standard error calculated from the biological replicates for each stage (calculated from the mean between the technical replicates). **(c)** Heat map of fold change relative to one. The gene expression between *stk* with WT, *rem24* with WT, and *rem24* with *stk* were compared. Fold change values are indicated for statistical differences found between absolute gene expression levels. * indicates statistical differences when comparing *stk* to WT. + indicates statistical differences between *rem24* and WT. Student's t-test, $\alpha = 0.05$. Red fill indicates upregulated genes. Black fill indicates downregulated genes.

AGO5 is also important for ovule development therefore its expression level was investigated (Fig. 37). *AGO5* mRNA was most abundant in the stages 1-7 and 8-9, where 100% of maximum transcript level was detected. From the flowers at the stage 10, the transcript levels were somewhat constant, varying between 56% and 83% of maximum transcript level (Fig. 37.a). The absolute expression level in *rem24* was similar to WT, and no statistical differences were observed for all developmental stages. On the contrary, *AGO5* mRNA level in the *stk* mutant was higher across all stages, and upregulation was detected in the stage 1-9 and 13-15. The fold change was 1.4 and 1.8, respectively. Despite the lack of deregulation in *rem24* and upregulation in *stk*, no significative differences were observed between the mutants (Fig. 37.b, c).

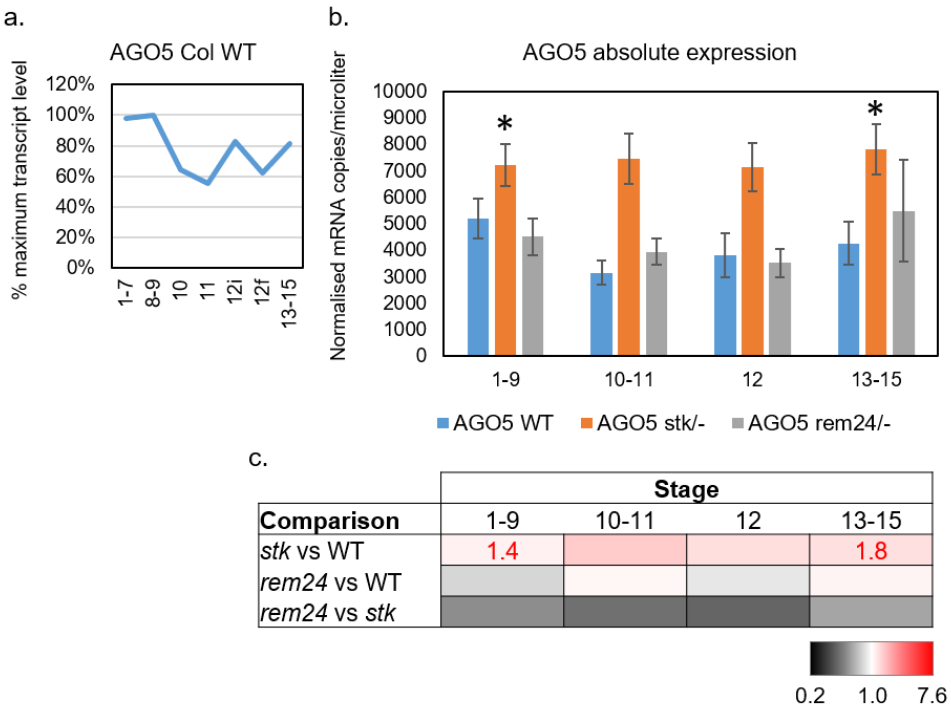

Fig. 37 – *AGO5* qPCR expression analysis throughout floral development. **(a)** *AGO5* transcript abundance across all the stages collected for WT plants. Transcript abundance was plotted considering the maximum absolute expression level corresponds to 100%. **(b)** *AGO5* absolute gene expression level in pulled stages of floral development for WT, *stk* and *rem24*. Error bars are the (±) standard error calculated from the biological replicates for each stage (calculated from the mean between the technical replicates). **(c)** Heat map of fold change relative to one. The gene expression between *stk* with WT, *rem24* with WT, and *rem24* with *stk* were compared. Fold change values are indicated for statistical differences found between absolute gene expression levels. * indicates statistical differences when comparing *stk* to WT. Student's t-test, α = 0.05. Red fill indicates upregulated genes. Black fill indicates downregulated genes.

In WT, *KNU* transcript level was at its highest in the stage 1-9, decreased abruptly in the stage 8-9 (only 30% of maximum transcript level), and it was practically null from the stage 12i to 13-15 (Fig. 38.a). The transcript abundance was somewhat similar in *rem24* and *stk,* relative to WT, in all flower stages. This was confirmed by the lack of statistical differences between *rem24* or *stk* and WT, and *rem24* with *stk* (Fig. 38.b, c).

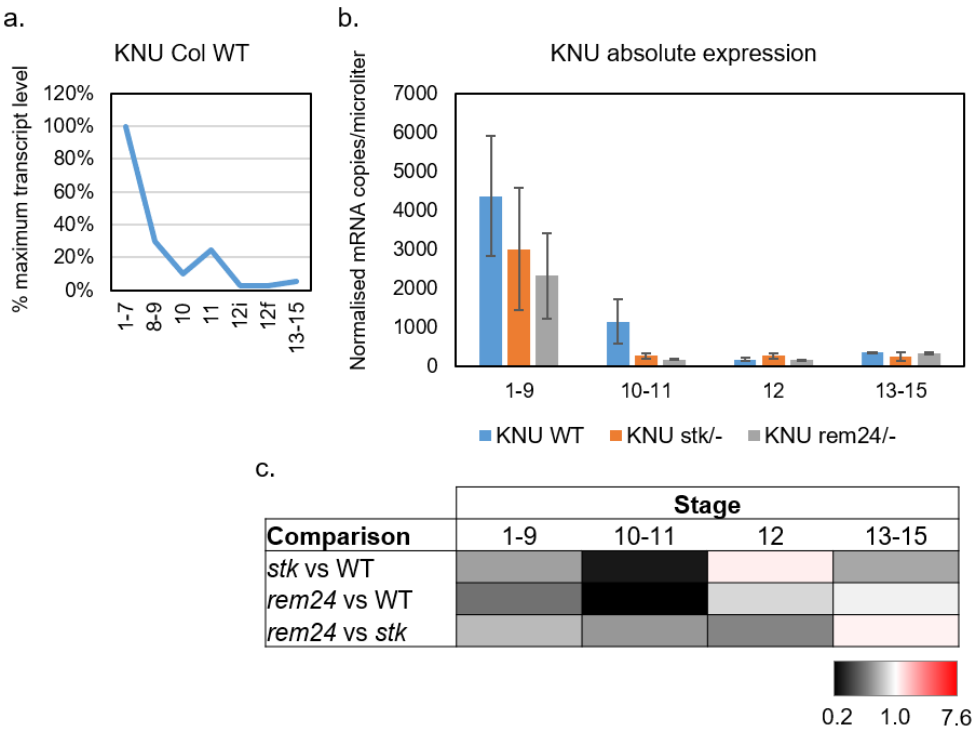

Fig. 38 - *KNU* qPCR expression analysis throughout floral development. **(a)** *KNU* transcript abundance across all the stages collected for WT plants. Transcript abundance was plotted considering the maximum absolute expression level corresponds to 100%. **(b)** *KNU* absolute gene expression level in pulled stages of floral development for WT, *stk* and *rem24*. Error bars are the (±) standard error calculated from the biological replicates for each stage (calculated from the mean between the technical replicates). **(c)** Heat map of fold change relative to one. The gene expression between *stk* with WT, *rem24* with WT, and *rem24* with *stk* were compared. Fold change values are indicated for statistical differences found between absolute gene expression levels. Student's t-test, $\alpha = 0.05$. Red fill indicates upregulated genes. Black fill indicates downregulated genes.

3.5.3. Genes co-expressed with *REM24*

The expression level of genes putatively co-expressed with *REM24* was evaluated in *rem24* and *stk* flowers.

Other target gene tested was *REM23.* In WT, the highest transcript level was in the first stages of flower development (1-7 and 8-9), and it decreased after stage 10. By stage 13-15 only 23% of maximum transcript level was detected in WT flowers (Fig. 39.a). *REM23* absolute transcript expression was higher in *rem24* flowers, compared to WT, however the differences weren't significative. On the other hand, in *stk, REM23* was upregulated in the stage 12, with a 1.7-fold change, and in the stage 13-15, with a fold change of 2.5. Although *rem24* wasn't significantly different from WT, and *REM23* upregulation was detected in *stk*, when comparing *rem24* to *stk*, the difference in absolute expression level wasn't significative (Fig. 39.b, c).

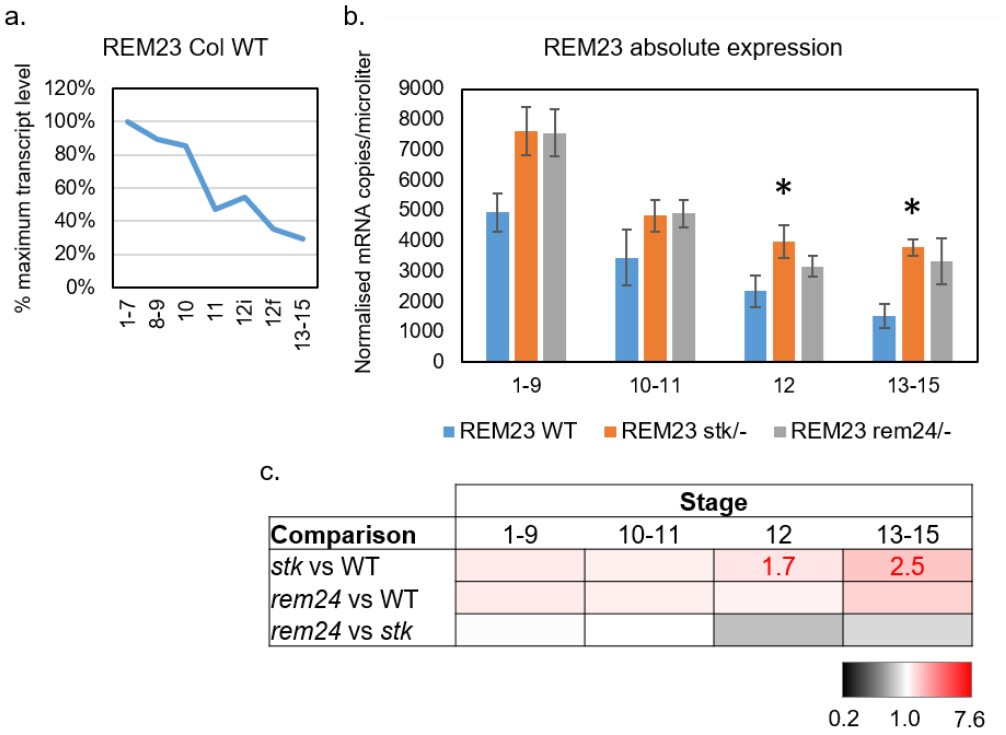

Fig. 39 – *REM23* qPCR expression analysis throughout floral development. **(a)** *REM23* transcript abundance across all the stages collected for WT plants. Transcript abundance was plotted considering the maximum absolute expression level corresponds to 100%. **(b)** *REM23* absolute gene expression level in pulled stages of floral development for WT, *stk* and *rem24*. Error bars are the (±) standard error calculated from the biological replicates for each stage (calculated from the mean between the technical replicates). **(c)** Heat map of fold change relative to one. The gene expression between *stk* with WT, *rem24* with WT, and *rem24* with *stk* were compared. Fold change values are indicated for statistical differences found between absolute gene expression levels. * indicates statistical differences when comparing *stk* to WT. Student's t-test, $\alpha = 0.05$. Red fill indicates upregulated genes. Black fill indicates downregulated genes.

During floral development, *HSP20* mRNA maximum transcript level occurred in WT flowers at the stage 1-7. The transcript level reduced abruptly from the stage 8-9, where only 16% of maximum transcript level was detected. From stage 11 to stage 13-15 *HSP20* was almost absent (Fig. 40.a). *HSP20* absolute transcript level in *rem24* and *stk* followed a similar trend. Relative to WT, only in the *rem24* flower at the stage 13-15 a significative upregulation of 3.2-fold change was found. In the flowers at the stage 12, it was possible to verify a statistical difference, between *rem24* and *stk* (Fig. 40.b, c).

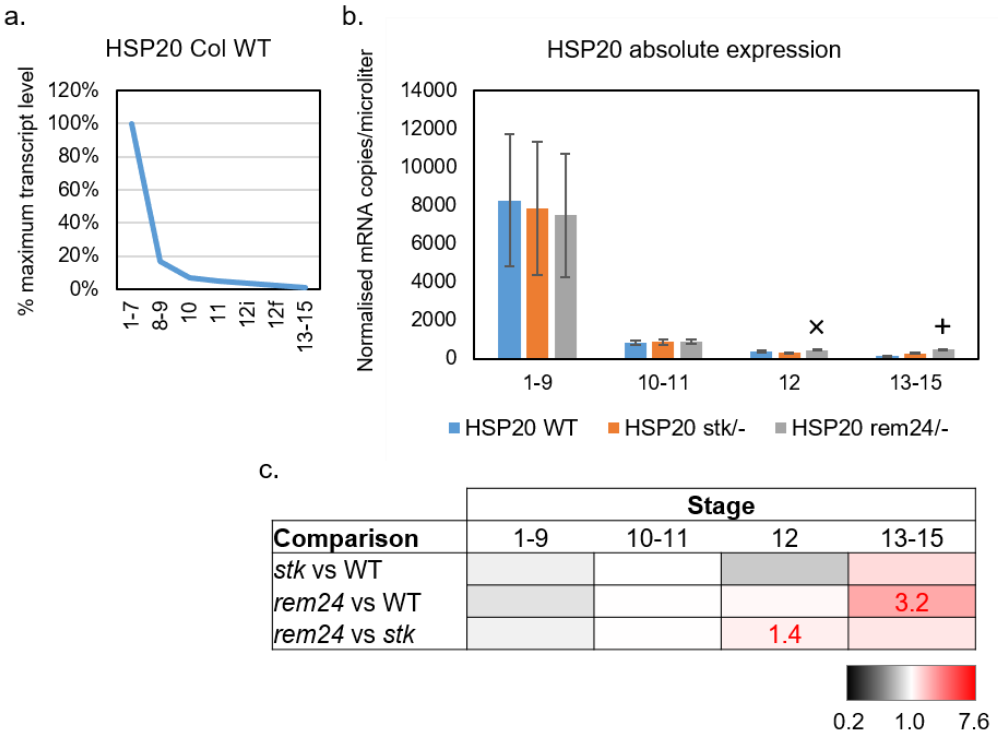

Fig. 40 – *HSP20* qPCR expression analysis throughout floral development. **(a)** *HSP20* transcript abundance across all the stages collected for WT plants. Transcript abundance was plotted considering the maximum absolute expression level corresponds to 100%. **(b)** *HSP20* absolute gene expression level in pulled stages of floral development for WT, *stk* and *rem24*. Error bars are the (±) standard error calculated from the biological replicates for each stage (calculated from the mean between the technical replicates). **(c)** Heat map of fold change relative to one. The gene expression between *stk* with WT, *rem24* with WT, and *rem24* with *stk* were compared. Fold change values are indicated for statistical differences found between absolute gene expression levels. x indicates statistical differences from the *rem24* versus *stk* comparison. + indicates statistical differences between *rem24* and WT. Student's t-test, α = 0.05. Red fill indicates upregulated genes. Black fill indicates downregulated genes.

4. Discussion

This work was centred on *STK*-related pathways necessary for early ovule development. Until now, scarce information connected *STK* to early ovule development. To describe the pathways deregulated in *stk*, a bioinformatic analysis of *stk* RNA-seq was performed (4.1.1. Analysis of GO terms in *stk* RNA-seq). After an intricate transcriptomic and *in silico* analysis, *REM24* was chosen as a putative *STK* target involved in MMC formation (4.1.2. Transcriptomic approach suitability; 4.1.3. Analysis of the candidate genes). The next objective was to characterize the gene in terms of gene expression and ovule phenotype (4.2. *REM24* expression pattern during ovule development; 4.3. *rem24* phenotype during ovule development). To finalize, a molecular network involving *REM24* and *STK* was proposed (4.5. A molecular pathway involving *REM24* and *STK*: qPCR analysis of relevant genes).

4.1. Bioinformatic analysis

4.1.1. Analysis of GO terms in *stk* RNA-seq

Since *STK* controls aspects of ovule, seed and carpel development (as reviewed in the introduction), it was expected that the genes downregulated in *stk* inflorescence were related to the reproductive process as verified. The enriched cell division and associated biological processes and cellular components GO terms of the downregulated genes in *stk* revealed that *STK* can be regulating mitotic and meiotic cell division. Especially because those GO terms weren't present when analysing the upregulated genes. Considering that *stk* seeds are smaller than WT ones (Pinyopich *et al*., 2003), and the fact that genes related to mitotic division are downregulated, perhaps *STK* influences cell division in the seed leading to its smaller size. Although *STK* is only known to regulate female-related development, remarkably, pollen development GO term was enriched among the downregulated genes. Perhaps indicating that *STK* may regulate genes that operate in both female and male reproductive development.

The examination of the upregulated genes showed that in the absence of *STK*, cell wall biogenesis may be more active. This was demonstrated by the enrichment in cell wall biogenesis-related GO terms. Interestingly, GO terms related to cellular respiration and photosynthesis were also increased. This leads to speculate if and how *STK* can lead to increased metabolic and photosynthetic rates. Moreover, the ribosome associated GO terms enrichment among the upregulated genes may be an indicative of increased translation of proteins for the production of molecules involved in all these processes.

4.1.2. Transcriptomic approach suitability

STK known regulatory functions are centred in positive interactions. *STK* promotes: the stabilization of the complex BEL1-AG-SEP3 for integument development (Brambilla *et al*., 2007; Brambilla *et al*., 2008; Battaglia *et al*., 2008), and *VDD* and *VAL* for FG cellular specification (Matias-Hernandez *et al*., 2010; Mendes *et al*., 2013; Mendes *et al*., 2016). Moreover, the *stk shp1 shp2* phenotype leads to the assumption that *STK* promotes ovule identity. Only one example clearly associates *STK* with repression: *STK* represses *ABS* and *BAN* to restrict PA production to the endothelium (Mizzotti *et al.,* 2014). Considering this information, it seemed plausible to restrict the search to the positively regulated *STK* targets.

To find *STK* targets involved in MMC formation, it was decided to narrow the *stk* RNA-seq DEG list by overlapping them with the nucellus transcriptome and the MMC transcriptome: several evidences connect the correct nucellar development with correct female germline formation (reviewed in the introduction). If a gene is positively regulated by *STK*, it could be downregulated in the *stk* inflorescence and upregulated in the WT nucellus, where *STK* is normally expressed (Mizzoti *et al*., 2014). *STK* is not expressed in the WT MMC as observed by the *STK-GFP* marker line (Mizzotti *et al*., 2014) and *STK* is downregulated in the MMC; consequently, *STK* shouldn't be able to directly regulate the transcription of a target gene expressed in the MMC. Thus, the genes downregulated in the MMC transcriptome were crossed with the genes downregulated in the *stk* inflorescence and upregulated in the nucellus. It was decided that the analysis should include also indirect *STK* targets. Which meant that the candidate gene could be up or downregulated in the MMC depending on its regulation by other genes expressed in the ovule. Moreover, it was relevant to find targets upregulated in the MMC to select genes that could be important for MMC formation themselves. Among all these hypothetical scenarios, an objective was defined: find targets expressed in the nucellus that can indirectly affect MMC formation, or targets expressed in the MMC therefore directly involved in its formation process, both positively regulated by *STK*. In the list of genes downregulated in *stk*, upregulated in the nucellus and downregulated in the MMC (Table 12) the higher expression level of each target was at early and later flower stages, or at different stages of the seed development. This demonstrates that this approach was successful in identifying potential *STK* targets, since *STK* is expressed during ovule and seed development (Mizzotti *et al.,* 2014). The genes downregulated in *stk*, upregulated in the nucellus and upregulated in the MMC (Table 13) were expressed in higher levels in the flower stage 9, flowers when MMC develop in the ovule primordia, in accordance to what was proposed: genes that could be directly involved in MMC formation.

For the analysis, the FDR in the *stk* RNA-seq was disregarded, since only 538 genes, 3.0% of the total genes detected in the RNA-seq, had a FDR below 0.05. Observing the two output lists it is possible to verify that only 5 genes would have a suitable FDR (< 0.05) (Table 12 and 13). Additionally, some of the genes with FDR > 0.05 presented higher fold changes in the nucellus and MMC, then the ones with FDR < 0.05. The genes with FDR < 0.05 never presented a fold change in the nucellus over 1.3x; regarding the MMC dataset, the fold change was never higher than 0.7x. Disregarding the FDR aimed to increase the possibility of finding genes closely related with the MMC/germline development. One of the genes present in the list with a FDR higher than 0.05 is *KLUH* (*KLU*), FDR = 0.10. *KLU* is a cytochrome P450 monooxygenase (Anastasiou *et al*., 2007) implicated in megasporogenesis: 26% *klu* ovule primordia show defective cell plate formation during meiosis (Zhao *et al*., 2014). Therefore, *KLU* could be a *STK* target, clearly involved in germline formation, illustrating the suitability of the approach taken.

Several available on-line tools were consulted to determine if the listed genes were related to reproduction. The analysis of the expression pattern aimed to restrict the candidate list for genes that were specifically expressed in the reproductive structures, in particular, early stages of flower development. The e-FP browser indications, the RNA-seq-based PCW tool, and the qPCR analysis in WT flowers resulted in similar WT patterns of expression for both *REM24* and *AGO9*. Relying on e-FP browser pattern of expression to determine which genes are more specifically involved in reproduction seemed a good strategy. 59% of the targets on Table 12 and 13 were specifically expressed in reproductive tissues. And only 5% of the genes were specifically expressed in the vegetative part of the plant. The literature review allowed to understand if they could relate to ovule development and if there were any hints that could support *STK* regulatory role toward a specific target.

4.1.3. Analysis of the candidate genes

AGO9 and *REM24* were considered the best targets to further investigate, since they were the top targets of each output.

Unlike most of the genes present on Table 12 and 13, *AGO9* showed a FDR < 0.05 for the *stk* RNA-seq, which supported the detection of 0.8 downregulation. *AGO9* functions were extensively detailed in the introduction. Summarizing, by targeting 24nt sRNAs, *AGO9* is a component of the RdDM pathway involved in post-transcriptional gene silencing (Durán-Figueroa *et al*., 2010; Havecker *et al*., 2010). In *ago9* mutant ovules, nucellar sub epidermal cells enlarge and acquire FG identity without undergoing meiosis. Therefore, *AGO9* should prevent the nucellar cells to enter megagametogenesis (Olmedo-Monfil *et al*., 2010). e-FP browser showed *AGO9* higher expression in flowers stage 12 harbouring ovules in different

stages of megagametogenesis. At the Araport platform it is possible to find a list of genes potentially co-expressed with the gene of interest. For *AGO9*, the most relevant genes were *AGO5*, *SEP1*, *SEP2*, *SHP1*, *SHP2*, *INO*, *STK* and *AG* (score ≥ 0.200). *AGO5* was recently implicated in ovule development (Tucker *et al*., 2012); *INO* is responsible for outer integument outgrowth (Baker *et al*., 1997) and it is indirectly regulated by *STK* (Brambilla *et al*., 2007; Brambilla *et al*., 2008; Battaglia *et al*., 2008); *SEP1, SEP2, SHP1, SHP2* and *AG* were already mentioned in the introduction. This analysis showed the involvement of *AGO9* with reproduction, more specifically ovule development.

In the *stk* RNA-seq, the FDR for *REM24* was 0.45 which indicated that it may not be downregulated. Nevertheless, since *REM24* showed such high fold change in the MMC (1.3) and also in the nucellus data (1.9), and the genes with FDR < 0.05 in the *stk* RNA-seq had a smaller fold change in the MMC datasets; it was determined that *REM24* could be a candidate to investigate. A *rem24* mutant (SALK_054142), with a T-DNA insertion in the 3'UTR was reported as a *knock-down* line, where *REM24* was 2.6-fold downregulated. The authors determined that this *rem24* mutant didn't have a phenotype, consequently *REM24* function was unknown. The authors of the article were consulted in order to better understand the assessment of *rem24* phenotype: ovule development was overlooked; likewise, the gene was still considered a good candidate to investigate. Mantegazza *et al.* (2014) performed an *in situ* hybridization to detect *REM24* RNA. *REM24* is expressed in the microsporocytes and tapetum of anthers in flowers at the stage 7-8 (Mantegazza *et al*., 2014; Wijeratne *et al*., 2007). The e-FP browser indicates that *REM24* is highly expressed in the inflorescence meristem and in the first stages of flower development, the stage 9 (when the MMC develops in the ovules). The level of expression in other organs is nearly null. This information points out that *REM24* may be a gene important for reproduction. At Araport, the genes putatively co-expressed with *REM24* were *REM15*, *REM22*, *REM23*, *AP1*, *LEAFY (LFY)*, *AGO5*, and *UNUSUAL FLORAL ORGANS* (*UFO*) (score ≥ 0.300). The *REM* genes are considered to have originated from duplication events (Romanel *et al*., 2009). Mantegazza *et al*. (2014), analysed microarray data available for *REM* and flower meristem initiation genes, like *AP1* and *LFY*. This analysis placed *REM22, REM23* and *REM24* in the same cluster. The expression pattern of these genes had good correlation with *LFY* and to a less degree with *AP1* expression pattern (Mantegazza *et al*., 2014). Additionally, *REM23* and *REM24 in situ* hybridization showed that they have similar expression patterns (Mantegazza *et al*., 2014). Since their expression pattern overlap, and *REM23* and *REM24* are phylogenetically close related (Romanel *et al*., 2009), *REM* TFs may share redundant functions. This information seems to indicate that *REM24* may be involved in inflorescence meristem development. However, *REM22* (Romanel *et al*., 2011), *REM23* and *REM24* (Mantegazza *et al*., 2014) transcripts aren't detected in the

inflorescence meristem, but in the floral meristem where stamens will originate. Interestingly, the *in situ* hybridization revealed *REM15* (Wellmer *et al*., 2006) and *REM22* (Romanel *et al*., 2011) transcripts at the carpel margin meristem where ovules form (Reyes-Olalde *et al*., 2013). Besides affecting stamen development, if *REM24* is indeed co-expressed with *REM15* and *REM22*, it may be involved in ovule initiation. *UFO* controls petal and stamen formation together with *LFY* (Lee *et al*., 1997).

Altogether the data point that *LFY* through *UFO* or *AP1* may regulate the activation of *REM24* for the formation of stamen. However, considering the likely overlap of the *REM* TFs expression pattern, it is possible that *REM24* may be expressed in the carpel margin meristem, also promoting ovule formation.

Another evidence for this possible dual role of *REM24* is the fact that it may be co-expressed with *AGO5*. As mentioned before *AGO5,* mutations in *MEL1*, closely related to *AGO5*, lead to male and female meiotic arrest and sterility (Nonomura *et al*., 2007). Additionally, *AGO5* is expressed in the sperm cells and comparative analysis of miRNA population in pollen, sperm cells and sporophytic tissues revealed that miRNAs which associate with *AGO5* are enriched in the male tissues, leading to the suggestion that *AGO5* may be also involved in male reproductive development (Borges *et al*., 2011).

As mentioned before, *VDD* and *VAL* are two *REM* TFs regulated directly by the STK-SEP3 complex (Matias-Hernandez *et al*., 2010; Mendes *et al*., 2013; Mendes *et al.,* 2016). *VAL* was found downregulated in the MMC data. Interestingly, like *REM24*, *VDD* was upregulated in the MMC transcriptome. The upregulation in the MMC, suggests that *REM24* (and *VDD*) can be indirectly regulated by *STK*.

The fact that *STK* directly regulates the transcription of two *REM* TFs, and that *REM* genes must be intimately involved in reproduction since almost all members are expressed exclusively in reproductive tissues (Mantegazza *et al*., 2014), were the main reasons to choose *REM24* as focus of this work.

4.1.4. Understanding the network

4.1.4.1. Analysis of genes putatively co-expressed with *REM24*

At the Plant Cell Wall (PCW) laboratory publicly available RNA-seq data was integrated in a platform such that one can investigate the expression pattern of a certain gene across different WT *A. thaliana* vegetative and reproductive structures. The sample staging was according to Klepikova *et al*., 2016. Among other functions, it can be used similarly to e-FP browser and to find genes putatively co-expressed with the gene of interest. According to this data, *REM24* was highly expressed in the flower primordia and floral meristem (flower stage 19) and early stages of flower development (flowers at the stage 15-18 and stage 12-14); in the young carpels (which correspond to flower stage 9, according to Smyth *et al*., 1990); and, in the anthers, although the level of expression in this structure was much lower. This was in accordance to the eFP browser information.

Considering only the floral tissues, the gene with the most similar expression pattern with *REM24* was *NUBBIN* (*NUB*), a TF belonging to the C2HC zinc fingers superfamily protein involved in regulating carpel and stamen growth. *In situ* hybridization detects *NUB* mRNA in stamen, and in carpel primordia where ovules arise (Dinneny *et al*., 2006). *SPL8*, a SBP-box TF with the associated biological processes GO terms, megasporogenesis and microsporogenesis shared a similar expression pattern with *REM24*. In *spl8* ovules megasporogenesis doesn't occur because the MMC degenerates, and, in the anther, archesporial cells fail to develop (Unte *et al*., 2003). *SPL8* was also implicated in correct carpel formation (Xing *et al*., 2013). Remarkably, *SPL8* was found also when considering vegetative tissues, reinforcing their potential co-expression. Another *REM24* potentially co-expressed gene was *YUCCA1* (*YUC1*), a flavin-binding monooxygenase family protein implicated in auxin biosynthesis (Stepanova *et al*., 2011). *YUC1* expression is detected in carpel and stamen primordia. It was verified that in *yuc1 yuc4* plant development is affected and the plants are completely sterile because functional floral organs are absent (Cheng *et al*., 2006). When just considering flower tissues, *FILAMENTOUS FLOWER* (*FIL)* and *REM24* present a similar expression profile. *FIL* is a YABBY TF acting in the inflorescence and floral meristem for the specification of the floral organs. *fil* flowers are flowers with altered number or rearrangement of the floral organs, or flowers where the floral organs are replaced by filamentous structures. Notably, *FIL* was downregulated in the *stk* RNA sequencing. This means that although *FIL* and perhaps *REM24* may be involved in early organ formation, *STK* may still be able to regulate their expression at later stages of flower development when ovules arise.

The genes potentially co-expressed with *REM24* support a role for *REM24* in carpel and stamen formation. Importantly, *REM24* biological role may involve an auxin signaling

pathway, very important for ovule development. For example, the correct expression domain expression of *ARF3* prevents the formation of ectopic MMCs (Su *et al*., 2017).

The potential redundancy of *REM* TFs was demonstrated by the fact that four other *REM* TFs seem to be co-expressed with *REM24* (Table 14 and 15). *REM15* was considered a potential co-expressed gene in this analysis but also in Araport. *REM15* is expressed in both anthers and MMC (Wynn *et al*., 2011). *REM16* was present on the list of genes co-expressed with *REM24* when considering just floral tissues, and its mRNA is also detected in the MMC (Wynn *et al*., 2011). This information provided further support for *REM24* involvement in MMC formation. As expected, *REM23* appeared to be co-expressed with *REM24* in this analysis.

4.1.4.2. *STK* positively regulated genes

The list of genes potentially co-expressed with *STK* was obtained to gain more insights in *STK*-dependant pathways. A gene positively regulated by *STK*, may have a similar expression pattern to the *STK* expression pattern. With this purpose, the list of the 18 genes most likely co-expressed with *STK* was crossed with the list of genes downregulated in the *stk* inflorescence. When considering all the samples tested, only *PTR5* (*AT5G01180*) was also downregulated in *stk*. It was suggested that *PTR5* is implicated in peptide transport into maturating pollen and ovules (Komarova *et al*., 2008). Interestingly, if only the genes expressed in the floral tissues were accounted, *AGO9* was the gene commonly downregulated in *stk.*

The assumption that genes sharing the same expression domain have a regulator-target relation is partially validated by the fact that *VAL* (a known *STK* direct target, Mendes *et al*., 2016) emerges as the first gene potentially co-expressed with *STK*, independent of sample clustering. The cross between *STK* co-expressed genes and downregulated genes in *stk*, seem to further support the idea that *AGO9* can be a *STK* target. On the other side, co-expressed genes may reflect an interaction relation as evidenced by the fact that *SHP2*, known to act with *STK* to promote ovule identity (Pinyopich *et al*., 2003), comes up as a *STK* co-expressed gene, when considering only floral samples.

The fact that *REM24* wasn't in the list of *STK* co-expressed genes, supports the suggestion that *REM24* could be an indirect target. Yet, *AT2G19910* (RNA-dependent RNA polymerase family protein) upregulation in *stk* and potential co-expression with *REM24* indicates that both *STK* and *REM24* may regulate or be involved in *RDR*-dependent pathways which are known to be important for ovule development (Olmedo *et al*., 2010; Su *et al*., 2017).

The co-expression analysis, regarding *STK* and *REM24* are summarized in Fig. 41. The functions related to the co-expressed genes are highlighted showing the potential involvement of *STK* and *REM24* in those processes. It is possible to observe the overlap of potential functions between *REM24* and *STK*.

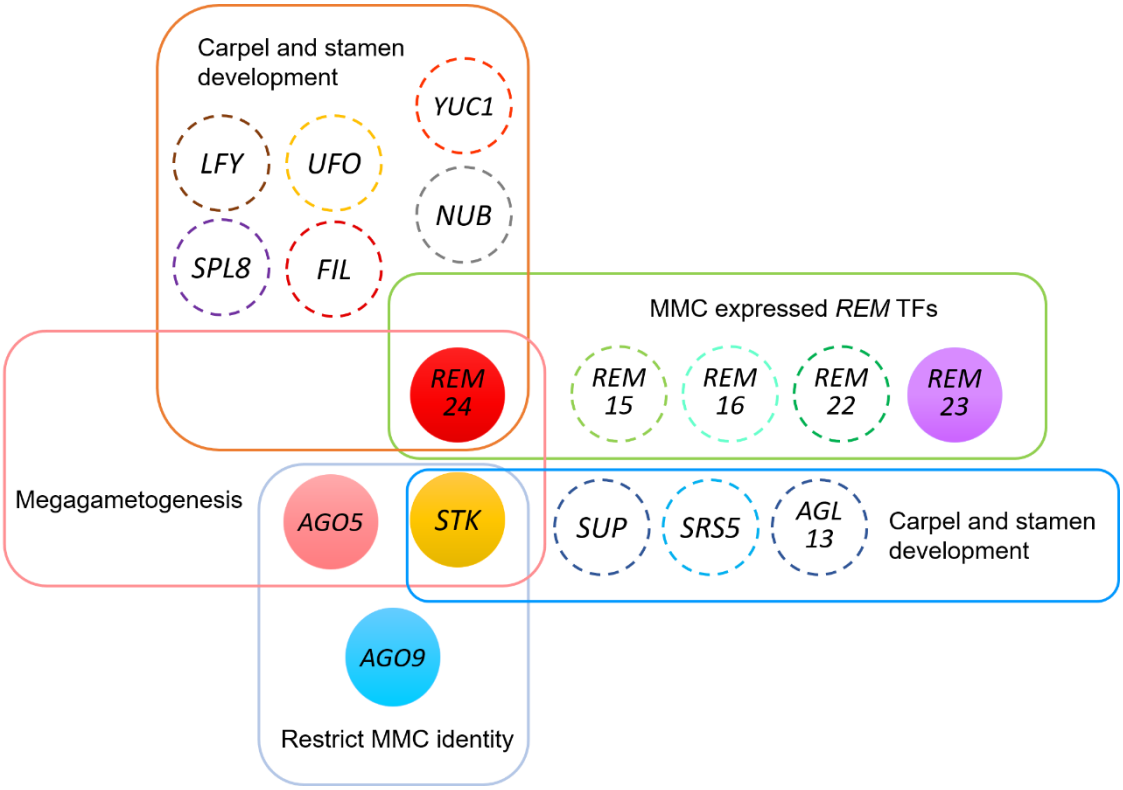

Fig. 41 – *STK* and *REM24* co-expression network. *STK* and *REM24* may share functions in megagametogenesis, carpel and stamen development and in MMC identity. Each square encases some of the genes found to be co-expressed using Araport or through the PCW tool with *STK* or *REM24*. The functions are described according to the functions of the genes in each square. *AGL13 – AGAMOUS-LIKE 13; AGO5 – ARGONAUTE 5; AGO9 – ARGONEUTE 9; FIL – FILAMENTOUS FLOWER; LFY – LEAFY*; MMC – Megaspore Mother Cell; *NUB – NUBBIN; REM – REPRODUCTIVE MERISTEM; SPL8 – SQUAMOSA binding PROTEIN-LIKE 8; SRS5 - SHI-RELATED SEQUENCE 5; STK – SEEDSTICK; UFO – UNUSUAL FLOWER ORGANS; YUC1 – YUCCA1.*

4.1.5. qPCR assay to confirm *stk* RNA-seq indicated targets

AGO9 and *FLA20* were evaluated by qPCR to understand if the expression of these potential targets was deregulated in *stk* as predicted by the RNA-seq.

Although *AGO9* known functions are related with early ovule formation, it seems that its highest level of expression occurs at later stages of development. Its expression pattern is very similar to the *STK* pattern, showing that *AGO9* can be regulated by *STK* throughout ovule development. *AGO9* absolute expression level was somewhat constant in *stk*, while in WT increased with development. No statistical differences were found, but that could be

because the standard error verified for WT was large. For example, in the stage 12 the *p*-value for the difference of *AGO9* mRNA level in *stk vs* WT was 0.05.

FLA20 could be positively regulated by *STK*, because *STK* and *FLA20* are expressed in the nucellus and *FLA20* was downregulated in the *stk* mutant. But like *REM24*, *FLA20* could be an indirect target, since *FLA20* was upregulated in the MMC, where *STK* is absent. Regarding the qPCR, the results pointed that *FLA20* wasn't deregulated in the *stk* inflorescence. The absolute expression level of *FLA20* was much higher in *stk* than in WT for the sample stage 1-9 but the variability among replicates, resulting in the large standard error, may explain the lack of differences detected. However, the non-significative FDR for *FLA20* in *stk* RNA-seq is in accordance with the lack of deregulation. *FLA20* was chosen to be analysed by qPCR, to the detriment of other targets, because of the known involvement of AGPs in reproduction (discussed ahead).

4.2. *REM24* expression pattern during ovule development

4.2.1. Confirming the nature of the mutant line *rem24*

rem24 mutant was reported as a *knock-down* line (Mantegazza *et al*., 2014), therefore it was necessary to confirm the downregulation. Moreover, to understand the flower stages where the downregulation could be relevant, *REM24* qPCR was performed. The transcript profile of *REM24* expression in WT flowers at different developmental stages followed what was predicted by e-FP browser and the PCW tool. Analysing the transcript abundance of the samples 1-7 and 8-9, the high level of expression observed for sample 1-9 should be majorly due to high expression in the floral meristem and flower primordia (stage 1-7); when ovules arise (stage 8-9) the transcript abundance decreases but it is still high. This signifies that *REM24* is mostly expressed before ovule initiation, perhaps to allow ovule initiation. Accordingly, the regulation of *REM24* by *STK* should occur only when ovules arise.

The qPCR experiment showed that *REM24* expression level during flower development wasn't altered in *rem24*. The absolute gene level in *rem24* was very similar to what was verified in WT, therefore differences due to sample variability shouldn't account for the lack of *REM24* downregulation in the mutant. The fact is that the T-DNA insertion in this line was in the 3'UTR of the gene (Mantegazza *et al*., 2014). Perhaps, the insertion would have some effect in the first generations of the mutant line, but that effect was lost; especially because the *rem24* seeds used here were descendants from Mantegazza *et al*. (2014) work. The specificity of the qPCR primers was verified by sequencing of the amplified products, and the consensus sequence was aligned against the Arabidopsis genome (BLAST) and the

only match was *REM24*. Therefore, the primer pair mustn't amplify other *REM* TFs, which could artificially increase *REM24* expression level.

Technical problems didn't allow to obtain the qPCRs results before the phenotypic characterization started. Unlike what was expected the mutant revealed WT expression of the target. Despite continuing the study of this line, a line with a T-DNA insertion in the first intron (WiscDsLoxHs200_02A) was ordered and the seeds sown. The importance of the first intron for this gene is supported by the fact that the T-DNA insertion in *vdd* is located in the first intron, and the mutation is lethal in homozygosity (Matias-Hernandez *et al*., 2010). Nonetheless it wasn't possible to obtain mutants for this line in time. If gene expression isn't altered also in this line, a RNAi line will be constructed. *REM24* is a promising gene involved in ovule development and the analysis performed here will be employed in the new mutants, now in a more effective manner.

4.2.2. *REM24* marker lines and *in situ* hybridization

The two marker lines were constructed to understand whether the first intron has any *cis*-regulatory sequences. The presence of CArG boxes (with the maximum of two mismatches) was detected in this region of *REM24* nucleotide sequencing (data not shown), indicating the putative binding of MADS TFs. Using phylogenetic footprinting and reporter gene analysis it was determined that the large second intron (3 kb) of *AG* possess six *cis*-regulatory elements necessary for its function (Hong *et al*., 2003). Despite the indications of the importance of the introns for correct gene expression, a construct harbouring 1022 bp upstream the predicted start codon of *REM22* and without the first intron (which is similar-sized to *REM24* intron) shows a comparable expression pattern to the one obtained with RNA *in situ* hybridization (Romanel *et al*., 2011). Therefore, it would be interesting to comprehend if *REM24*, or other *REM* TFs (like *REM21*, *23*, *25* which present a similar first intron), have important *cis*-regulatory elements in that region.

Regarding the *in situ* hybridization, the dot blot worked, indicating the success of transcription and incorporation of the labelled UTP but the *in situ* technique didn't work probably because the protocol needs to be optimized for the robot used.

In situ hybridization for *REM15* and *REM16,* potentially co-expressed with *REM24*, show that these TFs are expressed in the MMC of WT ovules and *REM22,* a putative *REM24* homolog (Mantegazza *et al*., 2014), is expressed in the ovule primordia (Wynn *et al*., 2011). Considering the time-line of expression detected for *REM24* by qPCR and according to other RNA *in situ* hybridization performed for closely related *REM*, it is plausible to assume that *REM24* is indeed expressed in the MMC, besides being expressed in the microsporocytes.

4.3. *rem24* phenotype during ovule development

4.3.1. Checking the presence of abnormal nucellar cells – clearing method

Analysis of cellular volume during early ovule development established that, in general, the MMC has a central position in the nucellar dome and it is surrounded by smaller nucellar cells (Lora *et al*., 2016). Using clearing techniques, it was established that only 3 to 6% of WT ovules appear to harbour enlarged nucellar cells, with a similar size to the MMC (Schneitz *et al*., 1995; Olmedo-Monfil *et al*., 2010; Zhao *et al*., 2017). Likewise, the emergence of higher frequency of enlarged nucellar cells in the ovule is abnormal and it can be assessed using a clearing technique.

It was possible to clearly distinguish ovules with enlarged nucellar cells in *rem24* and *stk*. The analysis of the frequencies of each morphology wasn't statistically different between genotypes. When observing WT cleared ovules, it was quite easy to distinguish the MMC by its prominent larger nucleolus. The surrounding nucellar cells usually didn't seem to have this kind of prominent nucleolus and when present their nucleolus was smaller. Ectopic MMC-like cells in *rbr1-2* develop by mitosis, and their size seem similar to that of the rest of the nucellar cells (Zhao *et al*., 2017). For that reason, the category MMC + small nucleolus was described as ovules where it was possible to observe the presence of the MMC nucleolus and a small nucleolus on its side. This included ovules where the MMC was sided by enlarged or small subepidermal nucellar cells which showed a prominent nucleolus. This category was described as such to avoid the subjectivity associated with categorizing the size of the cell next to the MMC. It was assumed that the percentage of ovules with WT subepidermal nucellar cells with a prominent nucleolus was similar in every genotype and that percentage would increase in an abnormal situation. Since 35% of WT ovules showed MMC + small nucleolus morphology, against the usual 3% of WT ovules showing enlarged nucellar cells, the category "MMC + small nucleolus" doesn't translate the percentage of ovules with enlarged nucellar cells. Therefore, it wasn't possible to confirm the differences observed for *stk* previously, which should have served as a positive control (Gatti, 2015). Concluding, it is plausible to conceive that the frequency of ovules with WT sub-epidermal cells with a prominent nucleolus decreases as the frequency of ovules with enlarged nucellar cells increases. To confirm this hypothesis, analysing the phenotype of *ago9* or *rdr6* mutant ovules based on the same principles and performing the analysis on all the genotypes but considering the cell size may resolve the problem.

Considering the analysis performed with mature ovules, it wasn't observed the development of a second embryo sac or an evident tetrad of megaspores. If the enlarged nucellar cells acquire MMC or FG identity, the results indicate they shouldn't divide further and constitute

major reproductive structures, as observed for *ago9* and *rdr6-11* (Olmedo-Monfil *et al*., 2010). For *rem24*, the results are in agreement with the lack of downregulation of the gene.

4.3.2. Analysis of callose deposition during megasporogenesis – aniline blue staining

During megasporogenesis, initially, callose accumulates around the MMC; after the division of the MMC, the callose is present on the newly formed cell plates; when the micropyle-most megaspores degenerate they also accumulate callose (Lora *et al*., 2016).

The aniline blue patterns in *rem24* or *stk* ovules at MMC stage weren't significantly different from the WT patterns observed. In *ago9-3* ovules the authors affirm that the enlarged nucellar cells present the typical accumulation of callose of the pre-meiotic MMC (Olmedo-Monfil *et al*., 2010). The clearing method wasn't very good in allowing to understand the internal morphology of the ovule. Analysing just the aniline blue deposition didn't allow to distinguish enlarged nucellar cells in ovules at MMC stage. Two cells with the same pattern of staining would be hard to distinguish without relying on the bright-field image. If the enlarged nucellar cells didn't possess any callose, the MMC would be pushed to the side, and the pattern would also be dislocated. Unfortunately, the position of the MMC aniline blue staining wasn't scored. Therefore, it is unclear whether the enlarged nucellar cells did or didn't accumulate callose. However, if present, the enlarged nucellar cells didn't seem to be isolated from the rest of the cells of the ovule or divide, because the aniline blue pattern observed was very similar between the three genotypes.

The three categories classified may translate a difference in development. Perhaps the callose deposits around the MMC in a small punctate pattern, and its starts to accumulate in bigger puncta as the MMC prepares to enter meiosis.

Analysing the tetrad stage allowed better resolution of the cell constitution of the nucellus. In the three genotypes it was possible to find enlarged nucellar cells that persisted until that stage that distorted the MMC position, pushing it to the side. Again, no especial callose deposition was observed in those enlarged cells, confirming that they don't divide. The lack of division doesn't immediately mean that the cells do not acquire MMC or FG identity. The abnormal nucellar cells of *ago9-3* that initially accumulate callose as the MMC, at the tetrad stage, don't stain for callose but acquire FG identity as shown by the expression of *pFM2:GUS* (Olmedo-Monfil *et al*., 2010). Additionally, in *tex1-5* mutant extra MMC cells (that express *pKNU:YFP*) form in the ovule primordia. In ovules at the tetrad stage, the ectopic cells don't stain with aniline blue, but divide mitotically to form an unreduced embryo sac (Su *et al*., 2017). Although the enlarged cells didn't divide further and didn't seem to

form any identifiable structures in *rem24* or *stk* ovules, they may still have MMC or FG identity, but the mutation is not sufficient to induce the meiotic or mitotic divisions of the abnormal cells.

Considering that the GO terms for the genes downregulated in the *stk* inflorescence were related to cell division and cell plate formation, it would be interesting to evaluate in depth potential alterations in meiotic divisions in *stk* ovules at tetrad stage. In fact, although no counting was performed, it was possible to observe abnormal aniline blue staining on *stk* ovules at tetrad stage that wasn't verified on WT ovules in the same stage. However, this needs further validation.

Although *stk* may show some callose deposition alterations at meiosis, the lack of differences observed in *rem24* at the MMC or tetrad stage are in accordance with *REM24* WT expression in *rem24*.

4.3.3. Characterising the identity of the enlarged nucellar cells

4.3.3.1. Crosses with marker lines

The clearing or aniline blue staining experiments do not clarify the identity of the abnormal cells present in the ovule. As depicted previously, the enlarged nucellar cells may have MMC, as the case of *tex1-5* (Su *et al*., 2017), or FG, as the case of *ago9* (Olmedo-Monfil *et al*., 2010), identity without possessing any distinct callose deposition pattern. Crossing the mutant plants with marker lines which allow this identification would clarify the mutant phenotypes.

The crosses were performed but, it was only possible to observe the first generation in time. 30.29% of *ago9/+* ovules display the abnormal enlarged nucellar cells phenotype, a smaller frequency than the homozygous mutant (Olmedo-Monfil *et al*., 2010). Likewise, it seemed reasonable to analyse the first generation of the crosses. *pKNU-YFP* is expressed in the nuclei of the MMC and not in the surrounding cells of the ovule (Tucker *et al*., 2012). Therefore, it was previously used to determine if abnormal cells present in ovule primordia acquire MMC identity (Su *et al*., 2017; Zhao *et al*., 2017). Even if the phenotype was absent in *stk*/+ or *rem24*/+ plants, the small percentage of ovules that present enlarged nucellar cells in WT could potentially express the YFP if they had MMC identity. The ovules were observed fresh to preserve the fluorescence; therefore, it wasn't possible to clearly detect the enlarged nucellar cells in the bright-field images. Thus, the hypothesis that *rem24/+* or *stk/+* presented enlarged nucellar cells in a higher frequency than WT wasn't demonstrated. *KNU* was expressed ectopically in one WT ovule, demonstrating that in WT ovules a second MMC may develop, validating the method. It is established that 3% of WT ovules harbour

enlarged nucellar cells, however the frequency of WT ovules expressing *pKNU-YFP* was 0.2%. The fact is the construct wasn't fully penetrant, so it is possible that not all the ovules with enlarged nucellar cells were expressing the construct. Other option would be that not all the enlarged nucellar cells gain germline fate. No ectopic *pKNU-YFP* expression was observed for *stk*/+, indicating that the heterozygous plants must have a WT-like frequency of ovules with enlarged nucellar cells. In the case of *rem24*/+ plants, this can also be explained by *REM24* expression at WT levels.

In the *dyad* mutant, meiosis stops after the first division in 75% of ovules (Mercier *et al*., 2001). As a preliminary study, *dyad* plants expressing p*KNU-YFP* were analysed. It was possible to observe the expression of the YFP in the spores long after the ovule stage when the dyad is formed, indicating that *KNU* is expressed in the spores and not only inherited (Supplemental Fig. 2). Accordingly, *rem24*/+ *pKNU-YFP*/+ and *stk*/+ *pKNU-YFP*/+ ovules express YFP in the FG nuclei of few ovules. These results indicate that the expression of p*KNU-YFP* identifies germline cells and not just the MMC. Therefore, when analysing the identity of ovule nucellar cells it is a good approach to use *KNU* marker line in combination with others that identify the FG. In the context of this work, combining the expression pattern observed in the p*KNU-YFP* crosses and the expression profile obtained with the *pFM1-GUS* crosses would better distinguish cellular identity.

GUS is expressed under the *FM1* promoter only in the FM and the resultant mitotic products, during megagametogenesis (Huanca-Mamani *et al*., 2005) and it has been previously used as FM/FG1 marker line (Olmedo-Monfil *et al*., 2010). If the enlarged nucellar cells didn't acquire MMC identity they could acquire FG identity, therefore *rem24* and *stk* were crossed with *pFM1-GUS* marker line. The enzymatic activity was detected in the FM/FG1 and never in enlarged nucellar cells in *rem24*/+ and *stk*/+. Again, *REM24* expression in the homozygous mutant may lead to the absence of differences. Around 40% of the *rem24*/+ or *stk*/+ ovules showed GUS staining. Considering that *pFM1-GUS* is a haploid marker and because the plants are heterozygous for the marker, it should be expressed in around 50% of the ovules. This means that *pFM1-GUS* was expressed in aproximatly 80% of FM harbouring the transgene, a higher frequency than what was obtained for *pKNU-YFP*. Ectopic expression of *pFM1-GUS* wasn't detected in any of the genotypes, therefore the question remains: the gametophytic identity isn't established in the enlarged nucellar cells or in heterozygosity the mutants don't display the phenotype? In some ovules (*rem24/*+ and *stk/*+) the stain generated by the enzyme spread out from the FM and into the nucellus. The enzymatic cleavage of X-gluc results in the production of soluble indoxyl which becomes insoluble indigo when it is oxidized and dimerized (Jefferson, 1987; Lojda, 1970). When this process is not rapid enough the soluble product may diffuse between cells (Mascarenhas and Hamilton, 1992). To minimize the background staining an equimolar ratio of potassium

hexacyanoferrate(II) trihydrate, and potassium hexacyanoferrate(III) is added to the X-gluc solution (Lojda, 1970). Perhaps higher concentration of these components would resolve the diffusion of the soluble product. Moreover, a WT control would be necessary.

The fact that no ectopic expression of the markers was found in *stk*/+ may be a cause of the absence of phenotype in heterozygosity. The presence of phenotype wasn't possible to verify in the mutant crosses. Accordingly, the identity of the enlarged nucellar cells is still to be clarified and the analysis of homozygous mutant ovules is of extreme relevance.

4.3.3.2. Immunolabelling of AGP and callose epitopes

AGPs are enigmatic molecules involved, among other processes, in many aspects of plant reproduction (Pereira *et al*., 2016). They are hydroxyproline-rich glycoproteins connected to the plasma membrane via a glycosylphosphatidylinositol (GPI) anchor (Schultz *et al*., 2002).

Early immunolocalization studies placed AGPs on the pathway where pollen tubes grow until reaching the ES (Coimbra *et al*., 2007). An example of that is *JAGGER*/*AGP4* predicted to be localized in the stigma, in the transmitting tract of the pistil, and in the micropylar region of the integuments. In *jagger*, two pollen tubes can be attracted to the same ovule because the persistent synergid doesn't degenerate upon fertilization (Pereira *et al*., 2016b). Moreover, AGPs function in early female gametophyte development. *AGP18* is necessary for the initiation of mitotic divisions in the FM, since null expression of *AGP18* cause the arrest of ovule development at FM stage (Acosta-García and Vielle-Calzada, 2004). Accordingly, the overexpression of *AGP18* leads to the survival of the micropylar-most megaspores which acquire FM identity (Demesa-Arévalo and Vielle-Calzada 2013). Also, *AGP22* and *AGP24* must be important for female germline specification. In the ovules, *AGP22* is expressed in the epidermal nucellar cells surrounding the MMC and *AGP24* is expressed in the FM. Additionally, transcriptomic analysis revealed that AGPs and FLAs represent a high proportion of the cell-wall related genes expressed in Arabidopsis, rice and *Hieracium* ovules (Tucker and Koltunow, 2014). These examples demonstrate the potential of AGPs serving as communication signals during reproductive development. Likewise, studying their distribution when reproductive development is impaired is of relevance.

In this work, it was shown that JIM13 recognizes AGP epitopes in the MMC cell wall of *rem24* ovules. Unlike desired, it wasn't feasible to produce sections of WT ovules at MMC stage in time. However, formerly it was shown that JIM13 doesn't bind AGP epitopes in the MMC cell wall of Arabidopsis ovules, but only when *AGP18* was overexpressed in that cell (Demesa-Arévalo and Vielle-Calzada, 2013). Accordingly, it was recently reported that JIM13 or JIM8 (which recognize other AGP sugar epitopes) monoclonal antibodies don't

label AGPs in the MMC cell wall (Lora *et al*., 2016). It is not known which AGPs does JIM13 recognize; nonetheless, 30 AGPs were found upregulated in the MMC relative to the nucellus (Schmidt *et al*., 2011) (Supplemental table 7). *AGP18* was slightly upregulated 0.1-fold change in the MMC. Curiously, *AGP4* is the fifth AGP more upregulated in the MMC, with a 0.9-fold change. These findings allow to speculate whether AGP expression or processing could be altered in *rem24* leading to their detection by JIM13. The hypothesis that technical issues may reflect this abnormal staining wasn't discarded. Additionally, repetition of this analysis with a *rem24 knock-out* line is essential, therefore, more studies are required.

Regarding the labelling observed at tetrad stage, other works related to AGP immunolocalization mention JIM13 labelling firstly in the WT FM (Coimbra *et al*., 2007; Demeso-Arévalo and Vielle-Calzada, 2013), therefore, JIM13 has been recognized as a gametophytic marker. AGP labelling by JIM13 in the cell walls of the megaspores has only been reported when *AGP18* is overexpressed causing the megaspores to skip the degeneration step (Demeso-Arévalo and Vielle-Calzada, 2013). On the other hand, JIM8 reacts to AGP epitopes present in the megaspore cell walls (Lora *et al*., 2016). Here we show that AGP epitopes were recognized by JIM13 in the cell walls of the megaspores in WT and *rem24* ovules. When the micropylar-most megaspores degenerate, the labelling is specific to the FM. The enlarged nucellar cells in WT or *rem24* ovules didn't present any labelling, thus, that they shouldn't possess gametophytic identity. On the other hand, these results indicate that WT megaspores express AGPs with sugars recognized by JIM13, and maybe megaspore degeneration is accompanied by AGP or their sugars degradation or turnover so that only the FM is labelled by JIM13.
Callose localization in the *rem24* MMC cell wall, and WT and *rem24* megaspore cell plates are in accordance to the WT aniline blue pattern obtained. Again, enlarged nucellar cells didn't present any labelling and ovules with two sets of tetrads were never observed, indicating that these cells do not enter meiosis. To note that it wasn't possible to find sections of ovules at MMC stage with enlarged nucellar cells due to time restrictions (not due to their absence). Consequently, we can't determine whether those cells would have any specific labelling at that time point that would be clearer to analyse than via aniline blue staining, as discussed previously.

Considering that *rem24* isn't a *knock-down* mutant, a WT control is essential, but perhaps the T-DNA insertion has a complex effect, and in this *rem24* insertion line, gametophytic lineage identity may be acquired earlier as demonstrated by the recognition of AGP

epitopes by JIM13 in the MMC and megaspores (which still degenerate). On the contrary, the enlarged nucellar cells do not gain this identity, as observed for WT.

4.4. Evaluating *REM24* and *STK* relation

4.4.1. Obtaining a double mutant *rem24 stk*

Although *rem24* T-DNA insertion line didn't show any downregulation of the gene, something may by altered in the mutant as shown by the lethality of the cross *stk* x *rem24* and the increased size of *rem24* x *stk* seeds.

Gene expression in the seed is partially biased, genomic imprinting occurs. Imprinted genes are genes in which the allelic variant from one of the progenitors is preferentially expressed over of the equivalent allele of the other progenitor (Gehring, 2013). In the case of a Maternally Expressed Genes (MEGs), if WT pollen fertilizes ovules mutated for that gene, seed development may be affected. This results because the gene won't be expressed since the maternal copy is mutated and the paternal copy isn't naturally expressed. But in the reciprocal cross that shouldn't be verified since the gene will be expressed from the maternal allele.

Endosperm-derived cDNA analysis revealed that *STK* is a putative MEG. In this study, *REM24* wasn't identified as an imprinted gene (Hsieh *et al*., 2010). If *STK* is a MEG or affects the expression of a MEG, *rem24* x *stk* should lead to a WT seed because *STK* isn't mutated in the maternal side from which it is expressed. This was not verified. On the other hand, *stk* x *rem24* would show an aberrant phenotype. Although this was true, since *rem24* presented *REM24* expression at WT levels, substituting *rem24* by WT pollen should result in the same phenotype, which didn't occur regarding the evident seed abortion. These results indicate that *STK* may not be an imprinted gene, and that the T-DNA insertion in *rem24* may have some effect on these crosses.

The unequal contribution of maternal and paternal genome has consequences for seed development. Generally, when maternal genomic contribution is higher the seed size decreases. Reversely, when paternal genomic contribution is higher the seed size increases. These phenotypes are associated with endosperm early arrest or prolonged development, respectively. When parental imbalance is overwhelming it may lead to seed abortion (Tiwari *et al*., 2010). The *dyad* allele affects only female fertility. The few fertile ovules from *dyad* originate unreduced female gametes leading to the formation of triploid shrunken seeds, related to the increase of maternal genomic contribution. Portion of *dyad* seeds are larger than WT, however they are diploid and the authors didn't discuss this phenomenon. Impaired female meiosis in *stk*, shouldn't explain *stk* and *rem24* reciprocal

crosses, because the phenotype should be verified also in autopollinated *stk* pistils, which doesn't occur. Moreover, the abortions were observed when *rem24* was the pollen donor, and it is known that *REM24* is expressed in stamen primordia (Mantegazza *et al*., 2014) while *STK* is absent from the male organs. Thus, the T-DNA insertion may affect some aspect of pollen development in *rem24*. Concluding, a combined effect of *STK* absence and *rem24* T-DNA insertion should account for the defects observed.

4.4.2. qPCR analysis of *STK* expression and *REM24*

Unlike what was detected in the *stk* RNA-seq, *REM24* transcript level was upregulated in the *stk* flowers at the stage 10-11, which harbour ovules at megasporogenesis, and 12, flowers containing ovules at megagametogenesis. Moreover, it may have been possible to find an upregulation of *REM24* in *stk* flowers at the stage 13-15 if the standard error was smaller, since the fold change was 2.8 compared to WT. At the stage 1-9 it was detected a statistical difference between *rem24* and *stk* which should be due to the decreased *REM24* expression in *rem24* and slight increase of *REM24* expression in *stk* at that stage. The standard error was large for the samples stage 1-9, perhaps the variability in expression level between the replicates explains the lack of statistical downregulation of *REM24* in *rem24*, relative to WT at that stage. However, even if detected the fold change would be 0.7 much different from the 2.6-fold downregulation detected previously (Mantegazza *et al*., 2014). On the contrary, in the flowers at the stage 10-11 the difference observed between *rem24* and *stk* should be due to *REM24* upregulation in *stk*, because *REM24* is expressed at WT levels.

STK expression pattern revealed that its transcript level increases along flower development, probably because the number of cells were *STK* is expressed increases during development with the increase in ovule size. The absence of *STK* expression in the sample stage 1-7 (flower meristem and flower primordia without ovule primordia) is in accordance with the fact that *STK* is specifically expressed in ovules (Mizzotti *et al*., 2014). A peak in *STK* expression in WT flowers was registered for flowers at the stage 8-9. On the one hand, it is possible that *STK* expression becomes more relevant in those flowers because ovules arise and the MMC forms, consistent with the fact that when *STK* is absent the ovules present enlarged nucellar cells (Gatti, 2015).
stk is described as a *knock-out* mutant (Mizzotti *et al*., 2014). In this work it was verified that despite a downregulation was detected, the gene was still expressed. The downregulation occurred for stages 12 and 13-15, the fold change of expression was 0.3 and 0.2x, respectively. Moreover, it may be possible that *STK* is downregulated in flowers at the stage

10-11 because a statistical difference was observed between the absolute expression level between *rem24* and *stk*. At that stage, *STK* absolute expression level was reduced compared either to WT or *rem24*, and *STK* expression level was similar between *rem24* and WT (and not statistically different). Likewise, the large standard error verified for WT, perhaps didn't allow the finding of differences between *stk* and WT.

STK wasn't deregulated in *rem24*. At the stage 12 is detected a difference in expression when comparing *rem24* to *stk*, which should be due to *STK* downregulation in the *stk* mutant. Moreover, despite *STK* downregulation in *stk* the flowers at the stage 13-15, the standard error in *rem24* was very large, not allowing to detect differences between *rem24* and *stk*. The absence of deregulation in *rem24*, is in accordance to the hypothesis that *REM24* acts downstream *STK*. However, considering *REM24* WT expression level in *rem24*, it is normal to think that the T-DNA insertion in *rem24* may not cause expression defects in the plants.

4.5. A molecular pathway involving *REM24* and *STK*: qPCR analysis of relevant genes

In order to characterise the ovule network involving *REM24* and *STK,* several relevant genes were evaluated by qPCR. Important gene expression differences were found in *stk*. No alterations were expected for *rem24* according to *REM24* expression in the mutant. However, the seed phenotype observed when performing the reciprocal crosses *rem24* x *stk*, lead to the search of molecular cues that could explain the effect of the T-DNA insertion, and, in fact, point alterations were discovered. The potential genetic interactions are summarized on Fig. 42.

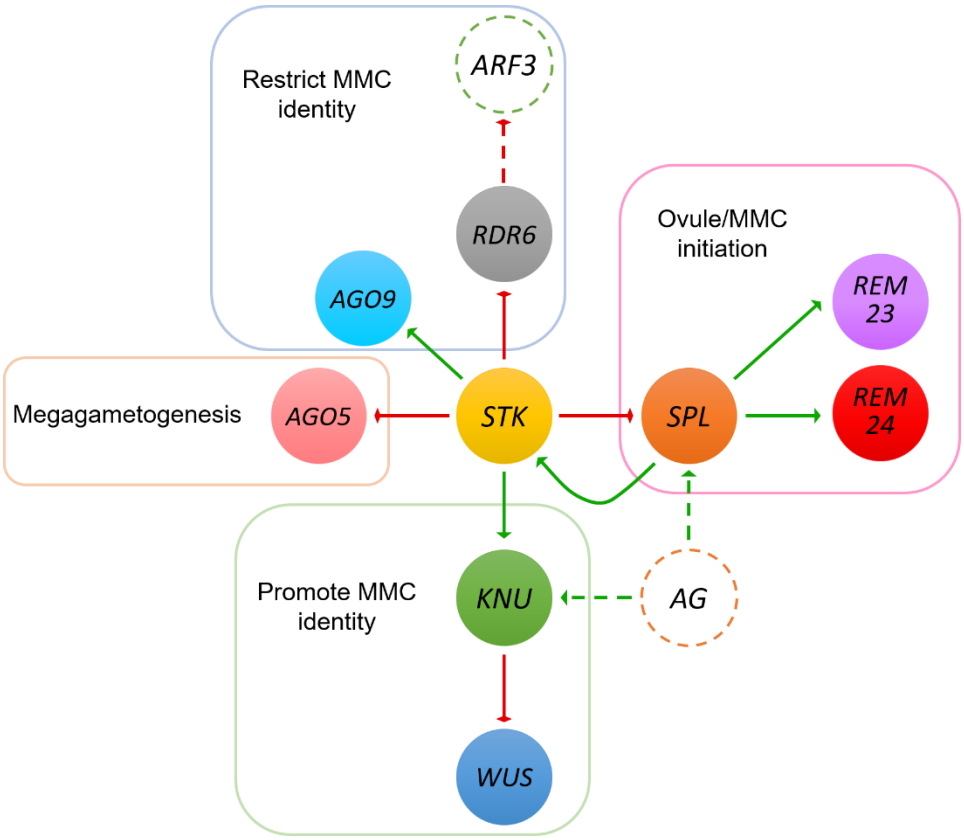

Fig. 42 - Gene network revealed by quantitative PCR analysis of relevant genes on *stk*. It is evidenced *SEEDSTICK (STK)* involvement in early ovule development. Although not tested, *STK* transcriptional regulation over *REPRODUCTIVE MERISTEM24 (REM24)* and *REM23* may be mediated by *SPOROCYTELESS (SPL)*. It has been previously proposed that *SPL* expression is promoted by *AGAMOUS* (*AG*) in anthers (Ito *et al*., 2004). *STK* may promote Megaspore Mother Cell (MMC) identity and support its development by indirectly promoting *KNUCKLES (KNU)* expression, leading to *WUSCHEL (WUS)* repression in the MMC. It has been previously reported that *AG* represses the expression of *WUS* through the transcriptional activation of *KNU* in the floral meristem (Sun *et al*., 2009). STK may function in megagametogenesis by repressing *ARGONAUTE5 (AGO5*). *STK* may be also implicated in restricting MMC identity in the surrounding nucellar cells by promoting *AGO9*. *RNA DEPENDENT RNA polymerase 6 (RDR6)* represses *AUXIN RESPONSIVE FACTOR3 (ARF3)* and this pathway restricts MMC identity (Su *et al*., 2017). Therefore, the upregulation of *RDR6* in *stk*, shouldn't be the cause of *stk* phenotype. Filled circles correspond to genes tested in this work, while dashed circles are genes previously known to regulate the target expression. The red arrows show the putative repression of a gene by another. The green arrows illustrate genes putatively transcriptionally activated by another. Dashed arrows indicated previously studied genetic interactions.

4.5.1. *STK* putative targets

Initially it was thought that *AGO9*, *FLA20* and *REM24* could be part of a *STK*-controlled pathway, since they showed at least a partial overlapping expression pattern with *STK* and were downregulated in *stk* (as revealed by the bioinformatic analysis). Therefore, if they were acting in the same pathway, *AGO9* or *FLA20* could act downstream *REM24*.

AGO9 absolute expression level in *rem24* was very similar to WT, which was translated by the lack of statistical differences. In *stk, AGO9* mRNA level in flowers at the stage 10-11 wasn't statistical different from the WT. However, the decreased *AGO9* absolute expression in *stk* flowers at the stage 10-11, was shown by the statistical difference between *rem24* and *stk.* Since *AGO9* expression level in *rem24* was similar to WT, and the standard error for *rem24* was smaller. The statistical difference among *stk* and *rem24* flowers stage 12 should account for the downregulation verified for *stk* (against WT). Despite the great differences in absolute gene expression between *rem24* to *stk* flowers at the stage 13-15, and the small standard errors, no statistical differences were found. One can argue that *AGO9* was downregulated in *stk* (as verified in the *stk* RNA-seq) however the variability among replicates didn't allow the finding of those differences, relative to WT. On the contrary, in *rem24*, *AGO9* absolute expression level was WT-like.
FLA20 was found in the same list as *REM24* and they showed similar transcript abundance profiles. No statistical differences were observed between the *rem24* and WT, indicating that if *rem24* present any molecular defects, those don't include *FLA20* expression.

4.5.2. Genes involved in ovule development

WUS, the homeobox transcription factor, is vital for ovule development. Despite being expressed in the nucellar cells surrounding the MMC, and never within the MMC, *WUS* participates in MMC formation. In *wus-1* mutant, 9 to 12% of ovules don't develop an MMC and in the remaining ovules, the MMC arrests its development. Additionally, evidences indicate that *WUS* time-dependent repression in the MMC is required for the MMC to enter meiosis (Zhao *et al*., 2017). Considering that the enlarged nucellar cells don't enter meiosis, it was speculated if *WUS* is expressed in these cells; if so, perhaps an upregulation of *WUS* was verified in the mutants compared to WT.
In situ hybridization revealed that *WUS* mRNA is strongly present in ovules at stage 2-II and 2-III, until the stage 3-I, afterwards its mRNA is absent from the ovule (Groß-Hardt *et al*., 2002), like what was observed in *WUS* WT expression pattern.
Although *WUS* absolute expression level was higher in *stk* and *rem24* in stage 10-11 and 12 relative to WT, a statistical difference was only verified for *rem24* flowers stage 10-11

with an important 2.4-fold change. For this stage, *WUS* absolute expression level was very similar between *stk* and *rem24*. It is possible that the large standard error verified for *stk* masks the increase in *WUS* expression in the mutant. Moreover, the similarity of the level of expression in *rem24* and *stk* flowers at the stage 12 (indicated by the lack of statistical differences) could indicate that the upregulation maintains at that stage, but no differences were found between the mutants and the WT, probably due to the large standard error.

RDR6 functions in the RdDM pathway, in the biogenesis of ta-siRNAs which repress *ARF3,* preventing the formation of extra MMCs (Su *et al*., 2017). In 43.3% of *rdr6-11* ovules subepidermal nucellar cells enlarge and acquire FG identity. This phenotype is identical to *ago9* phenotype, suggesting that *RDR6* and *AGO9* act in the same pathway (Olmedo-Monfil *et al*., 2010). Since *AGO9* could be deregulated in *stk* (as predicted by the *stk* RNAseq), it was decided to analyse *RDR6* in *stk* and *rem24*.
RDR6 function seems to be relevant for ovule initiation since its transcript abundance is higher at early stages of flower development. Interestingly, this didn't occur in the mutants, and important upregulation fold changes were detected. In *rem24, RDR6* mRNA levels were very similar to WT in the first two stages, however it was significantly upregulated in flowers at the stage 12. For *stk,* there was a general high upregulation of *RDR6,* although the large standard errors may have masked it in flowers at the stage 10-11. Despite the expression level being very different between *rem24* and *stk*, no differences were found when comparing *rem24* to *stk,* excepting in the flowers at the stage 12. Generally, *RDR6* is highly upregulated in *stk* across all developmental stages and upregulated at later stages of flower development in *rem24*. A question arises: how can *RDR6* upregulation relate to a potential phenotype associated with abnormally enlarged nucellar cells? Perhaps a compensation mechanism is triggered to try to restrict the phenotype and this involves *RDR6* action. Or *RDR6* upregulation may lead to more gene silencing, and a balance of gene expression is lost, causing the phenotype.

SPL (Schiefthaler *et al*., 1999) is a key gene responsible for ovule and MMC formation. In *spl* mutants, ovule development is arrested and the archesporial cell doesn't develop into MMC (Wei *et al*., 2015). Thus, it was important to analyse *SPL* expression level.
SPL higher expression in early flower stages and decrease along development reflects its importance in the flower meristem and in ovule formation.
The T-DNA insertion in *rem24* may be causing the *SPL* upregulation in *rem24* flowers stage 10-11. However, *SPL* may regulate *REM24* expression indirectly. *SPL* impairs microsporogenesis in a parallel manner to what is verified for megasporogenesis, in the anthers archesporial cells can't be detected (Schiefthaler *et al*., 1999). Wijeratne *et al* (2007), using a transcriptomic approach identified *REM24* in a cluster of genes

downregulated in the *spl* anthers at meiosis. An *in situ* hybridization allowed the verification of *REM24* mRNA in the microsporocytes of WT anthers. In *REM24* cluster several known meiotic genes were enriched (such as *DMC1*). The authors suggested that proteins acting downstream of *SPL*, can regulate the transcription of genes present in *REM24* cluster (Wijeratne *et al.,* 2007). It is known that male and female sporogenesis share common pathways, as evidenced by the lack of MMC and Microspore Mother Cell (MiMC) formation in *spl* (Schiefthaler *et al*., 1999), or its incorrect development in *krp4 krp6 krp7* and *rbr1-2* (Zhao *et al*., 2017), and the common changes in chromatin reprogramming (She and Baroux, 2015). Moreover, *REM* TFs, such as *REM15*, *REM16* and *REM22* are expressed in both anthers and MMC (Wynn *et al*., 2011). Put together, the data seems to point, that *REM24* could be indirectly regulated by *SPL* in the ovule. To support this is the fact that in the *stk* mutant, both *SPL* and *REM24* are upregulated. The most obvious assumption would be that *SPL* upregulation may lead to *REM24* upregulation. Knowing that *REM24* is expressed at WT levels in the mutant *rem24*, perhaps other effect associated with the T-DNA insertion is causing the miss regulation of *SPL*.

In *stk*, it was verified *SPL* upregulation in sample stage 1-9 and 10-11 with a fold change over 2x, pointing that *STK* may repress *SPL.* On the contrary to what occurs in *spl* mutant, maybe *SPL* upregulation promotes archesporial cell formation and the abnormal enlarged nucellar cells arise in the mutant. *STK* and *SPL* interaction isn't linear. *STK* is 0.79-fold downregulated in *spl* ovules at the stage 11 relative to WT (Yu *et al*., 2005). Considering that *SPL* and *STK* are expressed in the integuments and nucellus at the same time in the ovule, it is likely that *SPL* may promote *STK* expression. Concluding, in a time dependent manner, *SPL* may promote *STK* transcription, and *STK* in a feed-back loop will repress *SPL* expression.

It seems that *SPL* and *RDR6* act in opposite fashion during ovule development: while *rdr6-11* mutation leads to the development of abnormal enlarged nucellar cells (Olmedo-Monfil *et al*., 2010), the *spl* mutation leads to the lack of germline development (Schiefthaler *et al*., 1999). Additionally, in microarray data obtained from *spl* stage 11 ovules, *RDR6* isn't deregulated (Yu *et al*., 2005). As demonstrated here, both genes are expressed at that stage in WT ovules. Therefore, *SPL* and *RDR6* may function in a parallel way in ovule development. Both *SPL* and *RDR6* are upregulated in *stk*. Can *STK* regulate two pathways of ovule development, one promoting germline formation and the other preventing germline fate in the nucellar cells? Moreover, *REM24* may be part of this dual mechanism since *RDR6* and *SPL* were also upregulated in the mutant, however its involvement it's not clear since *rem24* wasn't a *knock-down*.

AGO5 was identified as potentially co-expressed with *AGO9* and *REM24*. Moreover, its biological function in reproduction has been studied making it a relevant target to assess in the mutant backgrounds. In the ovule, like *AGO9*, *AGO5* is expressed in the nucellar epidermis and it is excluded from the female germline (Tucker *et al*., 2012). However, while *AGO9* restricts the megagametogenesis pathway in the nucellar cells, *AGO5* seems to be important for the correct development of the FM into an ES.

In WT flowers, *AGO5* was expressed in a somewhat constant level across development. WT expression of *AGO5* in *rem24* relates to the absence of altered *REM24* expression.

AGO5 expression level was constantly high in *stk*. However, large standard errors verified for flowers stage 10-11 and 12 didn't allow the finding of a statistical difference. Nonetheless, *AGO5* upregulation in *stk* flowers stage 1-9 and 13-15, may indicate that *STK* repress *AGO5* expression.

KNU encodes a C2H2-type zinc finger protein (Payne *et al*., 2004). *KNU* has been used as MMC identity marker (Su *et al*., 2017; Zhao *et al*., 2017) because it is expressed in the MMC and not in the surrounding cells (Tucker *et al*., 2012). Hypothetically, if enlarged nucellar cells have MMC identity, perhaps it would be possible to detect *KNU* upregulation in the mutants.

A GUS reporter line allowed the establishment of *KNU* expression pattern in WT flowers (Payne *et al*. 2004). More specifically, *KNU* is detected in the floral meristem, in the MMC, in the meiotic products and in the cells of the ES during megametogenesis. In the anthers, *KNU* is present until anthesis (Payne *et al*., 2004). This pattern of expression is consistent to what was observed in the qPCR for WT flowers. Since *KNU* is ectopically expressed in MMC-like cells (Su *et al*., 2017; Zhao *et al*., 2017), it was hypothesized that if the enlarged nucellar cells in 47% of *stk* ovules (Gatti, 2015) had MMC identity, *KNU* would be upregulated in *stk* mutant flowers at the stage 9 to 11. Such hypothesis wasn't confirmed, no statistical differences were found between *stk* to WT.

KNU role in germline fate commitment isn't understood. Known *KNU* functions are related to meristem development. In a time-dependent manner, *AG* removes histone marks from the *KNU* promoter leading to its transcriptional activation. At the same time *WUS* is repressed causing stem cell fate termination. Since their expression domains don't overlap, the epigenetic activation of *KNU* must lead to *WUS* repression (Sun *et al*., 2009). This relation between *WUS* and *KNU* may be replicated in flower development supported by the complementary *KNU* and *WUS* expression patterns observed. Considering the potential *KNU* downregulation in *stk* and the fact that *WUS* is potentially upregulated in *stk*, maybe *KNU* isn't activated at the WT levels in the mutant causing *WUS* elevated expression. As discussed this could lead to the repression of meiosis in the enlarged cells.

4.5.3. Genes co-expressed with *REM24*

Other target gene tested was *REM23* since it is phylogenetically close related to *REM24* (Romanel *et al*., 2009). *REM* genes must be important for reproduction because almost all *REM* genes are expressed preferentially during flower and seed development (Mantegazza *et al*., 2014). It seemed reasonable to investigate *REM23* expression level in the mutants: perhaps, if *REM24* was downregulated in *stk,* as it was predicted, *REM23* would be upregulated to compensate *REM24* lack of expression, or *STK* could regulate both genes in the same manner.

REM23 expression profile in WT flowers followed the same trend as *REM24*, higher levels in the initial stages which decreased along development. However, *REM23* is expressed in much higher levels than *REM24* in all stages. Considering that the *REM* family originated from duplication events, the more restricted expression pattern of *REM24* compared to *REM23* may suggest that *REM24* has more specific functions.

The lack of *REM23* deregulation in *rem24* could be a result of *REM24* expression in the mutant. *REM23* was upregulated in *stk* flowers at the stage 12 and 13-15. This result supports the hypothesis that *STK* may regulate *REM23* in a similar manner as it regulates *REM24*. According to *in situ* hybridization experiments, *REM23* and *REM24* aren't expressed in the inflorescence meristem (Mantegazza *et al*., 2014); on the contrary, the eFP browser, the RNA-seq data from the PCW tool and the expression level of these genes in the sample 1-7 indicate that *REM23* and *REM24* may be highly expressed in the inflorescence meristem. At that stage *STK* is practically absent, so *REM23* and *REM24* most likely are controlled by other regulators, maybe explaining why *REM23* and *REM24* aren't upregulated also in *stk* sample 1-9.

The bioinformatic analysis highlighted *HSP20* (*AT5G47600*) as a potential component of *REM24* pathway since they appear to have partial overlapping expression patterns, and *HSP20* was upregulated in *stk*. Besides being expressed under stressing conditions, some small HSPs are expressed under normal conditions associated with reproduction processes (Morrow and Tanguay, 2012; Sun *et al*., 2002). Therefore, *HSP20* expression pattern was evaluated.

The WT expression profile of *HSP20* was similar to *REM24*, confirming the co-expression data.

HSP20 was upregulated in *rem24* flowers stage 13-15. A statistical difference between *rem24* and *stk* flowers at stage 12 was detected. The lack of upregulation in *rem24* flowers stage 12 (relative to WT) may be because the standard error was smaller in *stk* (28.3), relative to WT (45.5), since *HSP20* absolute expression level was higher in *rem24* than in

stk or WT. *REM24* is expressed at WT levels in *rem24*, but *HSP20* was deregulated. The T-DNA insertion may affect other aspects of *REM24* expression leading to miss regulation of *HSP20*. Although *HSP20* was significantly upregulated in *stk* RNA-seq (FDR < 0.05), that wasn't verified in the qPCR analysis. On the contrary, *REM24* showed FDR > 0.05 but it was significantly upregulated in *stk* flowers. This, partially confirms that considering the FDR in *stk* RNA-seq allowed to expand the list of potential *STK* targets.

5. Conclusion

The objective of this work was to uncover *STK*-dependent pathways acting on early ovule development and the characterisation of a potential *STK* target involved in this process.

The bioinformatic analysis performed on *stk* RNA-seq suggested that *STK*-dependent pathways may involve an epigenetic control of gene expression. This was proposed earlier, but the data collected now seems to further support the hypothesis. The RNA-seq and the bioinformatic analysis pointed that *AGO9* could be a *STK* target. By qPCR it was demonstrated that *RDR6* and *AGO5* were upregulated in *stk*. Additionally, *AGO3* was identified as a putative *STK* co-expressed gene.

Previously, ovule development was evaluated in *stk* and enlarged nucellar cells were found next to the MMC. *ago9* ovules showed an enlarged nucellar cells phenotype, that was a good indication of *STK* involvement in cellular specification during ovule formation. A putative *STK* target was *REM24*. Moreover, the evidences pointed *REM24* expression in the MMC. Consequently, *REM24* was chosen as the candidate gene focus of this study because it could be the molecular puzzle piece linking *STK* expression in the sporophytic tissues to its control of MMC development.

The analysis of *REM24* expression in *rem24*, revealed that the gene wasn't *knock down* as previously demonstrated (Mantegazza *et al*., 2014). The genetic analysis were already underway so we continued, because it wasn't possible to establish another mutant line in time. *REM24* expression profile in WT indicated that it may function in early flower development. When ovules enter meiosis, *STK* seems to repress *REM24*, suggesting that further reproductive development is accompanied by *REM24* repression by *STK*. All the indications pointed *REM24* involvement in early ovule development, so the analysis here performed will be employed on the new mutant line (already being established), ensuring that *REM24* involvement in MMC formation will be clarified.

The phenotypic analysis preformed during this work didn't completely clarified *stk* or *rem24* phenotypes during ovule development so more experiments need to be performed to fully characterize the frequency of ovules with enlarged nucellar cells in both mutants. The analysis of the aniline blue pattern during ovule development indicated that the enlarged nucellar cells do not proceed into meiosis, in both *stk* and *rem24*. The immunolocalization study performed on *rem24* showed that the enlarged nucellar cells do not present any distinctive characteristic in terms of callose deposition and presence of AGPs recognizable by JIM13, relative to WT. However, it is possible that MMC and megaspores identity may be slightly altered as shown by the JIM13 labelling on the MMC cell wall, and apparent more intense labelling on the *rem24* megaspores cell wall, relative to WT. Finally, the identity of

the enlarged nucellar cells in *stk* couldn't be defined since, in heterozygosity, the mutant may not show the phenotype.

Reciprocal crosses between *rem24* and *stk* uncovered a potential complex effect of the T-DNA insertion in *rem24* line and a possible parent-of-origin effect caused by *STK knock-out* expression.

Key genes important for ovule development were assessed through qPCR, in *rem24* and *stk*. Although *REM24* expression level wasn't different from WT in *rem24*, perhaps the T-DNA insertion causes other effects leading to somewhat altered gene expression of *WUS*, *RDR6* and *SPL*. The molecular information gathered for *STK* indicates that it may repress *SPL*, *AGO5*, *RDR6*, *REM23* and perhaps *WUS*, and promote *AGO9* expression*;* highlighting the relevant role of *STK* for initiation of ovule development. *SPL* upregulation in *stk* supports the enlarged nucellar cell phenotype reported for *stk*. Considering *AGO9* downregulation, and the absence of *KNU* upregulation in *stk,* these cells may not acquire MMC identity. Importantly, these results also point that *STK* may have regulatory functions over more *REM* TFs.

Considering all the data together, when *STK* is knocked out, it is possible that the nucellar cells are able to perceive a germline initiation signal. Thus, they enlarge just as occurs for the MMC. Yet, that signal is not sufficient to commit the cells completely to the germline fate and their development stops. Regarding *REM24*, its involvement in MMC development isn't clarified yet. Whilst, *REM24* seems to be controlled by *STK*, showing it was a good candidate to further study. Additionally, *REM24* potential functions in MMC development may be shared with other *REM* TFs, such as *REM15*, *REM22* or *REM23.*

The ovule presents an outstanding model to study cellular communication and cellular identity establishment. Although ovules' simple structure and small size, much is yet to understand. What are the signals conveyed that dictate the nucellar versus MMC identity? How is the communication established? Does callose have essential functions in this process? These questions may still take some time to answer, but now we know that *STK* must be implicated in MMC identity, probably through a non-cell autonomous pathway involving *AGO9*, *RDR6* and possibly *REM* transcription factors.

6. References

Abe M, Kobayashi Y, Yamamoto S, Daimon Y, Yamaguchi A, Ikeda Y, Ichinoki H, Notaguchi M, Goto K, Araki T (2005) FD, a bZIP protein mediating signals from the floral pathway integrator FT at the shoot apex. Science 309: 1052-6.

Acosta-Garcia G and Vielle-Calzada JP (2004). A classical arabinogalactan protein is essential for the initiation of female gametogenesis in Arabidopsis. Plant Cell 16: 2614-2628.

Anastasiou E, Kenz S, Gerstung M, MacLean D, Timmer J, Fleck C, Lenhard M (2007) Control of plant organ size by KLUH/CYP78A5-dependent intercellular signaling. Dev Cell 13: 843-856.

Appelhagen I, Lu GH, Huep G, Schmelzer E, Weisshaar B, Sagasser M (2011) TRANSPARENT TESTA1 interacts with R2R3-MYB factors and affects early and late steps of flavonoid biosynthesis in the endothelium of Arabidopsis thaliana seeds. Plant J 67: 406-419.

Baker SC, Robinson-Beers K, Villanueva JM, Gaiser JC, Gasser CS (1997) Interactions among genes regulating ovule development in Arabidopsis thaliana. Genetics 145: 1109–1124

Baroux C and Autran D (2015) Chromatin dynamics during cellular differentiation in the female reproductive lineage of flowering plants. Plant J 83: 160–176

Battaglia R, Brambilla V, Colombo L (2008) Morphological analysis of female gametophyte development in the bel1 stk shp1 shp2 mutant. Plant Biosyst 142: 643-649

Benlloch R, Kim MC, Sayou C, Thévenon E, Parcy F, Nilsson O (2011) Integrating long-day flowering signals: a LEAFY binding site is essential for proper photoperiodic activation of APETALA1. Plant J 67: 1094-102

Ben-Tov D, Abraham Y, Stav S, Thompson K, Loraine A, Elbaum R, de Souza A, Pauly M1, Kieber JJ, Harpaz-Saad S (2015) COBRA-LIKE2, a member of the glycosylphosphatidylinositol-anchored COBRA-LIKE family, plays a role in cellulose deposition in arabidopsis seed coat mucilage secretory cells. Plant Physiol 167: 711-24

Bicknell, RA and Koltunow, AM (2004) Understanding apomixis: recent advances and remaining conundrums. Plant Cell 16 Suppl. 1, S228-S245.

Borges F, Pereira PA, Slotkin RK, Martienssen RA, Becker JD (2011) MicroRNA activity in the Arabidopsis male germline. J Exp Bot 62: 1611-20

Borges F and Martienssen RA (2015) The expanding world of small RNAs in plants. Nat Rev Mol Cell Biol 16: 727–741

Bouman F (1984) The ovule. In 'Embryology of angiosperms'. (Ed. BM Johri) pp. 123–157. (Springer-Verlag: Berlin Heidelberg)

Brambilla V, Battaglia R, Colombo M, Masiero M, Bencivenga S, Kater MM, Colombo L (2007) Genetic and Molecular Interactions between BELL1 and MADS Box Factors Support Ovule Development in Arabidopsis. Plant Cell 19: 2544–2556

Brambilla V, Kater MM, Colombo L (2008) Ovule integument identity determination in Arabidopsis. Plant Signal Behav 3: 246-247

Burton RA, Shirley NJ, King BJ, Harvey AJ, Fincher GB (2004) The CesA gene family of barley. Quantitative analysis of transcripts reveals two groups of co-expressed genes. Plant Physiol 134: 224-236.

Burton RA, Jobling SA, Harvey AJ, Shirley NJ, Mather DE, Bacic A, Fincher GB (2008) The genetics and transcriptional profiles of the cellulose synthase-like HvCslF gene family in barley. Plant Physiol 146: 1821-1833.

Cecchetti V, Altamura MM, Falasca G, Costantino P, Cardarelli M (2008) Auxin Regulates Arabidopsis Anther Dehiscence, Pollen Maturation, and Filament Elongation. Plant Cell Online 20: 1760-1774

Cheng Y, Dai X, Zhao Y (2006) Auxin biosynthesis by the YUCCA flavin monooxygenases controls the formation of floral organs and vascular tissues in Arabidopsis. Genes Dev 20: 1790–1799

Chevalier D, Batoux M, Fulton L, Pfister K, Yadav RK, Schellenberg M, Schneitz K (2005) STRUBBELIG defines a receptor kinase-mediated signaling pathway regulating organ development in Arabidopsis. Proc Natl Acad Sci U S A 102: 9074-9079.

Christensen CA, King EJ, Jordan JR, Drews GN (1997) Megagametogenesis in Arabidopsis wild type and the Gf mutant. Sex Plant Reprod 10: 49–64

Clough SJ, Bent AF (1988) Floral dip: a simplified method for Agrobacterium-mediated transformation of Arabidopsis thaliana. Plant J 16: 735-43.

Coen ES, Meyerowitz EM (1991) The war of the whorls: Genetic interactions controlling flower development. Nature 353: 31–37

Coimbra S, Almeida J, Junqueira V, Costa ML, Pereira LG (2007) Arabinogalactan proteins as molecular markers in Arabidopsis thaliana sexual reproduction. J Exp Bot 58: 4027-4035.

Colombo L, Franken J, Koetje E, van Went J, Dons HJM, Angenent GC, van Tunenai, AJ (1995) The Petunia MADS Box Gene FBPI7 Determines Ovule Identity. Plant Cell 7: 1859-1868

Debeaujon I, Nesi N, Perez P, Devic M, Grandjean O, Caboche M, Lepiniec L (2003) Proanthocyanidin-accumulating cells in Arabidopsis testa: regulation of differentiation and role in seed development. Plant Cell 15: 2514–2531

Demesa-Arévalo E and Vielle-Calzada JP (2013) The classical arabinogalactan protein AGP18 mediates megaspore selection in Arabidopsis. Plant Cell 25: 1274-1287.

d'Erfurth I, Jolivet S, Froger N, Catrice O, Novatchkova M, Simon M, Jenczewski E, Mercier R (2008) PLOS Genet 4(11): e1000274

Devaiah, B. N., Madhuvanthi, R., Karthikeyan, A. S., Raghothama, K. G Phosphate Starvation Responses and Gibberellic Acid Biosynthesis Are Regulated by the MYB62 Transcription Factor in Arabidopsis. Mol Plant 2: 43-58

Devic M, Guilleminot J, Debeaujon I, Bechtold N, Bensaude E, Koornneef M, Pelletier G, Delseny M (1999) The BANYULS gene encodes a DFR-like protein and is a marker of early seed coat development. Plant J 19: 387–398

Dinneny JR, Weigel D, Yanofsky MF (2006) NUBBIN and JAGGED define stamen and carpel shape in Arabidopsis. Development 133: 1645-55

Durán-Figueroa N, Vielle-Calzada J-P (2010) ARGONAUTE9-dependent silencing of transposable elements in pericentromeric regions of Arabidopsis. Plant Signal Behav 5: 1476-1479

Edwards K, Johnstone C, Thompson C (1991) A simple and rapid method for the preparation of plant genomic DNA for PCR analysis. Nucleic Acids Res 19(6): 1349

Ehlers K, Bhide AS, Tekleyohans DG, Wittkop B, Snowdon RJ, Becker A (2016) The MADS Box Genes ABS, SHP1, and SHP2 Are Essential for the Coordination of Cell Divisions in Ovule and Seed Coat Development and for Endosperm Formation in Arabidopsis thaliana. PLoS ONE 11: e0165075.

Enugutti B, Kirchhelle C, Oelschner M, Torres Ruiz RA, Schliebner I, Leister D, Schneitz K (2012) Regulation of planar growth by the Arabidopsis AGC protein kinase UNICORN. Proc Natl Acad Sci U S A 109: 15060-5

Food and Agriculture Organization of the United Nations. (2016). FAO's work on climate change. United Nations Conference. 36pp

Favaro R, Pinyopich A, Battaglia R, Kooiker M, Borghi L, Ditta G, Yanofsky MF, Kater MM, Colombo L (2003) MADS-Box Protein Complexes Control Carpel and Ovule Development in Arabidopsis. Plant Cell 15: 2603–2611

Franco-Zorrilla JM, Cubas P, Jarillo J, Fernàndez-Calvìn B, Salinas J, Martınez-Zapater JM (2002) AtREM1, a member of a new family of B3 domain-containing genes, is preferentially expressed in reproductive meristems. Plant Physiol 128: 418–427

Gatti S (2015) Genetic and epigenetic control of Megaspore Mother Cell (MMC) formation in Arabidopsis thaliana (L.) Dissertation

Gehring M (2013) Genomic imprinting: insights from plants. Ann Rev Genet 47: 187-208

Gupta SC, Sharma A, Mishra M, Mishra R, Chowdhuri DK (2010) Heat shock proteins in toxicology: how close and how far? Life Sci 86: 377-384

Havecker ER, Wallbridge LM, Hardcastle TJ, Bush MS, Kelly KA, Dunn RM, Schwach F, Doonan JH, Baulcombe DC (2010) The Arabidopsis RNA-Directed DNA Methylation Argonautes Functionally Diverge Based on Their Expression and Interaction with Target Loci. Plant Cell 22: 321–334

Hayashi S, Ishii T, Matsunaga T, Tominaga R, Kuromori T, Wada T, Shinozaki K, Hirayama T (2008) The glycerophosphoryl diester phosphodiesterase-like proteins SHV3 and its homologs play important roles in cell wall organization. Plant Cell Physiol. 49: 1522-35

Himber C, Dunoyer P, Moissiard G, Ritzenthaler C, Voinnet O (2003) Transitivity-dependent and -independent cell-to-cell movement of RNA silencing. EMBO J. 22, 4523–4533

Hong RL, Hamaguchi L, Busch MA, Weigel D (2003) Regulatory elements of the floral homeotic gene AGAMOUS identified by phylogenetic footprinting and shadowing. Plant Cell 15: 1296-1309.

Hsieh TF, Shin J, Uzawa R, Silva P, Cohen S, Bauer M J, ..., Fischer RL (2011) Regulation of imprinted gene expression in Arabidopsis endosperm. Proc Natl Acad Sci 108: 1755-1762.

Hsu WH, Yeh TJ, Huang KY, Li JY, Chen HY, Yang CH (2014) AGAMOUS-LIKE13, a putative ancestor for the E functional genes, specifies male and female gametophyte morphogenesis. Plant J 77: 1-15

Huanca-Mamani W, Garcia-Aguilar M, León-Martínez G, Grossniklaus U, Vielle-Calzada JP (2005) CHR11, a chromatin-remodeling factor essential for nuclear proliferation during female gametogenesis in Arabidopsis thaliana. Proc Natl Acad Sci USA 102: 17231-17236.

Jauvion V, Elmayan T, Vaucheret H (2010) The conserved RNA trafficking proteins HPR1 and TEX1 are involved in the production of endogenous and exogenous small interfering RNA in Arabidopsis. Plant Cell 22: 2697–2709.

Jefferson RA (1987) Assaying chimeric genes in plants: the GUS gene fusion system. Plant Mol Biol Rep 5: 387-405

Jing HC1, Schippers JH, Hille J, Dijkwel PP (2005) Ethylene-induced leaf senescence depends on age-related changes and OLD genes in Arabidopsis. J Exp Bot 56: 2915-2923

Ito T, Ng K-H, Lim T-S, Yu H, Meyerowitz EM. (2007) The Homeotic Protein AGAMOUS Controls Late Stamen Development by Regulating a Jasmonate Biosynthetic Gene in Arabidopsis. Plant Cell19: 3516-3529

Kaufmann K, Melzer R, Theiβen G (2005) MIKC-type MADS-domain proteins: structural modularity, protein interactions and network evolution in land plants. Genes 347: 183–198

Kaufmann K, Wellmer F, Muiño JM, Ferrier T, Wuest SE, Kumar V, Serrano-Mislata A, Madueño F, Krajewski P, Meyerowitz EM, Angenent GC, Riechmann JL (2010) Orchestration of floral initiation by APETALA1. Science 328: 85–89.

Kaufmann K (2012) Characterization of MADS-domain transcription factor complexes in Arabidopsis flower development. Proc Natl Acad Sci U S A 109: 1560–1565

Kawashima T, Berger F (2014) Epigenetic reprogramming in plant sexual reproduction. Nat Rev Genet 15: 613–624

Keerthisinghe, S, Nadeau, JA, Lucas, JR, Nakagawa, T, Sack, FD (2015) The Arabidopsis leucine-rich repeat receptor-like kinase MUSTACHES enforces stomatal bilateral symmetry in Arabidopsis. Plant J 81: 684-94

Klepikova AV, Kasianov AS, Gerasimov ES, Logacheva MD, Penin AA (2016) A high resolution map of the Arabidopsis thaliana developmental transcriptome based on RNA-seq profiling. Plant J 88: 1058–1070

Kim S, Yamaoka Y, Ono H, Kim H, Shim D, Maeshima M, Martinoia E, Cahoon EB, Nishida I, Lee Y (2013) AtABCA9 transporter supplies fatty acids for lipid synthesis to the endoplasmic reticulum. Proc Natl Acad Sci U S A 110: 773-778

Komarova NY, Thor K, Gubler A, Meier S, Dietrich D, Weichert A, Suter Grotemeyer M, Tegeder M, Rentsch D (2008) AtPTR1 and AtPTR5 transport dipeptides in planta. Plant Physiol 148: 856-869.

Kumakura N, Takeda A, Fujioka Y, Motose H, Takano R, Watanabe Y (2009) SGS3 and RDR6 interact and colocalize in cytoplasmic SGS3/RDR6-bodies. FEBS Lett 583: 1261–1266

Kurdyukov S, Faust A, Trenkamp S, Bär S, Franke R, Efremova N, Tietjen K, Schreiber L, Saedler H, Yephremov A (2006) Genetic and biochemical evidence for involvement of HOTHEAD in the biosynthesis of long-chain alpha-,omega-dicarboxylic fatty acids and formation of extracellular matrix. Planta 224: 315-29

Kuusk S, Sohlberg JJ, Magnus Eklund D, Sundberg E (2006) Functionally redundant SHI family genes regulate Arabidopsis gynoecium development in a dose-dependent manner. Plant J 47: 99-111

Lee I, Wolfe DS, Nilsson O, Weigel D (1997) A LEAFY co-regulator encoded by UNUSUAL FLORAL ORGANS. Curr Biol 7: 95-104

Lee YR, Giang HM, Liu B (2001) A novel plant kinesin-related protein specifically associates with the phragmoplast organelles. Plant Cell 13: 2427-39.

Li M, Lopato S, Hrmova M, Pickering M, Shirley N, Koltunow AM, Langridge P (2014) Expression patterns and protein structure of a lipid transfer protein END1 from Arabidopsis. Planta 240: 1319-34

Liljegren SJ, Ditta, GS, Eshed Y, Savidge B, Bowman JL, Yanofsky MF (2000) SHATTERPROOF MADS-box genes control seed dispersal in Arabidopsis. Nature 13;404(6779)

Liu WX, Zhang FC, Zhang WZ, Song LF, Wu WH, Chen YF (2013) Arabidopsis Di19 functions as a transcription factor and modulates PR1, PR2 and PR5 expressions in response to drought stress. Mol Plant 6: 1487-502

Lora J, Herrero M, Tucker MR, Hormaza JI (2016) The transition from somatic to germline identity shows conserved and specialized features during angiosperm evolution. New Phytol 216: 495–509

Lojda Z (1970) Indigogenic methods for glycosidases: I. An improved method of β-D-glucosidase and its application to localization studies of intestinal and renal enzymes. Histochemie 22: 347-361

Lu F, Cui X, Zhang S, Jenuwein T, Cao X (2011) Arabidopsis REF6 is a histone H3 lysine 27 demethylase. Nat Genet 43: 715–719.

Lugassi N, Nakayama N, Bochnik R, Zik M (2010) A novel allele of FILAMENTOUS FLOWER reveals new insights on the link between inflorescence and floral meristem organization and flower morphogenesis. BMC Plant Biol 28;10:131

Macquet A, Ralet MC, Loudet O, Kronenberger J, Mouille G, Marion-Poll A, North HM (2007) A naturally occurring mutation in an Arabidopsis accession affects a beta-D-galactosidase that increases the hydrophilic potential of rhamnogalacturonan I in seed mucilage. Plant Cell 19: 3990-4006

Mantegazza O, Gregis V, Mendes MA, Morandini P, Alves-Ferreira M, Patreze CM, Nardeli SM, Kater MM, Colombo L (2014) Analysis of the arabidopsis REM gene family predicts functions during flower development. Ann Bot 114: 1507-15

Mascarenhas JP and Hamilton DA (1992) Artifacts in the localization of GUS activity in anothers of petunia transformed with a CaMV 35S-GUS construct. Plant J 2: 405-408

Matias-Hernandez LM, Battaglia R, Galbiati F, Rubes M, Eichenberger C, Grossniklaus U, Kater MM, Colombo L (2010) VERDANDI is a direct target of the MADS domain ovule identity complex and affects embryo sac differentiation in Arabidopsis. Plant Cell 22: 1702–1715

Mendes MA, Guerra RF, Berns MC, Manzo C, Masiero S, Finzi L, Kater M, Colombo L (2013) MADS Domain Transcription Factors Mediate Short-Range DNA Looping That Is Essential for Target Gene Expression in Arabidopsis. Plant Cell 25: 2560–2572

Mendes MA, Guerra RF, Castelnovo B, Silva-Velazquez Y, Morandini P, Manrique S, Baumann N, Groß-Hardt R, Dickinson H, Colombo L (2016) Live and let die: a REM complex promotes fertilization through synergid cell death in Arabidopsis. Development 143: 2780-2790

Mercier R, Grelon M, Vezon D, Horlow C, Pelletier G (2001) How to characterize meiotic functions in plants?. Biochimie 83: 1023-1028.

Mizzotti C, Ezquer I, Paolo D, Rueda-Romero P, Guerra RF, Battaglia R, Rogachev I, Aharoni A, Kater MM, Caporali E, Colombo L (2014) SEEDSTICK is a Master Regulator of Development and Metabolism in the Arabidopsis Seed Coat. PLoS Genet 10: e1004856

Mizzotti C, Mendes MA, Caporali E, Schnittger A, Kater MM, Battaglia R, Colombo L (2012) The MADS box genes SEEDSTICK and ARABIDOPSIS Bsister play a maternal role in fertilization and seed development. Plant J 70: 409–420

Morrow G & Tanguay RM (2012) Small heat shock protein expression and functions during development. Int J Bioch Cell Biol 44: 1613-1621

Nakamichi N, Takao S, Kudo T, Kiba T, Wang Y, Kinoshita T, Sakakibara H (2016) Improvement of Arabidopsis Biomass and Cold, Drought and Salinity Stress Tolerance by Modified Circadian Clock-Associated PSEUDO-RESPONSE REGULATORs. Plant Cell Physiol 57: 1085-97

Nesi N, Debeaujon I, Jond C, Stewart AJ, Jenkins GI, Caboche M, Lepiniec L (2002) The TRANSPARENT TESTA16 locus encodes the ARABIDOPSIS BSISTER MADS domain protein and is required for proper development and pigmentation of the seed coat. Plant Cell 14: 2463–2479

Nonomura K-I, Morohoshi A, Nakano M, Eiguchi M, Miyao A, Hirochika H, Kurata N (2007) A germ cell specific gene of the ARGONAUTE family is essential for the progression of premeiotic mitosis and meiosis during sporogenesis in rice. Plant Cell 19: 2583-2594.

Okada T, Hu Y, Tucker MR, Taylor JM, Johnson SD, Spriggs A, Tsuchiya T, Oelkers K, Rodrigues JCM and Koltunow AM (2013) Enlarging cells initiating apomixis in Hieracium praealtum transition to an embryo sac program prior to entering mitosis. Plant Physiol. 163: 216-231.

Olmedo-Monfil V, Durán-Figueroa N, Arteaga-Vázquez M, Demesa-Arévalo E, Autran D, Grimanelli D, Slotkin RK, Martienssen RA, Vielle-Calzada J-P (2010) Control of female gamete formation by a small RNA pathway in Arabidopsis. Nature 464: 628–632

Payne T, Johnson SD, Koltunow AM (2004) KNUCKLES (KNU) encodes a C2H2 zinc-finger protein that regulates development of basal pattern elements of the Arabidopsis gynoecium. Development 131: 3737-3749.

Peragine A, Yoshikawa M, Wu G, Albrecht HL, Poethig RS (2004) SGS3 and SGS2/SDE1/RDR6 are required for juvenile development and the production of trans-acting siRNAs in Arabidopsis. Genes Dev 18: 2368–2379.

Pereira AM, Lopes AL, Coimbra S (2016) Arabinogalactan Proteins as Interactors along the Crosstalk between the Pollen Tube and the Female Tissues. Front Plant Sci 7.

Pereira AM, Nobre MS, Pinto SC, Lopes AL, Costa ML, Masiero S, Coimbra S (2016b) “Love Is Strong, and You're so Sweet”: JAGGER is essential for persistent synergid degeneration and polytubey block in Arabidopsis thaliana. Mol Plant 9: 601-614.

Pinyopich A, Ditta GS, Savidge B, Liljegren SJ, Baumann E, Wisman E, Yanofsky MF (2003) Assessing the redundancy of MADS-box genes during carpel and ovule development. Nature 424: 85–88

Rédei GP (1965) Non-mendelian megagametogenesis in Arabidopsis. Genetics 51: 857-872

Reiser L, Modrusan Z, Margossian L, Samach A, Ohad N, Haughn GW, Fischer RL (1995) The BELL1 gene encodes a homeodomain protein involved in pattern formation in the Arabidopsis ovule primordium. Cell 83: 735–742

Reyes-Olalde JI, Zuñiga-Mayo VM, Chávez Montes RA, Marsch-Martínez N, de Folter S (2013) Inside the gynoecium: at the carpel margin. Trends Plant Sci 18: 644-55

Robinson-Beers K, Pruitt RE, Gasser CS (1992). Ovule development in wild-type Arabidopsis and two female-sterile mutants. Plant Cell 4: 1237–1249

Rodríguez-Leal D, León-Martínez G, Abad-Vivero U, Vielle-Calzada JP (2015) Natural variation in epigenetic pathways affects the specification of female gamete precursors in Arabidopsis. Plant Cell 27: 1034-45

Romanel EA, Schrago CG, Couñago RM, Russo CAM, Alves-Ferreira M (2009) Evolution of the B3 DNA binding superfamily: new insights into REM family gene diversification. PLoS One 4: e5791.

Romanel E, Das P, Amasino RM, Traas J, Meyerowitz E, Alves-Ferreira M (2011) Reproductive Meristem22 is a unique marker for the early stages of stamen development. Int J Dev Biol. 55: 657-64

Rounsley SD, Ditta GS, Yanofsky MF (1995) Diverse Roles for MADS Box Genes in Arabidopsis Development. Plant cell 7: 1259-1269

Ruhlmann, JM, Kram, BW, Carter, CJ (2010) CELL WALL INVERTASE 4 is required for nectar production in Arabidopsis. J Exp Bot 61: 395-404

Saito T, Fujikawa H, Haga N, Suzuki T, Machida Y, Ito M (2015) Genetic interaction between G2/M phase-specific transcription factor MYB3R4 and MAPKKK ANP3 for execution of cytokinesis in Arabidopsis thaliana. Plant Signal Behav 10(3):e990817

Sakai H, Medrano LJ, Meyerowitz EM (1995) Role of SUPERMAN in maintaining Arabidopsis floral whorl boundaries. Nature 378: 199 - 203

Sauveplane V, Kandel S, Kastner PE, Ehlting J, Compagnon V, Werck-Reichhart D, Pinot F (2009) Arabidopsis thaliana CYP77A4 is the first cytochrome P450 able to catalyze the epoxidation of free fatty acids in plants. FEBS J 276:719-35

Sawa S, Ito T, Shimura Y, Okada K (1999) FILAMENTOUS FLOWER controls the formation and development of arabidopsis inflorescences and floral meristems. Plant Cell. 11: 69-86

Schiefthaler U, Balasubramanian S, Sieber P, Chevalier D, Wisman E, Schneitz K (1999) Molecular analysis of NOZZLE, a gene involved in pattern formation and early sporogenesis during sex organ development in Arabidopsis thaliana. Proc Natl Acad Sci USA 96: 11664-11669.

Schmidt A, Wuest SE, Vijverberg K, Baroux C, Kleen D, Grossniklaus U (2011) Transcriptome Analysis of the Arabidopsis Megaspore Mother Cell Uncovers the Importance of RNA Helicases for Plant Germline Development. PLoS Biol 9: e1001155

Schmidt A, Schmid Mw, Grossniklaus U (2015) Plant germline formation: common concepts and developmental flexibility in sexual and asexual reproduction. Development 142: 229-241

Schneitz K, Hülskamp M, Pruitt RE (1995) Wild-type ovule development in Arabidopsis thaliana: a light microscope study of cleared whole-mount tissue. Plant J 7: 731–749

Schröder F, Lisso J, Muessig C (2011) EXORDIUM-LIKE1 promotes growth during low carbon availability in Arabidopsis. Plant Physiol 156: 1620-30

Schultz CJ, Rumsewicz MP, Johnson KL, Jones BJ, Gaspar YM, Bacic A (2002) Using genomic resources to guide research directions. The arabinogalactan protein gene family as a test case. Plant Physiol 129: 1448-63

She W and Baroux C (2015) Chromatin dynamics in pollen mother cells underpin a common scenario at the somatic-to-reproductive fate transition of both the male and female lineages in Arabidopsis. Front Plant Sci 6.

She W, Grimanelli D, Rutowicz K, Whitehead MWJ, Puzio M, Kotlinski M, Jerzmanowski, A and Baroux C (2013) Chromatin reprogramming during the somatic-to-reproductive cell fate transition in plants. Development 140: 4008-4019

Singh M, Goel S, Meeley RB, Dantec C, Parrinello H, Michaud C, Leblanc O, Grimanelli D (2011) Production of viable gametes without meiosis in maize deficient for an ARGONAUTE protein. Plant Cell 23:443-458.

Smaczniak C, Immink RGH, Muiño JM, Blanvillaind R, Busscherb M, Busscher-Langeb J, Dinh QD, Liuh S, Westphali AH, Boereni S, Parcy F, Xuh L, Carles CC, Angenent GC,

Smyth DR, Bowman JL, Meyerowitz EM (1990). Early flower development in Arabidopsis. Plant Cell 2: 755-767.

Stepanova AN, Yun J, Robles LM, Novak O, He W, Guo H, Ljung K, Alonso JM (2011) The Arabidopsis YUCCA1 Flavin Monooxygenase Functions in the Indole-3-Pyruvic Acid Branch of Auxin Biosynthesis. Plant Cell 23: 3961-73

Su Z, Zhao L, Zhao Y, Li S, Won S, Cai H, Wang L, Li Z, Chen P, Qin Y, Chen X (2017) The THO Complex Non-Cell-Autonomously Represses Female Germline Specification through the TAS3-ARF3 Module. Curr Biol 27: 1597–1609

Sun W, Van Montagu M, Verbruggen N (2002) Small heat shock proteins and stress tolerance in plants. BBA Gene Struct Expr 1577: 1-9.

Sun B, Xu Y, Ng KH, Ito T (2009) A timing mechanism for stem cell maintenance and differentiation in the Arabidopsis floral meristem. Genes Dev 23: 1791-1804.

Swaminathan K, Peterson K, Jack T (2008) The plant B3 superfamily. Trends in Plant Science 13: 647–655.

Theißen G, Melzer R, Rümpler F (2016) MADS-domain transcription factors and the floral quartet model of flower development: linking plant development and evolution. Development 143: 3259-3271

Tiwari S, Spielman M, Schulz R, Oakey RJ, Kelsey G, Salazar A, Zhang K, Pennell R, Scott RJ (2010). Transcriptional profiles underlying parent-of-origin effects in seeds of Arabidopsis thaliana. BMC plant biol 10: 72.

Tucker MR and Koltunow AMG (2009) Sexual and asexual (apomictic) seed development in flowering plants: molecular, morphological and evolutionary relationships. Functional Plant Biology 36: 490-504

Tucker MR and Koltunow AMG (2014) Traffic monitors at the cell periphery: the role of cell walls during early female reproductive cell differentiation in plants. Curr Opp Plant Biol 17: 137-145.

Tucker MR, Okada T, Hu Y, Scholefield A, Taylor JM, Koltunow AMG (2012) Somatic small RNA pathways promote the mitotic events of megagametogenesis during female reproductive development in Arabidopsis. Development 139: 1399-1404

Turbant A, Fournet F, Lequart M, Zabijak L, Pageau K, Bouton S, Van Wuytswinkel O (2016) PME58 plays a role in pectin distribution during seed coat mucilage extrusion through homogalacturonan modification. J Exp Bot 67: 2177-90

Unte US, Sorensen AM, Pesaresi P, Gandikota M, Leister D, Saedler H, Huijser P (2003) SPL8, an SBP-Box Gene That Affects Pollen Sac Development in Arabidopsis. Plant Cell 15: 1009-19

Vandesompele J, De Preter K, Pattyn F, Poppe B, Van Roy N, De Paepe A, Speleman F (2002) Accurate normalization of real-time quantitative RTPCR data by geometric averaging of multiple internal control genes. Genome Biol 3: 1–11

Villanueva JM, Broadhvest J, Hauser BA, Meister RJ, Schneitz K, Gasser CS (1999) INNER NO OUTER regulates abaxial – adaxial patterning in Arabidopsis ovules. Gene Development 13: 3160–3169

Vitha S, Beneš K, Phillips JP, Gartlan KMA (1995) Histochemical GUS Analysis. In *Agrobacterium Protocols*, K.M.A. Gartland and M.R. Davey, eds (Totowa, NJ: Humana Press), pp. 185-193

Wang Y, Law SR, Ivanova A, van Aken O, Kubiszewski-Jakubiak S, Uggalla V, van der Merwe M, Duncan O, Narsai R, Whelan J, Murcha MW (2014) The mitochondrial protein import component, TRANSLOCASE OF THE INNER MEMBRANE17-1, plays a role in defining the timing of germination in Arabidopsis. Plant Physiol 166(3): 1420-35.

Watanabe K and Okada K (2003) Two Discrete cis Elements Control the Abaxial Side–Specific Expression of the FILAMENTOUS FLOWER Gene in Arabidopsis. Plant Cell 15: 2592-2602

Watanabe K, Pacher M, Dukowic S, Schubert V, Puchta H, Schubert I (2009) The STRUCTURAL MAINTENANCE OF CHROMOSOMES 5/6 Complex Promotes Sister Chromatid Alignment and Homologous Recombination after DNA Damage in Arabidopsis thaliana. Plant Cell 21: 2688-99.

Webb, MC and Gunning, BES (1990) Embryo sac development in Arabidopsis thaliana. Sex Plant Reprod 3: 244

Wellmer F, Alves-Ferreira M, Dubois A, Riechmann JL, Meyerowitz EM (2006) Genome-wide analysis of gene expression during early Arabidopsis flower development. PLoS Genet 2: e117

Wei B, Zhang J, Pang C, Yu H, Guo D, Jiang H, Ding M, Chen Z, Tao Q, Gu H, Qu L-J, Qin G (2015) The molecular mechanism of *SPOROCYTELESS/NOZZLE* in controlling Arabidopsis ovule development. Cell Res 25:121-134

Weigel D, Alvarez J, Smyth DR, Yanofsky MF, Meyerowitz EM (1992) LEAFY controls floral meristem identity in Arabidopsis. Cell 69:843-59.

Weis C, Hückelhoven R, Eichmann R (2013) LIFEGUARD proteins support plant colonization by biotrophic powdery mildew fungi. J Exp Bot 64: 3855-67

Whitton J, Sears C, Baack E, Otto S (2008) The dynamic nature of apomixis in the angiosperms. Int J Plant Sci 169: 169–182.

Wijeratne AJ, Zhang W, Sun Y, Liu W, Albert R, Zheng Z, Oppenheimer DG, Zhao D, Ma H (2007) Differential gene expression in Arabidopsis wild-type and mutant anthers: insights into anther cell differentiation and regulatory networks. Plant J 52: 14-29.

Wilkinson MD and Haughn GW (1995) UNUSUAL FLORAL ORGANS Controls Meristem Identity and Organ Primordia Fate in Arabidopsis. 7: 1485-1499

Wynn AN, Rueschhoff EE, Franks RG (2011) Transcriptomic characterization of a synergistic genetic interaction during carpel margin meristem development in Arabidopsis thaliana. PLoS One 6: e26231.

Xiang Y, Nakabayashi K, Ding J, He F, Bentsink L, Soppe WJ (2014) REDUCED DORMANCY5 Encodes a Protein Phosphatase 2C That Is Required for Seed Dormancy in Arabidopsis. Plant Cell 26: 4362-75

Xing S, Salinas M, Garcia-Molina A, Höhmann S, Berndtgen R, Huijser P (2013) SPL8 and miR156-targeted SPL genes redundantly regulate Arabidopsis gynoecium differential patterning. Plant J 75: 566-577.

Yadegari R and Drews GN (2004) Female gametophyte development. Plant Cell 16 (suppl 1) S133-S141

Yan W, Chen D, Kaufmann K (2016) Molecular mechanisms of floral organ specification by MADS domain proteins. Curr Opin Plant Biol 29:154–162

Yelina NE, Smith LM, Jones AM, Patel K, Kelly KA, Baulcombe DC (2010) Putative Arabidopsis THO/TREX mRNA export complex is involved in transgene and endogenous siRNA biosynthesis. Proc Natl Acad Sci USA 107: 13948–13953.

Yoshikawa M, Peragine A, Park, MY, Poethig RS (2005) A pathway for the biogenesis of trans-acting siRNAs in Arabidopsis. Genes Dev 19: 2164–2175.

Yu HJ, Hogan P, Sundaresan V (2005) Analysis of the female gametophyte transcriptome of Arabidopsis by comparative expression profiling. Plant Physiol 139: 1853-1869.

Zhao L, He J, Cai H, Lin H, Li Y, Liu R, Yang Z, Qin Y (2014) Comparative expression profiling reveals gene functions in female meiosis and gametophyte development in Arabidopsis. Plant J 80: 615-628.

Zhao XA, Bramsiepe J, Van Durme M, Komaki S, Prusicki MA, Maruyama D, ..., Lu, Y. (2017) RETINOBLASTOMA RELATED1 mediates germline entry in Arabidopsis. Science 356(6336) eaaf6532.

Zhang Z, Liu X, Guo X, Wang XJ, Zhang X (2016) Arabidopsis AGO3 predominantly recruits 24-nt small RNAs to regulate epigenetic silencing. Nat Plant 2: 16049

7. Supplemental material

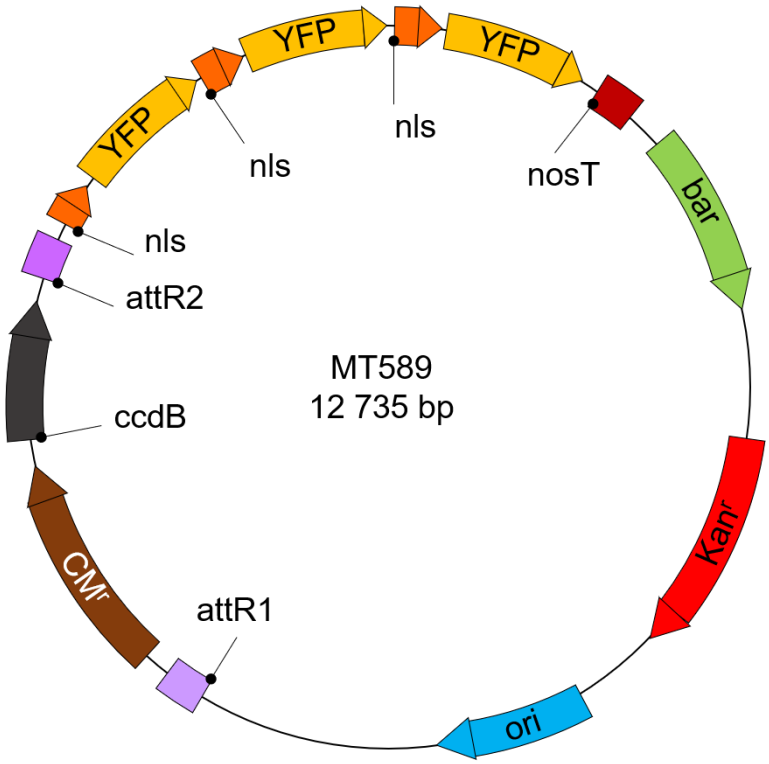

Supplemental Fig. 1 - Schematic representation of the destination vector MT589 used for gateway cloning. attR1/attR2 – recombination sites; bar – gene which confers resistance to the herbicide bialaphos (BASTA); ccdB - codes for the toxic protein (CcdB) that ultimately causes cell death; CM^r - gene wich confers chloramphenicol resistance; Kan^r – gene wich confers kanamycin resistance; nls – nuclear localization signal; nosT – nopaline synthase terminator; ori – origin of replication; YFP – encodes yellow fluorescent protein.

Primer name	Gene/Reference	Sequence	Ta	Product size (bp)	Use
OSP_003	AT4G09960	GCTTGTTCTGATAGCACCAACACTAGCA	60	350(wt) 400(mt)	genotyping *stk*
OSP_004		GGAACTCAAAGAGTCTCCCATCAG			
OSP_005	AT2G16210	AGGATGGATGTGAGGGTGTC	57	OSP5+25=400(mt)	genotyping *rem24* SALK_054142
OSP_006		GGTCATCCTTCTCAGACGTG		OSP5+6=351(wt)	
OSP_025	LBb1.3	ATTTTGCCGATTTCGGAAC	-	-	mutant primer SALK lines
OSP_031	AT2G16210	ATCTGGATTGTGGAGGTTGC	76	142	qPCR for *REM24*
OSP_032		TCTGGCTGGGAGAAGTTTGT			
OSP_033	AT5G21150	CACCTTTCGTTCCAGCAAAT	77	154	qPCR for *AGO9*
OSP_034		CCGCTTGGTTTGTTGAACTT			
OSP_035	AT2G35310	AAAAGCTCGATGGGGAAGTT	74	122	qPCR for *REM23*
OSP_036		GAAACTCACTGGCTCCCAAG			
OSP_037	AT3G49500	TACTGTCCCTGGCGATCTCT	77	187	qPCR for *RDR6*
OSP_038		CCACCTCACACGTTCCTCTT			
OSP_041	AT5G47600	TTAGGGACGGTGATCCAGAG	77	130	qPCR for *HSP20*-like
OSP_042		CAGCAATGCCTGAGTACGAA			
OSP_043	AT4G27330	CTTGGGAAGCCTTGTAGCAC	77	148	qPCR for *SPL/NZZ*
OSP_044		AGCTCGAGCGTCAGAGAATC			
OSP_045	AT4G09960	CCAGATCCAGAACCAGCAGT	75	121	qPCR for *STK*
OSP_046		TGGAGAGGTATCAACAACACCA			
OSP_047	AT5G40940	TGGATAAGTAGCCGGAATCG	78	145	qPCR for *FLA20*
OSP_048		AGCTCGAAGAACGCATCAAT			
OSP_055	pREM24_F	GTGAAAGCAATGAGCATTTC	55	OSP55+57= 1161	amplifying *pREM24*
OSP_056	pREM24_F1	GAGCATTTCATTTTGTTCTC	55	OSP56+61= 2189	amplifying *pREM24:intron1*
OSP_057	pREM24_R	CTCTCTAATTCAAGCTCACC	55	OSP55+57= 1161	amplifying *pREM24*
OSP_059	REM24_ISH_F1	CTTGGAGAAGAAGTTACTACG	56	206	amplifying *REM24* probe on 3'UTR
OSP_060	REM24_ISH_R	AAAAGGTTACCATTGAGTTGA	56		

OSP_061	pREM24_intron_R	GCAAATAAAATGAAGAGACG	55	OSP56+61= 2189	amplifying *pREM24:intron1*
OSP_069	MT589_seq	TTCCCTGTAGTTGAAGAAACG	-	-	sequencing *pREM24* and *pREM24:intron1* in MT589
AtCyclo_qF	AtCyclophilin	TGGCGAACGCTGGTCCTAATACA			qPCR for AtCyclophilin - control
AtCyclo_qR	AtCyclophilin	GTCAGCCAAGTCAACAACTCTCTG			
AtGAPdH_qF	AtGAPdH	TGGTTGATCTCGTTGTGCAGGTCTC			qPCR for AtGAPdH - control
AtGAPdH_qR	AtGAPdH	GTCAGCCAAGTCAACAACTCTCTG			
AtActin_qF	AtActin	GAGTTCTTCACGCGATACCTCCA			qPCR for AtActin - control
AtActin_qR	AtActin	GACCACCTTTATTAACCCCATTTACCA			
AtTubulin_qF	AtTubulin	ATGTGGGTCAGGGTATGGAA			qPCR for AtTubulin - control
AtTubulin_qR	AtTubulin	CCGACAACCTTCTTAGTCTCCTCT			
GUSAS	GUS_F	GTTTACGCGTTGCTTCCGCCA	55	1250	genotyping GUS
GUSSSENSE	GUS_R	GGTGGGAAAGCGCGTTACAAG			
q_WUS_F	AT2G17950	GCGATGCTTATCTGGAACATC	80	164	qPCR for *WUS* tested
q_WUS_R		AACTTCCGATTGGCCATACTT			
q_KNU_F	AT5G14010	CGTCCTCGCTAACTCTCCAC	78	110	qPCR for *KNU* tested
q_KNU_R		ACGGATGAAACGGATCGTAG			
q_AGO5_F	AT2G27880	ACCCATCAGGGAGCTAAGGTTC	73	141	qPCR for *AGO5* tested
q_AGO5_R		TAGACGGGTCTTGTGTCACTCC			
M13_F	universal primer	GTAAAACGACGGCCAG	-	-	colony PCR and sequencing of *pREM24* and *pREM24:intron* in pCR8; sequencing *REM24* ISH probe
TL40_R	universal primer	CCTACGGCAAGCTGACCC	-	OSP56+TL40_R= 1429/2467	colony PCR of *pREM24* and *pREM24:intron1* in MT589

Supplemental table 1 - List of primers used for genotyping, amplifying fragments of interest, sequencing and qPCR analysis. Ta = annealing temperature.

Construct	Vector	Enzyme combo	Buffer	Expected fragments (bp)	Use
pREM24	pCR8	EcoRI-HF	CutSmart	1160	insert presence
pREM24	pCR8	HindIII-HF XbaI	CutSmart	270+3700	insert orientation
pREM24:YFP	MT589	HindIII-HF NcoI-HF	CutSmart	1700+10500	insert orientation
pREM24:intron1	pCR8	EcoRI-HF	CutSmart	2209+2797	insert presence
pREM24:intron1	pCR8	NdeI, XhoI	CutSmart	1860+3146	insert orientation
pREM24:intron1 :YFP	MT589	XbaI	CutSmart	3074+10222	insert orientation
ISH_REM24	pCRII	NdeI, NcoI-HF	CutSmart	2464+1715	insert presence/orientation
ISH_REM24	pCRII	BamHI-HF	CutSmart	4179	linearization for transcription with T7
ISH_REM24	pCRII	XbaI	CutSmart	4179	linearization for transcription with SP6

Supplemental table 2 – List of enzymes used to confirm insert presence and orientation for cloning fragments of interest.

GO term	Description	p-value	FDR
GO:0044699	single-organism process	2.3e-20	6.7e-17
GO:0007018	microtubule-based movement	2.0e-12	2.8e-09
GO:0007049	cell cycle	2.3e-11	1.6e-08
GO:0006928	movement of cell or subcellular component	2.0e-11	1.6e-08
GO:0051301	cell division	1.0e-08	5.8e-06
GO:0007017	microtubule-based process	1.2e-08	5.8e-06
GO:0022402	cell cycle process	1.9e-08	7.0e-06
GO:0000278	mitotic cell cycle	2.0e-08	7.0e-06
GO:0071103	DNA conformation change	2.5e-08	7.7e-06
GO:1903047	mitotic cell cycle process	3.0e-08	8.6e-06
GO:0048229	gametophyte development	6.3e-08	1.5e-05
GO:0007275	multicellular organism development	6.1e-08	1.5e-05
GO:0022414	reproductive process	1.2e-07	2.5e-05
GO:0000003	reproduction	1.3e-07	2.5e-05
GO:0032501	multicellular organismal process	1.3e-07	2.5e-05
GO:0044707	single-multicellular organism process	1.6e-07	2.9e-05
GO:0044702	single organism reproductive process	1.8e-07	3.0e-05
GO:0044767	single-organism developmental process	5.6e-07	8.8e-05
GO:0048827	phyllome development	6.3e-07	9.1e-05
GO:0051321	meiotic cell cycle	6.4e-07	9.1e-05
GO:0048856	anatomical structure development	6.9e-07	9.3e-05
GO:0009555	pollen development	8.2e-07	1.1e-04
GO:0044710	single-organism metabolic process	9.5e-07	1.2e-04
GO:0032502	developmental process	2.2e-06	2.6e-04
GO:0000910	cytokinesis	5.1e-06	5.7e-04

GO:0000280	nuclear division	5.3e-06	5.8e-04
GO:0006260	DNA replication	6.8e-06	7.1e-04
GO:0048367	shoot system development	7.8e-06	7.9e-04
GO:0044763	single-organism cellular process	8.1e-06	8.0e-04
GO:0030261	chromosome condensation	9.7e-06	9.2e-04
GO:0048731	system development	1.0e-05	9.6e-04
GO:0048437	floral organ development	1.2e-05	1.0e-3
GO:0048285	organelle fission	1.2e-05	1.0e-3
GO:0048608	reproductive structure development	1.5e-05	1.2e-03
GO:0061458	reproductive system development	1.5e-05	1.2e-03
GO:0048646	anatomical structure formation involved in morphogenesis	2.0e-05	1.6e-03
GO:0003006	developmental process involved in reproduction	2.7e-05	2.0e-03
GO:0006629	lipid metabolic process	3.0e-05	2.3e-03
GO:0099402	plant organ development	3.3e-05	2.4e-03
GO:0006720	isoprenoid metabolic process	3.4e-05	2.4e-03
GO:0008283	cell proliferation	3.8e-05	2.6e-03
GO:0044711	single-organism biosynthetic process	4.6e-05	3.1e-03
GO:0008299	isoprenoid biosynthetic process	5.2e-05	3.4e-03
GO:0007067	mitotic nuclear division	5.6e-05	3.6e-03
GO:0009908	flower development	6.2e-05	3.9e-03
GO:0006323	DNA packaging	8.1e-05	4.9e-03
GO:0055114	oxidation-reduction process	8.2e-05	4.9e-03
GO:0048438	floral whorl development	8.0e-05	4.9e-03
GO:0090567	reproductive shoot system development	8.9e-05	5.2e-03
GO:0051726	regulation of cell cycle	9.3e-05	5.3e-03
GO:0006259	DNA metabolic process	1.1e-04	5.9e-03
GO:1902589	single-organism organelle organization	1.3e-04	7.2e-03
GO:0000819	sister chromatid segregation	1.4e-04	7.4e-03
GO:0045229	external encapsulating structure organization	1.4e-04	7.6e-03
GO:0007389	pattern specification process	1.5e-04	7.6e-03
GO:0008152	metabolic process	1.5e-04	7.6e-03
GO:0008610	lipid biosynthetic process	1.7e-04	8.4e-03
GO:0019748	secondary metabolic process	1.9e-04	9.4e-03
GO:0016043	cellular component organization	2.1e-04	0.001
GO:0000226	microtubule cytoskeleton organization	2.4e-04	0.012
GO:0052543	callose deposition in cell wall	2.5e-04	0.012
GO:0007059	chromosome segregation	3.0e-04	0.013
GO:0052386	cell wall thickening	2.9e-04	0.013
GO:0048653	anther development	2.9e-04	0.013
GO:0044106	cellular amine metabolic process	2.9e-04	0.013
GO:0010584	pollen exine formation	2.9e-04	0.013
GO:0009653	anatomical structure morphogenesis	3.0e-04	0.013
GO:0000281	mitotic cytokinesis	3.2e-04	0.013
GO:0009791	post-embryonic development	3.2e-04	0.013
GO:0006721	terpenoid metabolic process	3.5e-04	0.014

GO:0098813	nuclear chromosome segregation	3.8e-04	0.015
GO:0048878	chemical homeostasis	4.4e-04	0.017
GO:0061640	cytoskeleton-dependent cytokinesis	4.5e-04	0.017
GO:0010073	meristem maintenance	4.5e-04	0.017
GO:0071840	cellular component organization or biogenesis	5.2e-04	0.019
GO:0048466	androecium development	5.3e-04	0.019
GO:0042127	regulation of cell proliferation	5.2e-04	0.019
GO:0048443	stamen development	5.3e-04	0.019
GO:0003002	regionalization	5.5e-04	0.02
GO:0016114	terpenoid biosynthetic process	5.7e-04	0.02
GO:0006857	oligopeptide transport	5.6e-04	0.02
GO:0015833	peptide transport	6.6e-04	0.023
GO:0007126	meiotic nuclear division	7.3e-04	0.025
GO:0006261	DNA-dependent DNA replication	7.3e-04	0.025
GO:0052545	callose localization	8.2e-04	0.027
GO:0009308	amine metabolic process	8.7e-04	0.028
GO:0043062	extracellular structure organization	8.8e-04	0.028
GO:0030198	extracellular matrix organization	8.8e-04	0.028
GO:0051276	chromosome organization	9.0e-04	0.029
GO:0042545	cell wall modification	9.1e-04	0.029
GO:0044550	secondary metabolite biosynthetic process	9.4e-04	0.029
GO:0006576	cellular biogenic amine metabolic process	9.5e-04	0.029
GO:1903046	meiotic cell cycle process	9.8e-04	0.03
GO:0085029	extracellular matrix assembly	1.0e-03	0.03
GO:0010927	cellular component assembly involved in morphogenesis	1.0e-03	0.03
GO:0010208	pollen wall assembly	1.0e-03	0.03
GO:0033037	polysaccharide localization	1.1e-03	0.033
GO:1902578	single-organism localization	1.2e-03	0.034
GO:0006310	DNA recombination	1.2e-03	0.034
GO:0042886	amide transport	1.2e-03	0.035
GO:0044765	single-organism transport	1.3e-03	0.036
GO:0000272	polysaccharide catabolic process	1.5e-05	0.041
GO:0010154	fruit development	1.8e-03	0.048
GO:0008643	carbohydrate transport	1.8e-03	0.049

Supplemental table 3 - Biological process gene ontology (GO) terms associated with the genes downregulated in the *stk* transcriptome. The significantly (*p*-value < 0.05 and FDR < 0.05) enriched GO terms are presented.

GO term	Description	p-value	FDR
GO:0009834	plant-type secondary cell wall biogenesis	8.8e-15	3.9e-11
GO:0044085	cellular component biogenesis	8.3e-14	1.8e-10
GO:0071669	plant-type cell wall organization or biogenesis	6.5e-12	9.5e-09
GO:0042546	cell wall biogenesis	1.6e-10	1.8e-07
GO:0045491	xylan metabolic process	2.4e-10	2.1e-07
GO:0045492	xylan biosynthetic process	7.3e-10	5.3e-07
GO:0009832	plant-type cell wall biogenesis	1.0e-09	6.4e-07
GO:0071554	cell wall organization or biogenesis	3.5e-09	1.9e-06
GO:0071840	cellular component organization or biogenesis	8.3e-09	4.1e-06
GO:0070592	cell wall polysaccharide biosynthetic process	1.7e-08	7.4e-06
GO:0022900	electron transport chain	2.1e-08	8.2e-06
GO:0044038	cell wall macromolecule biosynthetic process	2.7e-08	9.0e-06
GO:0070589	cellular component macromolecule biosynthetic process	2.7e-08	9.0e-06
GO:0022613	ribonucleoprotein complex biogenesis	6.5e-08	2.0e-05
GO:0055114	oxidation-reduction process	1.4e-07	4.0e-05
GO:0010410	hemicellulose metabolic process	5.6e-07	1.5e-04
GO:0042254	ribosome biogenesis	7.7e-07	2.0e-04
GO:0010383	cell wall polysaccharide metabolic process	2.4e-06	5.9e-04
GO:0006979	response to oxidative stress	3.7e-06	8.6e-04
GO:0015979	photosynthesis	7.4e-06	1.6e-03
GO:0034637	cellular carbohydrate biosynthetic process	1.1e-05	2.3e-03
GO:0033692	cellular polysaccharide biosynthetic process	1.4e-05	2.8e-03
GO:0006869	lipid transport	1.8e-05	3.4e-03
GO:0009698	phenylpropanoid metabolic process	2.2e-05	4.0e-03
GO:0044264	cellular polysaccharide metabolic process	2.8e-05	4.8e-03
GO:0044036	cell wall macromolecule metabolic process	3.8e-05	6.3e-03
GO:0009773	photosynthetic electron transport in photosystem I	3.9e-05	6.3e-03
GO:0010876	lipid localization	4.6e-05	7.1e-03
GO:0019748	secondary metabolic process	5.0e-05	7.5e-03
GO:0044262	cellular carbohydrate metabolic process	7.0e-05	0.01
GO:0010417	glucuronoxylan biosynthetic process	8.0e-05	0.011
GO:0010413	glucuronoxylan metabolic process	8.0e-05	0.011
GO:0009808	lignin metabolic process	8.7e-05	0.012
GO:0009699	phenylpropanoid biosynthetic process	1.1e-04	0.014
GO:0009767	photosynthetic electron transport chain	1.4e-04	0.017
GO:0009853	photorespiration	1.4e-04	0.017
GO:0000271	polysaccharide biosynthetic process	1.4e-04	0.017
GO:0010023	proanthocyanidin biosynthetic process	1.5e-05	0.017
GO:0044710	single-organism metabolic process	2.1e-04	0.023
GO:0005976	polysaccharide metabolic process	2.1e-04	0.023
GO:0044550	secondary metabolite biosynthetic process	2.3e-04	0.025
GO:0071555	cell wall organization	2.7e-04	0.028
GO:0006091	generation of precursor metabolites and energy	3.3e-04	0.034
GO:0016051	carbohydrate biosynthetic process	5.0e-04	0.049

Supplemental table 4 - Biological process gene ontology (GO) terms associated with the genes upregulated in the *stk* transcriptome. The significantly (*p*-value < 0.05 and FDR < 0.05) enriched GO terms are presented.

GO term	Description	p-value	FDR
GO:0005840	ribosome	3.5e-23	3.3e-20
GO:0022626	cytosolic ribosome	8.0e-21	3.8e-18
GO:0032991	macromolecular complex	1.4e-20	4.4e-18
GO:0044391	ribosomal subunit	2.8e-20	6.7e-18
GO:0044445	cytosolic part	7.9e-20	1.5e-17
GO:0044444	cytoplasmic part	1.1e-19	1.8e-17
GO:0005746	mitochondrial respiratory chain	2.1e-19	2.9e-17
GO:1990204	oxidoreductase complex	2.4e-19	2.9e-17
GO:0098796	membrane protein complex	9.5e-19	1.0e-16
GO:1990904	ribonucleoprotein complex	1.2e-18	1.0e-16
GO:0030529	intracellular ribonucleoprotein complex	1.2e-18	1.0e-16
GO:0044436	thylakoid part	1.8e-18	1.4e-16
GO:0044422	organelle part	2.3e-18	1.6e-16
GO:0070469	respiratory chain	2.2e-18	1.6e-16
GO:0034357	photosynthetic membrane	2.7e-18	1.6e-16
GO:0009535	chloroplast thylakoid membrane	2.7e-18	1.6e-16
GO:0044446	intracellular organelle part	2.8e-18	1.6e-16
GO:0055035	plastid thylakoid membrane	3.0e-18	1.6e-16
GO:0009534	chloroplast thylakoid	5.2e-18	2.6e-16
GO:0031976	plastid thylakoid	5.8e-18	2.8e-16
GO:0009579	thylakoid	8.0e-18	3.4e-16
GO:0042651	thylakoid membrane	8.2e-18	3.4e-16
GO:0098803	respiratory chain complex	7.8e-18	3.4e-16
GO:0098798	mitochondrial protein complex	5.5e-17	2.2e-15
GO:0022625	cytosolic large ribosomal subunit	4.4e-16	1.7e-14
GO:0098800	inner mitochondrial membrane protein complex	6.9e-16	2.5e-14
GO:0044455	mitochondrial membrane part	1.0e-15	3.7e-14
GO:0015934	large ribosomal subunit	4.0e-15	1.4e-13
GO:0016020	membrane	4.8e-13	1.6e-11
GO:0005743	mitochondrial inner membrane	1.5e-12	4.8e-11
GO:0031966	mitochondrial membrane	2.8e-12	8.6e-11
GO:0005740	mitochondrial envelope	3.4e-12	1.0e-10
GO:0005747	mitochondrial respiratory chain complex I	6.6e-12	1.9e-10
GO:0045271	respiratory chain complex I	1.1e-11	3.0e-10
GO:0030964	NADH dehydrogenase complex	1.4e-11	3.7e-10
GO:0019866	organelle inner membrane	1.9e-11	5.1e-10
GO:0044425	membrane part	8.1e-11	2.1e-09

GO:0044434	chloroplast part	1.2e-10	3.0e-09
GO:0009536	plastid	1.3e-10	3.1e-09
GO:0044435	plastid part	1.4e-10	3.4e-09
GO:0031975	envelope	1.5e-10	3.4e-09
GO:0031967	organelle envelope	1.5e-10	3.4e-09
GO:0009507	chloroplast	2.5e-10	5.5e-09
GO:0031984	organelle subcompartment	5.7e-10	1.2e-08
GO:0043232	intracellular non-membrane-bounded organelle	6.3e-10	1.3e-08
GO:0043228	non-membrane-bounded organelle	6.3e-10	1.3e-08
GO:0044429	mitochondrial part	1.0e-09	2.1e-08
GO:0005576	extracellular region	3.0e-09	6.0e-08
GO:0005737	cytoplasm	3.6e-09	7-0e-07
GO:0022627	cytosolic small ribosomal subunit	4.7e-08	9,00E-07
GO:0005829	cytosol	6.5e-08	1.2e-06
GO:0009521	photosystem	1.4e-07	2.6e-06
GO:0010598	NAD(P)H dehydrogenase complex (plastoquinone)	1.6e-07	3.0e-06
GO:0031970	organelle envelope lumen	2.3e-07	4.0e-06
GO:0043234	protein complex	4.6e-07	8.1e-06
GO:0005758	mitochondrial intermembrane space	6.4e-07	1.1e-05
GO:0015935	small ribosomal subunit	7.0e-07	1.2e-05
GO:0070069	cytochrome complex	9.8e-07	1.6e-05
GO:0031225	anchored component of membrane	1.2e-06	1.9e-05
GO:0005750	mitochondrial respiratory chain complex III	1.8e-06	2.8e-05
GO:0031090	organelle membrane	1.8e-06	2.8e-05
GO:0045275	respiratory chain complex III	1.8e-06	2.8e-05
GO:0031224	intrinsic component of membrane	2.3e-06	3.5e-05
GO:1902494	catalytic complex	2.2e-05	3.3e-04
GO:1990351	transporter complex	2.8e-05	4.2e-04
GO:1990726	Lsm1-7-Pat1 complex	3.3e-05	4.8e-04
GO:0044423	virion part	6.7e-05	9.2e-04
GO:0019013	viral nucleocapsid	6.7e-05	9.2e-04
GO:0019012	virion	6.7e-05	9.2e-04
GO:0019028	viral capsid	6.7e-05	9.2e-04
GO:1902495	transmembrane transporter complex	8.2e-05	1.1e-03
GO:0098807	chloroplast thylakoid membrane protein complex	8.2e-05	1.1e-03
GO:0097526	spliceosomal tri-snRNP complex	9.3e-05	1.2e-03
GO:0030095	chloroplast photosystem II	9.3e-05	1.2e-03
GO:0031977	thylakoid lumen	9.7e-05	1.2e-03
GO:0009522	photosystem I	1.0e-04	1.3e-03
GO:0005618	cell wall	1.9e-04	2.3e-03
GO:0030312	external encapsulating structure	1.9e-04	2.3e-03
GO:0031978	plastid thylakoid lumen	2.2e-04	2.6e-03
GO:0009543	chloroplast thylakoid lumen	2.2e-04	2.6e-03
GO:0009523	photosystem II	2.5e-04	2.9e-03
GO:0016021	integral component of membrane	2.8e-04	3.2e-03
GO:0048046	apoplast	2.8e-04	3.2e-03

GO:0005688	U6 snRNP	4.6e-04	5.2e-03
GO:0016469	proton-transporting two-sector ATPase complex	4.8e-04	5.4e-03
GO:0071013	catalytic step 2 spliceosome	5.9e-04	6.4e-03
GO:0071944	cell periphery	5.8e-04	6.4e-03
GO:0005732	small nucleolar ribonucleoprotein complex	5.8e-04	6.4e-03
GO:0009941	chloroplast envelope	9.1e-04	9.7e-03
GO:0033176	proton-transporting V-type ATPase complex	9.1e-04	9.7e-03
GO:0009526	plastid envelope	9.5-04	0.01
GO:0071011	precatalytic spliceosome	1.1e-03	0.011

Supplemental table 5 - Cellular component gene ontology (GO) terms associated with the genes upregulated in the *stk* transcriptome. The significantly (*p*-value < 0.05 and FDR < 0.05) enriched GO terms are presented.

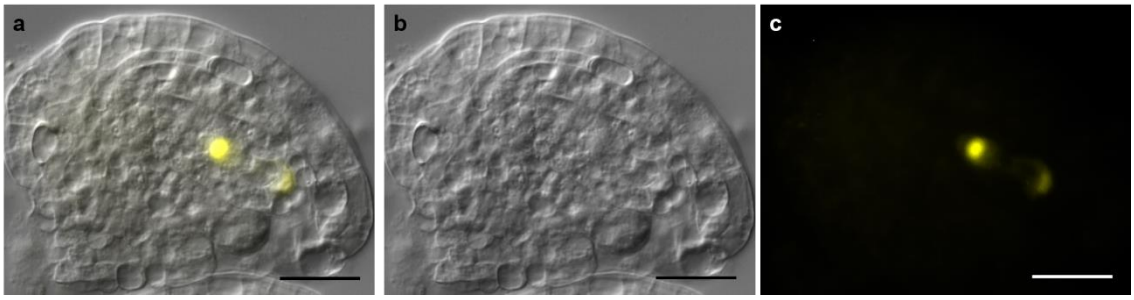

Supplemental Fig. 2 – *pKNU-YFP* expression in *dyad* ovules. The promoter of *KNU* (*pKNU*) drives the expression of the yellow fluorescent protein (YFP) in the spore dyad nuclei. **(a)** Merge of bright-field Differential Interference Contrast (DIC) and YFP fluorescence under UV images. **(b)** Bright-field DIC image. **(c)** The yellow signal corresponds to the YFP fluorescence under UV light. Scale bars = 20 μm.

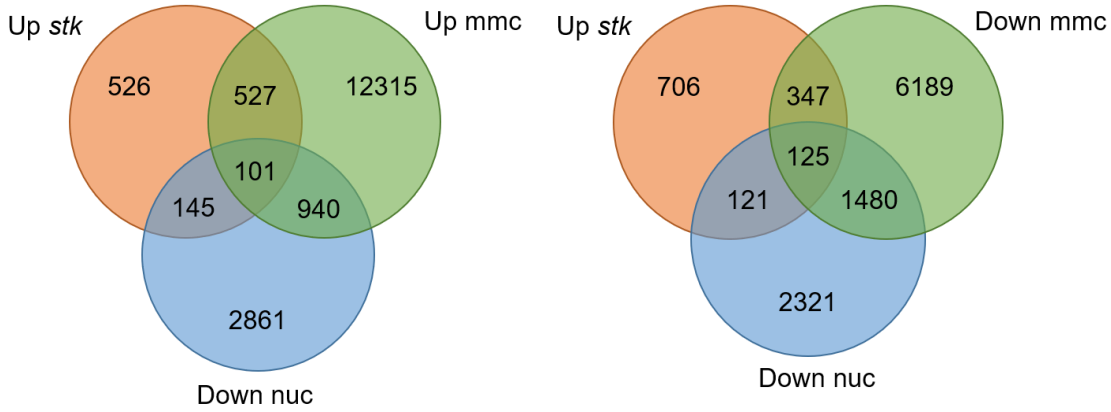

Supplemental Fig. 3 - Venn diagrams showing the cross of the upregulated genes in *stk* RNA sequencing (Up *stk*), downregulated in the nucellus microarray (Down nuc) with the upregulated genes in the MMC microarray (Up mmc, left) or downregulated in the MMC microarray (Down mmc, right).

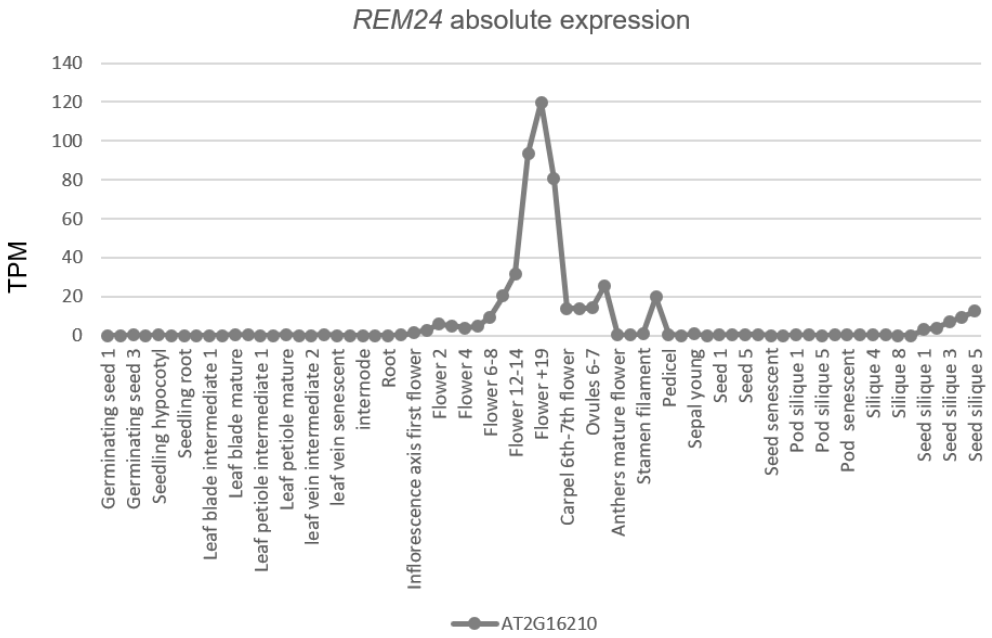

Supplemental Fig. 4 – *REM24* absolute expression level in various wild type Arabidopsis tissues, obtained by RNA sequencing. *REM24* mRNA level is higher during flower development, especially in younger stages. *REM24* is absent from vegetative structures, seeds and siliques. Gene level is shown as transcripts per million (TPM). Tissue was collected as described in Klepikova *et al*., 2016. This expression profile was used to obtain a list of the 18 genes with the most similar expression pattern to *REM24*, considering vegetative and floral tissues.

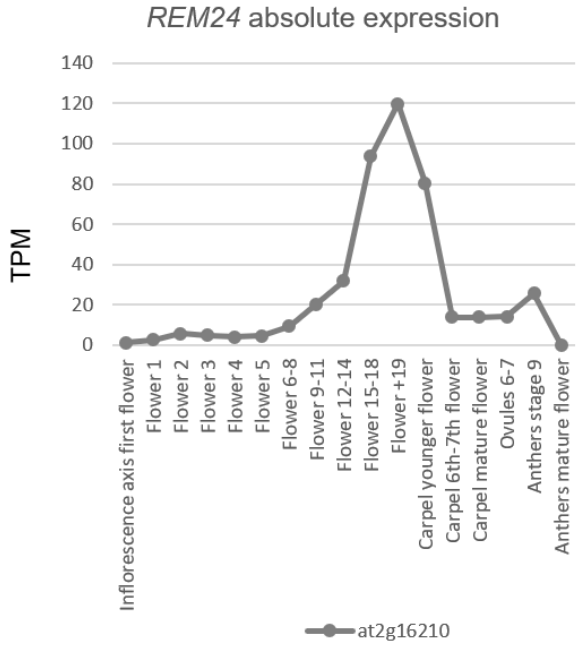

Supplemental Fig. 5 – *REM24* absolute expression level in reproductive wild type Arabidopsis tissues, obtained by RNA sequencing. *REM24* is expressed in carpels, ovules and anthers stage9. *REM24* is almost absent from the older flower stages. Gene level is shown as transcripts per million (TPM). Tissue was collected as described in Klepikova *et al*., 2016. This expression profile was used to obtain a list of the 18 genes with the most similar expression pattern to *REM24*, enriched for floral tissues.

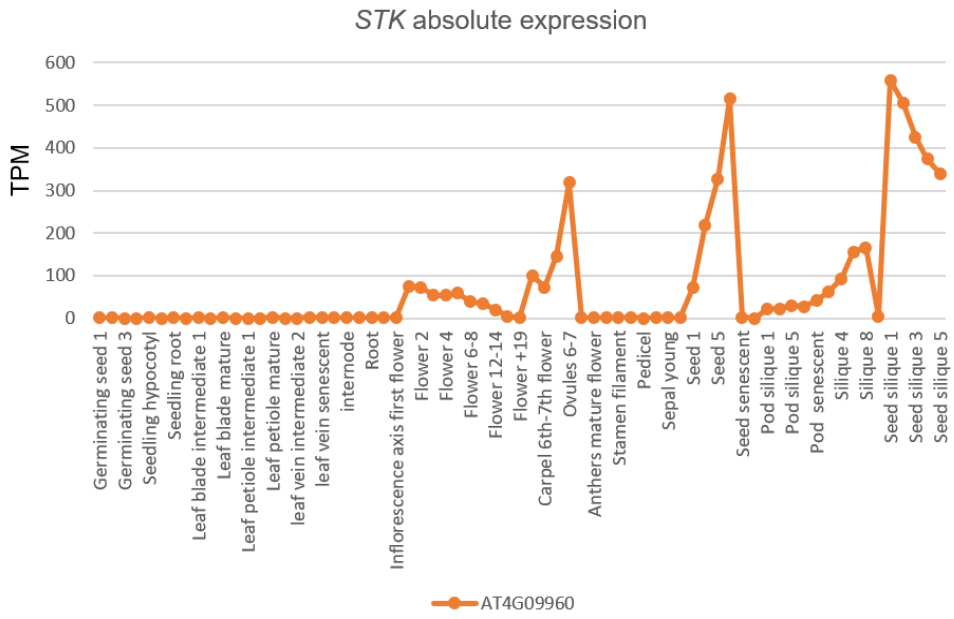

Supplemental Fig. 6 – *STK* absolute expression level in various wild type Arabidopsis tissues, obtained by RNA sequencing. *STK* mRNA level is higher in reproductive structures, throughout flower, silique and seed developmental stages. *STK* is absent from vegetative structures. Gene level is shown as transcripts per million (TPM). Tissue was collected as described in Klepikova *et al*., 2016. This expression profile was used to obtain a list of the 18 genes with the most similar expression pattern to *STK*, considering vegetative and floral tissues.

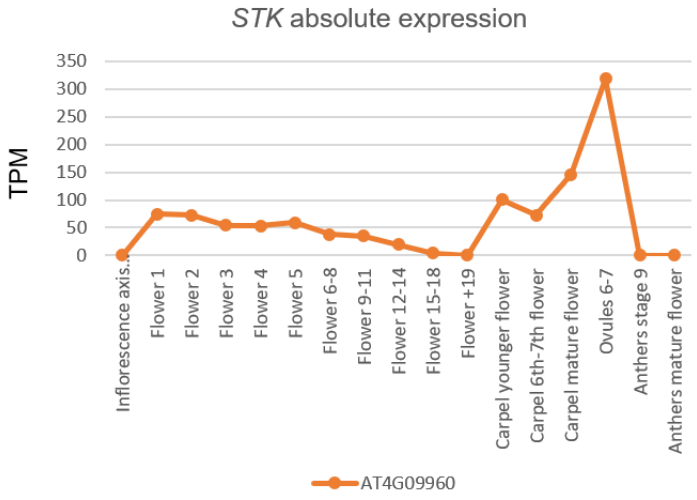

Supplemental Fig. 7 - *STK* absolute expression level in reproductive wild type Arabidopsis tissues, obtained by RNA sequencing. In the flower, *STK* expression is higher in ovules of flowers stage 6-7. *STK* is absent from the anthers. Gene level is shown as transcripts per million (TPM). Tissue was collected as described in Klepikova *et al*., 2016. This expression profile was used to obtain a list of the 18 genes with the most similar expression pattern to *STK*, enriched for floral tissues.

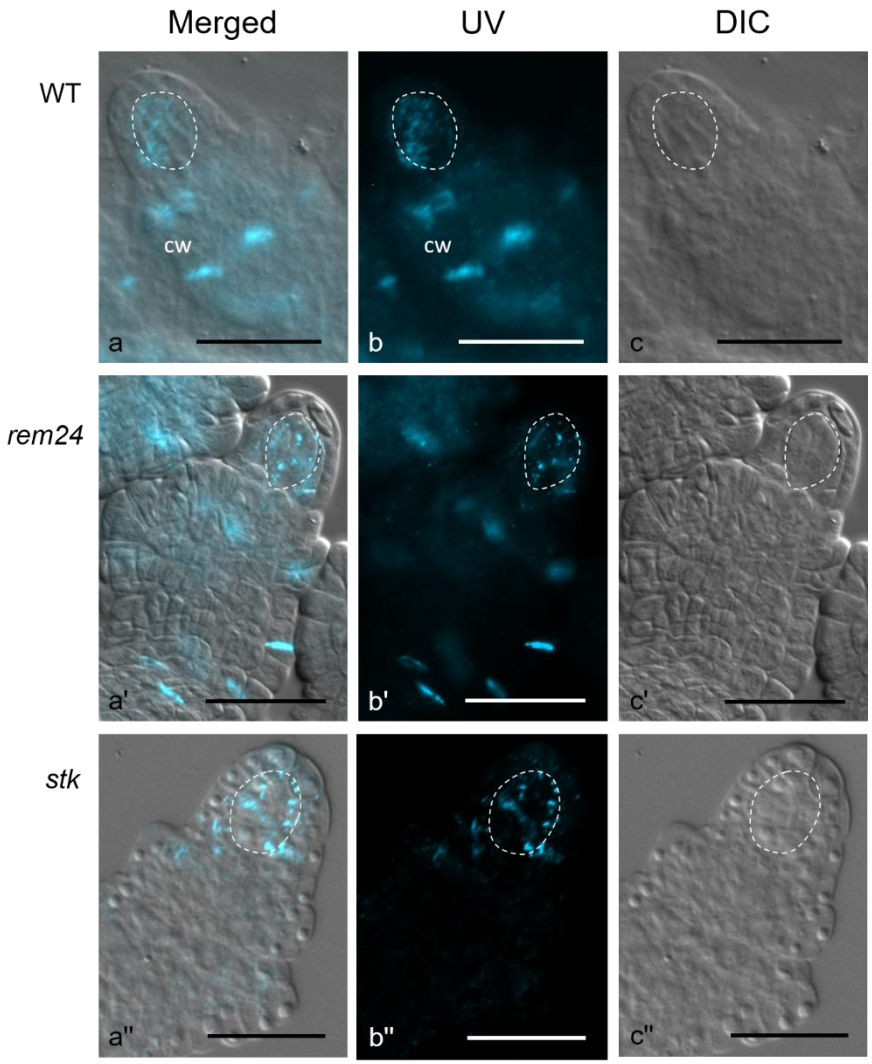

Supplemental Fig. 8 - Representative images of ovules at megaspore mother cell (MMC) stage with wild type-like aniline blue pattern. Wild type (WT) **(a – c)**, *rem24* **(a' – c')** and *stk* **(a'' – c'')** ovules showing the aniline blue staining in a small punctate pattern, surrounding the MMC, on the border between the MMC and the nucellar epidermis. **(a, a', a'')** Merge of bright-field Differential Interference Contrast (DIC) and UV channel images. **(b, b', b'')** The blue signal corresponds to the aniline blue fluorescence under UV light. **(c, c', c'')** Bright-field DIC microscopy. White dashed lines outline the MMC. MMC stage stands for ovules from stage 2-I to stage 2-III (according to Schneitz *et al*., 1995). Scale bars = 20 μm.

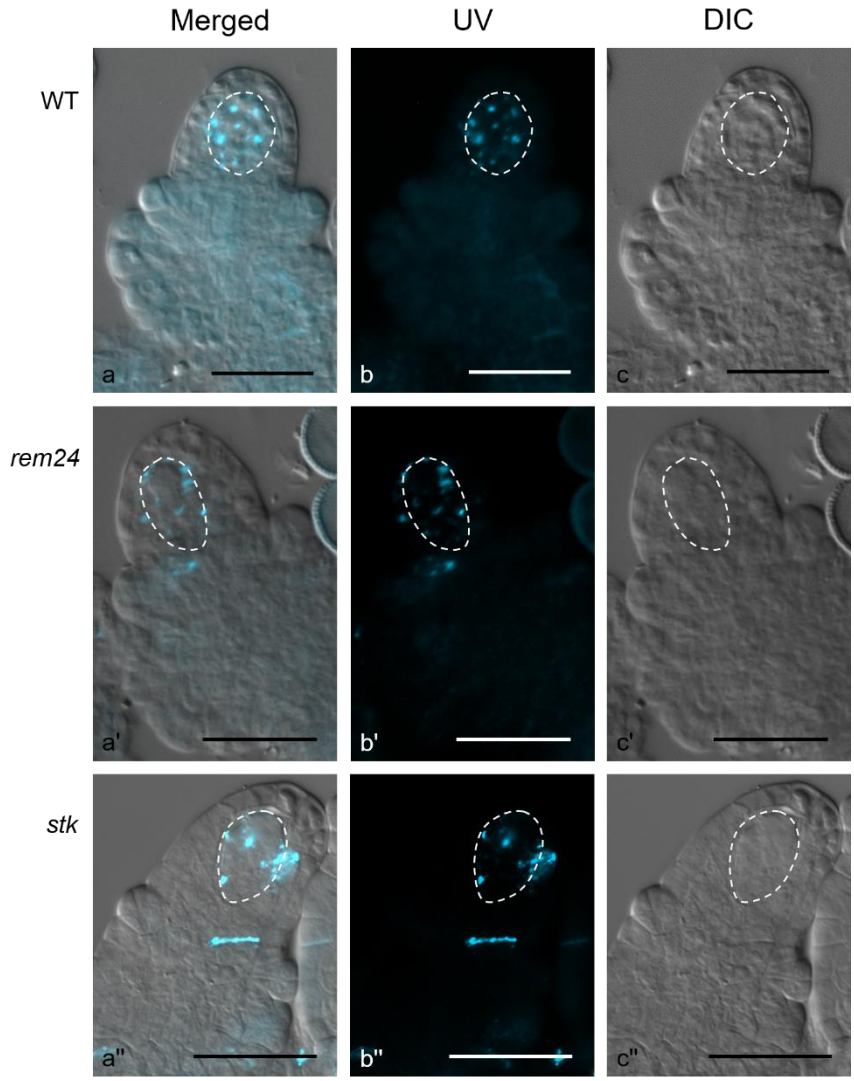

Supplemental Fig. 9 - Representative images of ovules at megaspore mother cell (MMC) stage with bigger spots aniline blue pattern. Wild type (WT) **(a – c)**, *rem24* **(a' – c')** and *stk* **(a'' – c'')** ovules showing accumulation of the stain creating bigger puncta, on the border between the MMC and the nucellar epidermis. **(a, a', a'')** Merge of bright-field Differential Interference Contrast (DIC) and UV channel images. **(b, b', b'')** The blue signal corresponds to the aniline blue fluorescence under UV light. **(c, c', c'')** Bright-field DIC microscopy. White dashed lines outline the MMC. MMC stage stands for ovules from stage 2-I to stage 2-III (according to Schneitz *et al*., 1995). Scale bars = 20 μm.

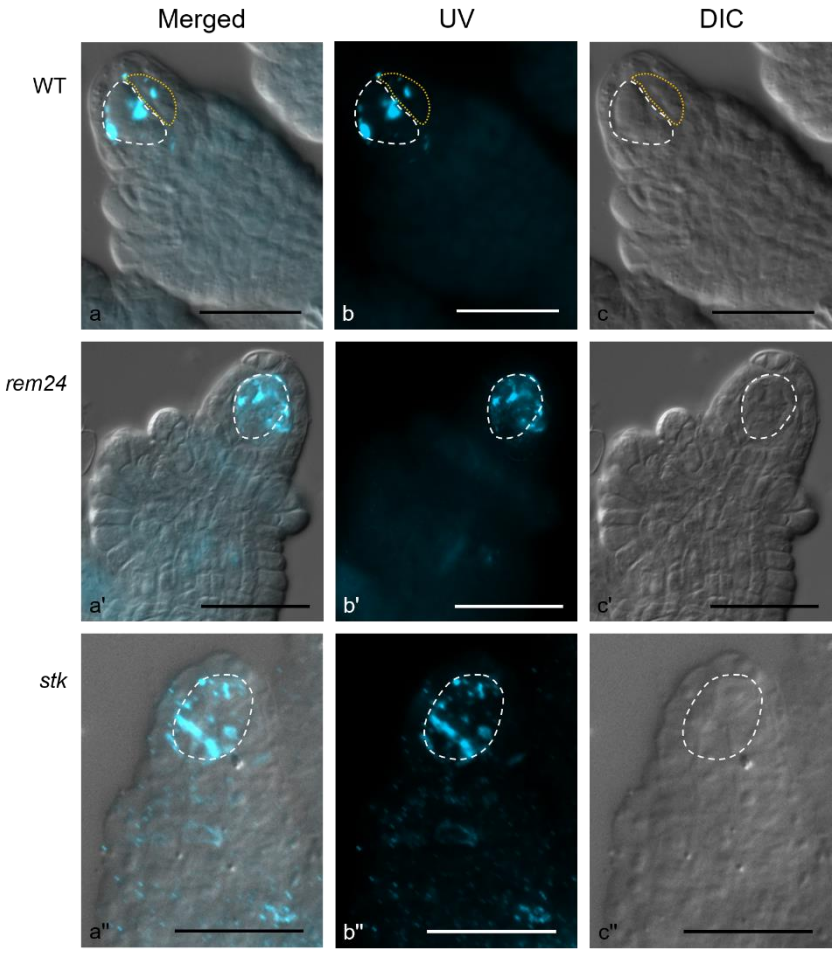

Supplemental Fig. 10 - Representative images of ovules at megaspore mother cell (MMC) stage with blobby aniline blue pattern. Wild type (WT) **(a – c)**, *rem24* **(a' – c')** and *stk* **(a'' – c'')** ovules showing accumulation of the stain in blobs, usually not forming a punctate pattern, but still surrounding the MMC. **(a, a', a'')** Merge of bright-field Differential Interference Contrast (DIC) and UV channel images. **(b, b', b'')** The blue signal corresponds to the aniline blue fluorescence under UV light. **(c, c', c'')** Bright-field DIC microscopy. White dashed lines outline the MMC. Yellow spotted line highlights the potential presence of nucellar cells next to the MMC. MMC stage stands for ovules from stage 2-I to stage 2-III (according to Schneitz *et al*., 1995). Scale bars = 20 μm.

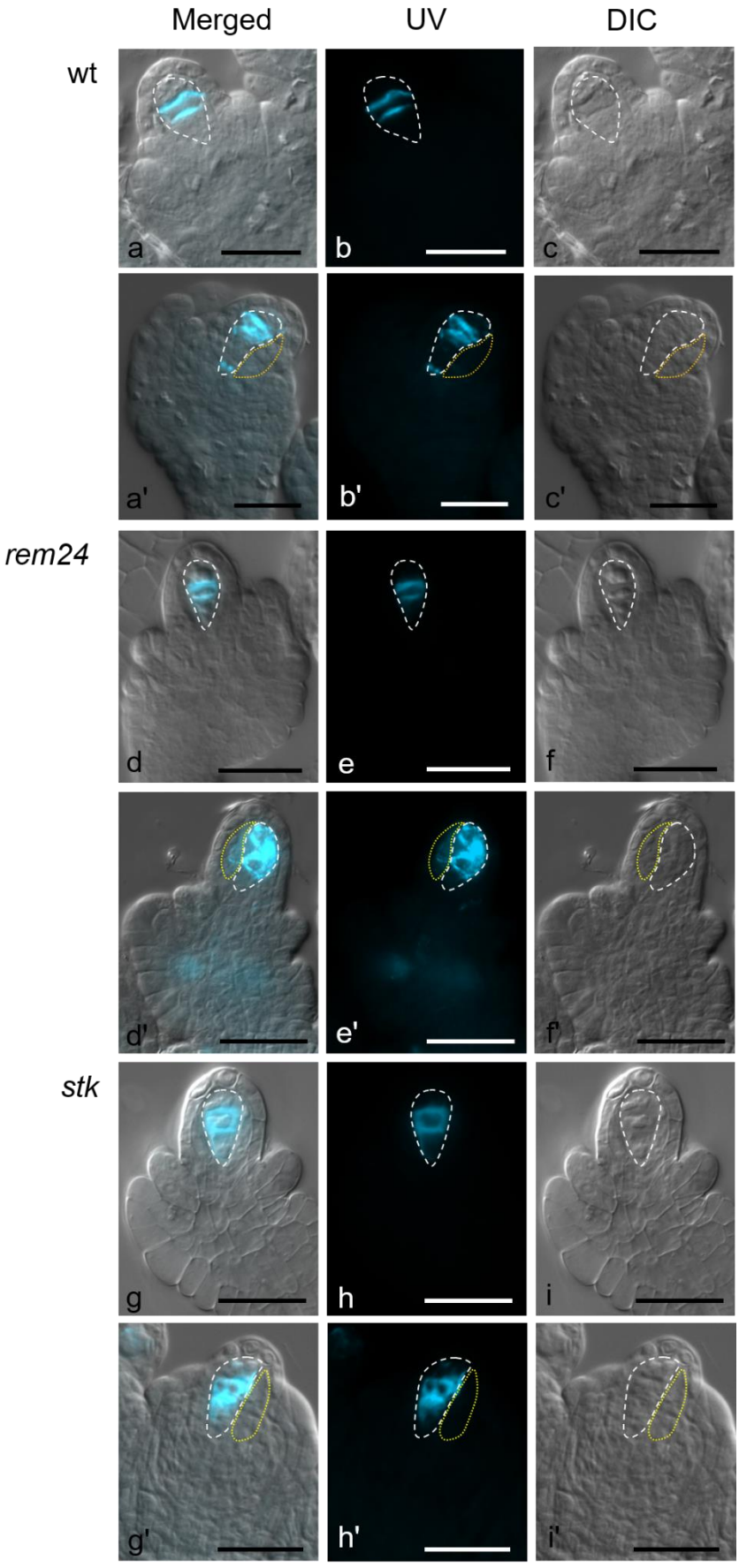

Supplemental Fig. 11 - Representative aniline blue patterns observed for wild type (WT), *rem24* and *stk* ovules at tetrad stage. Linear tetrads were observed for WT **(a, b, c)**, *rem24* **(d, e, f)** and *stk* **(g, h, i)** ovules. It was possible to find ovules with squashed tetrads for WT **(a', b', c')**, *rem24* **(d', e', f')** and *stk* **(g', h', i').** Linear tetrad: the tetrad occupies the nucellar dome, the aniline blue stains the cell plates dividing the spores parallelly, indicative of a linear tetrad. Squashed tetrad: the aniline blue staining pattern is representative of the linear tetrad, but the tetrad in is a lateral position pushed by a potential enlarged nucellar cell. **(a, a', d, d', g, g')** Merge of bright-field Differential Interference Contrast (DIC) and UV channel images. **(b, b', e, e', h, h')** The blue signal corresponds to the aniline blue fluorescence under UV light. **(c, c', f, f', i, i')** Bright-field DIC microscopy. White dashed lines outline the megaspore tetrad. Yellow spotted line highlights the presence of potential enlarged nucellar cells next to the MMC. Tetrad stage stands for ovules at stage 2-IV/V (according to Schneitz *et al*., 1995). Scale bars = 20 μm.

		Stage			
Gene	**Comparison**	1-9	10-11	12	13-15
AGO9	*stk* vs WT	1.0	0.8	0.6	0.4
	rem24 vs WT	1.2	1.3	1.1	0.8
	rem24 vs *stk*	1.2	1.6	1.9	2.1
WUS	*stk* vs WT	1.4	2.4	2.0	0.8
	rem24 vs WT	1.3	2.4	2.0	3.7
	rem24 vs *stk*	1.0	1.0	1.0	4.7
REM24	*stk* vs WT	1.1	1.8	1.8	2.8
	rem24 vs WT	0.7	0.8	1.1	1.8
	rem24 vs *stk*	0.6	0.4	0.6	0.6
RDR6	*stk* vs WT	2.5	2.3	4.4	7.6
	rem24 vs WT	1.2	1.1	1.7	3.2
	rem24 vs *stk*	0.5	0.5	0.4	0.4
SPL	*stk* vs WT	2.1	2.2	3.9	0.9
	rem24 vs WT	1.5	1.8	1.9	0.4
	rem24 vs *stk*	0.7	0.8	0.5	0.5
STK	*stk* vs WT	0.5	0.6	0.3	0.2
	rem24 vs WT	0.8	1.1	0.8	0.7
	rem24 vs *stk*	1.5	1.8	2.5	3.3
AGO5	*stk* vs WT	1.4	2.4	1.9	1.8
	rem24 vs WT	0.9	1.3	0.9	1.3
	rem24 vs *stk*	0.6	0.5	0.5	0.7
KNU	*stk* vs WT	0.7	0.2	1.5	0.7
	rem24 vs WT	0.5	0.2	0.9	1.0
	rem24 vs stk	0.8	0.7	0.6	1.3
REM23	*stk* vs WT	1.5	1.4	1.7	2.5
	rem24 vs WT	1.5	1.4	1.3	2.2
	rem24 vs stk	1.0	1.0	0.8	0.9
FLA20	*stk* vs WT	5.1	0.3	1.4	4.3
	rem24 vs WT	2.7	0.5	1.4	3.0
	rem24 vs *stk*	0.5	1.8	1.0	0.7
HSP20	*stk* vs WT	0.9	1.0	0.8	1.9
	rem24 vs WT	0.9	1.0	1.2	3.2
	rem24 vs *stk*	1.0	1.0	1.4	1.7

Supplemental table 6 - Heat map of fold change, relative to zero for all the conditions tested in all qPCR performed. The gene expression between *stk* with WT, *rem24* with WT, and *rem24* with *stk* were compared. Red fill indicates upregulated genes. Black fill indicates downregulated genes.

Locus	FC MMC-NUC	Gene description
AT1G15190	1,2	Fasciclin-like arabinogalactan family protein
AT4G16980	1,1	Arabinogalactan-protein family
AT5G56540	1,0	Arabinogalactan protein 14
AT1G35230	1,0	Arabinogalactan protein 5
AT5G10430	0,9	Arabinogalactan protein 4
AT5G14380	0,9	Arabinogalactan protein 6
AT3G01700	0,9	Arabinogalactan protein 11
AT3G06360	0,8	Arabinogalactan protein 27
AT3G60900	0,8	Fasciclin-like arabinogalactan-protein 10
AT5G06920	0,8	Fasciclin-like arabinogalactan protein 21 precursor
AT5G03170	0,8	Fasciclin-like arabinogalactan-protein 11
AT1G30800	0,7	Fasciclin-like arabinogalactan family protein
AT5G65390	0,7	Arabinogalactan protein 7
AT3G52370	0,7	Fasciclin-like arabinogalactan protein 15 precursor
AT5G40940	0,6	Fasciclin-like arabinogalactan protein 20
AT3G12660	0,6	Fasciclin-like arabinogalactan protein 14 precursor
AT2G22470	0,6	Arabinogalactan protein 2
AT5G53250	0,6	Arabinogalactan protein 22
AT3G55820	0,5	Fasciclin-like arabinogalactan family protein
AT2G33790	0,5	Arabinogalactan protein 30
AT2G20520	0,5	Fasciclin-like arabinogalactan 6
AT3G20865	0,3	Arabinogalactan protein 40
AT5G44130	0,3	Fasciclin-like arabinogalactan protein 13 precursor
AT2G35860	0,3	Fasciclin-like arabinogalactan protein 16 precursor
AT2G24450	0,2	Fasciclin-like arabinogalactan protein 3 precursor
AT2G23130	0,2	Arabinogalactan protein 17
AT3G11700	0,2	Fasciclin-like arabinogalactan protein 18 precursor
AT4G26320	0,1	Arabinogalactan protein 13
AT4G40090	0,1	Arabinogalactan protein 3
AT4G37450	0,1	Arabinogalactan protein 18

Supplemental table 7 - Arabinogalactan proteins and Fasciclin-like arabinogalactan protein upregulated in the Megaspore Mother Cell (MMC) microarray. For each gene is described the locus, fold change (FC) in the MMC relative to the nucellus (NUC) and its description.